RICE UNIVERSITY

Robust Constrained Optimization Approach to Control Design for International Space Station Centrifuge Rotor Auto Balancing Control System

By

Barry Dirk Postma

A THESIS SUBMITTED
IN PARTIAL FULFILLMENT OF THE
REQUIREMENTS FOR THE DEGREE

Master of Science

APPROVED, THESIS COMMITTEE:

Pol D. Spanos, Professor, L.B. Ryon
Endowed Chair in Engineering
Mechanical Engineering & Material Science

Satish Nagarajaiah, Associate Professor
Mechanical Engineering & Material Science

Marcia K. O'Malley, Assistant Professor
Mechanical Engineering & Material Science

Jiann-Woei Jang, Technical Supervisor
The Charles Stark Draper Laboratory

HOUSTON, TEXAS
APRIL 2005

Note: The views expressed in this thesis are those of the author and do not reflect the official policy or position of the United States Air Force, Department of Defense, or the U.S. Government

ABSTRACT

Robust Constrained Optimization Approach to Control Design for International Space Station Centrifuge Rotor Auto Balancing Control System

by

Barry Dirk Postma

This thesis discusses application of a robust constrained optimization approach to control design to develop an Auto Balancing Controller (ABC) for a centrifuge rotor to be implemented on the International Space Station. The design goal is to minimize a performance objective of the system, while guaranteeing stability and proper performance for a range of uncertain plants. The performance objective is to minimize the translational response of the centrifuge rotor due to a fixed worst-case rotor imbalance. The robustness constraints are posed with respect to parametric uncertainty in the plant. The proposed approach to control design allows for both of these objectives to be handled within the framework of constrained optimization. The resulting controller achieves acceptable performance and robustness characteristics.

ACKNOWLEDGEMENTS

First, I would like to thank my academic advisor, Dr. Pol Spanos, for his knowledge and willingness to provide guidance throughout the preparation of this thesis. Dr. Spanos' expertise was especially helpful in the area of Monte Carlo Simulation where he introduced me to the fundamentals of the Monte Carlo method.

I would like to thank Dr. Satish Nagarajaiah for his guidance and instruction in the area of classical and multivariable control.

Also, I would like to thank Dr. Marcia O'Malley for her instruction in the area of mechatronics and practical experience in control systems.

I would like to thank my technical supervisor at Draper Laboratory in Houston, TX, Dr. Jiann-Woei Jang, for reviewing my research and scrutinizing my thesis. His advice and guidance have greatly influenced the quality of this thesis.

I would also like to thank my program manager at Draper Laboratory, Dr. Nazareth Bedrossian, for his willingness to spend his time working with me and reviewing my work on a consistent basis. Without the help of Dr. Bedrossian this thesis would be much less "robust".

I would like to thank my wife Stephanie for her love and support during this process. Without her, I would not have been able to make the progress that I made.

Finally, I would like to thank God for the opportunity to come to Rice to conduct this research and pursue a graduate degree.

ASSIGNMENT

Draper Laboratory Report Number T-1509

In consideration for the research opportunity and permission to prepare my thesis by and at The Charles Stark Draper Laboratory, Inc., I hereby assign my copyright of the thesis to The Charles Stark Draper Laboratory, Inc., Cambridge, Massachusetts.

Barry D. Postma April 13, 2005

Table of Contents

List of Figures

List of Tables

1 Introduction

The Japanese Aerospace Exploration Agency (JAXA) plans to participate in the development of the International Space Station (ISS) by providing a centrifuge to be used for scientific experiments. The centrifuge will be housed in the Centrifuge Accommodation Module to be assembled with the ISS in the configuration shown in Figure 1-1 [1].

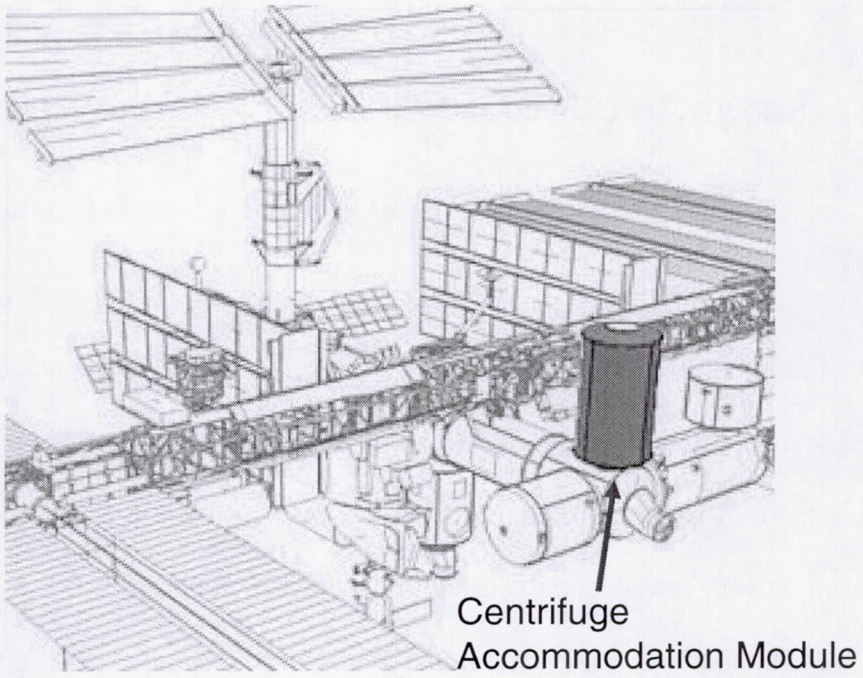

Figure 1-1. Location of the Centrifuge Accommodation Module

The centrifuge would serve as a home for a number of rodents (or other test specimen). The rodents are allowed to move within habitats that are housed in the centrifuge rotor as shown in Figure 1-2.

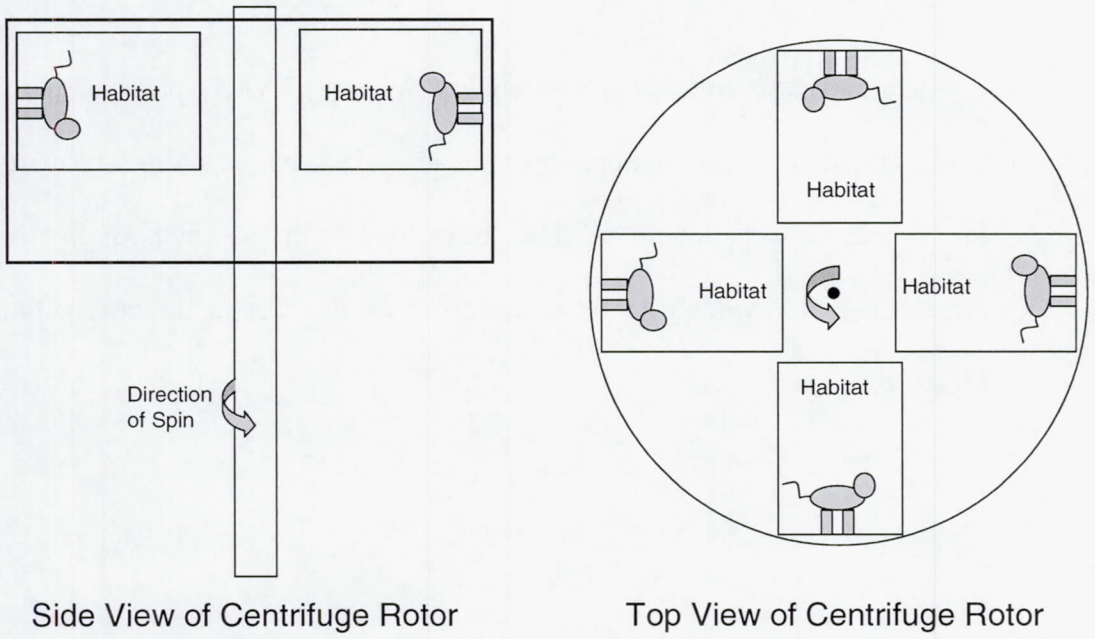

Figure 1-2. Side/Top View of Rodents in Habitats

Rodent movement within the habitats introduces an imbalance in the rotor that causes rotor vibration while the rotor is spinning. This imbalance must be cancelled to avoid the transfer of disturbances from the centrifuge rotor to the ISS. An active control system must be introduced to cancel imbalances in the rotor.

Methodologies for limiting the vibration of spinning rotors have been presented in the literature. These methods can be divided into two techniques: direct active vibration control and active balancing techniques using mass redistribution. Direct active vibration control uses magnetic bearings that generate an external lateral force on the rotor, while active balancing uses a mass redistribution device to eliminate the rotor imbalance. Meirovitch presented an overview of active vibration control in [2]. These methods can be applied to the direct active vibration control for a spinning rotor. Knopse presented

extensive work in [3]-[6] using adaptive open-loop control to suppress the rotor vibration using magnetic bearings as actuators. Herzog presented a method in [7] that also employed magnetic bearings and used notch filters in the control system. Fan introduced a vibration control method in [8] for an asymmetrical rotor using magnetic bearings.

The Auto Balancing Controller (ABC) for the centrifuge rotor is classified as a mass redistribution type of controller. Using mass redistribution techniques, Van De Vegte first proposed a modal balancing method for the balancing of spinning rotors during operation [9]. Gosiewski proposed a control method based on modal analysis of the rotor vibrations using a computer as the controller in [10] and [11]. Dyer and Ni introduced a balancing method based on influence coefficients to achieve on-line estimation and active control [12]. Many of these methods were developed for the case of a constant rotational rotor speed. More recently, Zhou and Shi developed several balancing methods for speed-varying rotors presented in [13]-[15]. A thorough summary of work in the area of active balancing and vibration control of rotor systems is presented in [16]. In those methods, it is assumed that a rotor speed is either known or estimated exactly; the issue of control system robustness is never addressed. It is important to account for the linear-time varying dynamics of the rotor when using these approaches. In this thesis, a constrained optimization approach is proposed to design an ABC that can robustly cancel rotor imbalances by redistributing mass in the presence of system uncertainty. With the proposed methodology, both time domain and frequency domain stability and performance requirements can be easily included in the design process.

The remainder of this thesis is divided into five chapters.

Chapter 2 provides relevant problem background. A description of the centrifuge rotor system and the ABC system is presented.

Chapter 3 presents technical background for the solution of the problem. System robustness for multivariable systems is discussed, and the solution method is introduced.

Chapter 4 explains the method used to solve the control problem. This section describes the implementation of the robust constrained optimization approach to control design and how it was applied to design an ABC system.

Chapter 5 presents the results of the control design. The system is analyzed in both the time domain and the frequency domain. Also, the results of Monte Carlo simulations are presented.

Chapter 6 summarizes the topics in this thesis and presents suggestions for possible future work related to this problem.

2 Problem Background

In order to delineate the methodology used to solve the ABC design problem, it is important to properly describe the centrifuge rotor system. In this section the centrifuge rotor system and the ABC system are described in detail. Following the system description is a general statement of the problem to be solved in the design of an ABC.

2.1 Centrifuge Rotor System

The purpose of the centrifuge is to simulate varying levels of gravity so that the effects on the rodents can be studied. The centrifuge achieves the effect of varying levels of gravity by spinning at different steady-state rates. In order to reach a desired level of simulated gravity the rotor must go through a "spin-up" when the spin rate is slowly increased to the desired level.

The spinning centrifuge imparts a centrifugal force on the rodents that serves to simulate gravity. The centrifugal force increases with increasing spin rate. An illustration of how the centrifugal force acts on the rodents is shown in Figure 2-1.

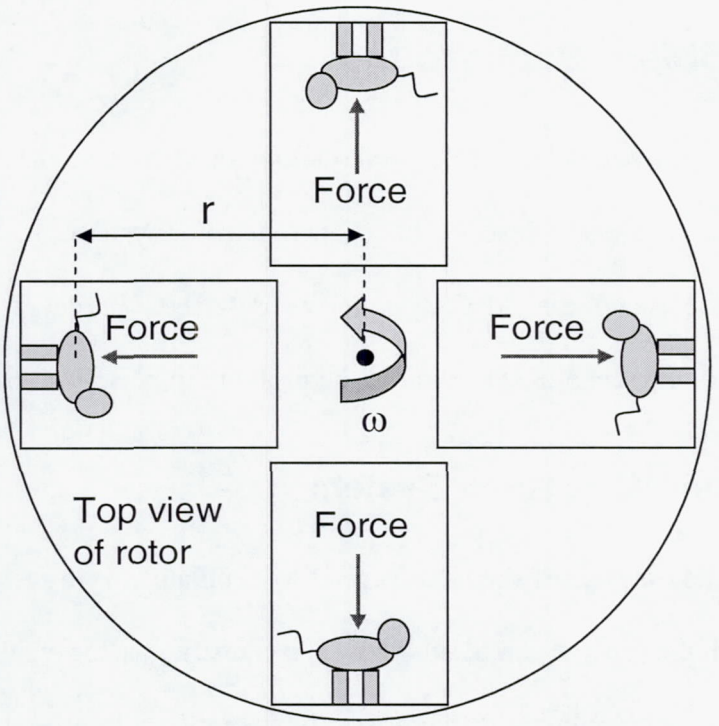

Figure 2-1. Illustration of Centrifugal Force Acting on Rodents

The centrifugal force acting on an individual rodent is specified by the equation

$$Force = M_{rodent} r\omega^2, \qquad (1)$$

where the symbol Force refers to the centrifugal force on the rodent (N), M_{rodent} is the mass of rodent (kg), r is the distance from spin axis to rodent (m), and ω represents the spin rate of centrifuge rotor (rad/sec).

The purpose of the ABC system is to balance the rotor when the rodents have imposed an imbalance. An illustration of the rotor and balancer masses is given in Figure 2-2.

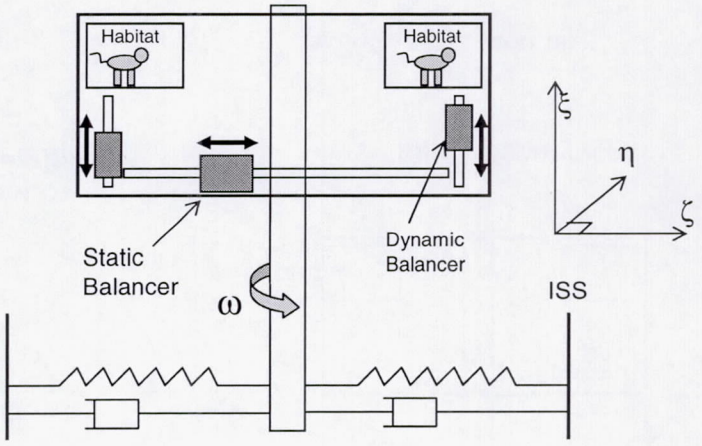

Figure 2-2. Rotor and Balancer Masses

If all of the rodents move to the same corner of their habitat, the center of mass of the rotor shifts in that direction. The ABC utilizes sliding balancer masses as pictured in Figure 2-2 within the rotor to cancel such imbalances. The static balancer masses are utilized to correct imbalances that cause the rotor to translate in the (ζ,η) plane. The dynamic balancer masses are utilized to correct imbalances that cause the rotor to tilt about the (ζ,η) axes. An illustration of the static balancer masses canceling an imbalance is given in Figure 2-3. The dynamic balancers work in a similar manner to cancel imbalances.

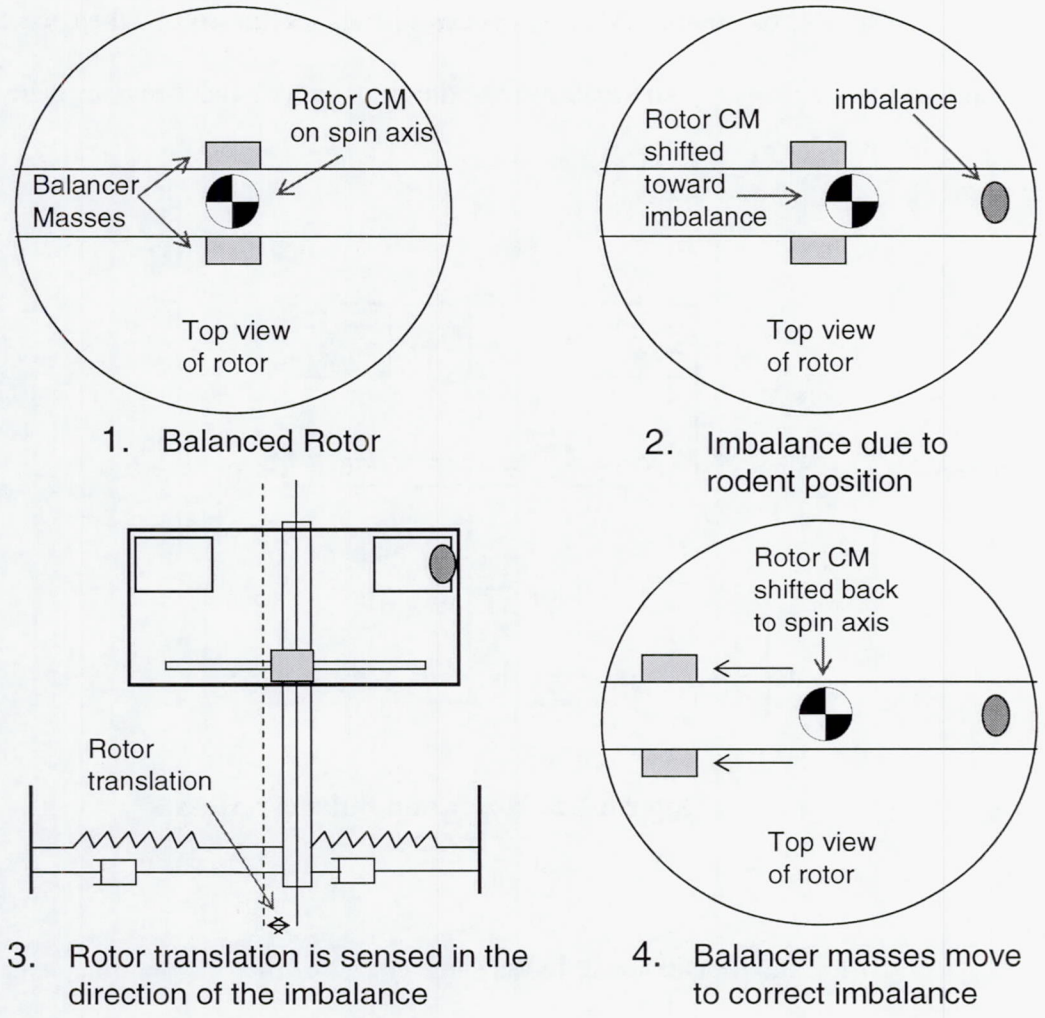

Figure 2-3. Illustration of Balancer Masses Canceling an Imbalance

The naming convention for the balancer masses and positions is described in Figure 2-4. There are two types of balancer masses: static balancer masses (rectangles in Figure 2-4) and dynamic balancer masses (circles in Figure 2-4). The set of static balancer masses moving in the same direction along the ζ-axis is denoted by the subscript b1 and the set of static balancer masses moving in the same direction along the η-axis is denoted by the subscript b2. The symbols ζ_{b1} and η_{b2} are used to describe the position of

the set of balancer masses along the respective axes. The dynamic balancer masses also work in pairs. Each mass is paired with the dynamic balancer mass diagonal to it. The masses in a pair of dynamic balancer masses move in opposite directions parallel to the ξ-axis (which is pointing out of the page in Figure 2-4). For instance, if the dynamic balancer mass in the upper right quadrant of Figure 2-4 moves up, the balancer mass in the lower left quadrant moves the same distance in a downward direction. These mass positions are denoted by ξ_{b3} and ξ_{b4} corresponding to balancer mass names in Figure 2-4.

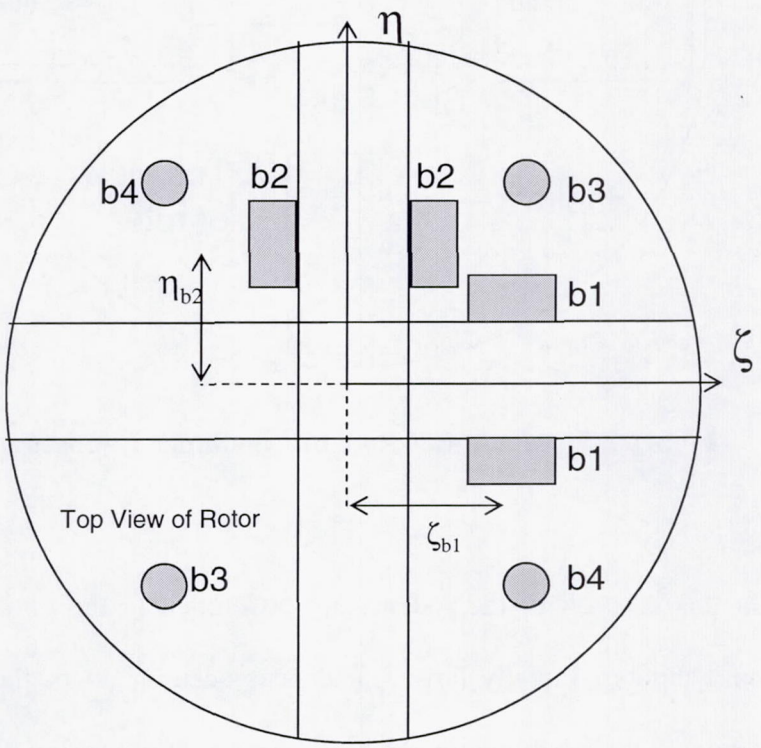

Figure 2-4. Balancer Mass Names and Positions

There exists a maximum imbalance that the rodents can impose on the system. The maximum imbalance occurs when all of the rodents are positioned in the same corner

of their habitats. This moves the center of mass of the rotor the furthest distance from the spin axis of the rotor. Such an imbalance is illustrated in Figure 2-5.

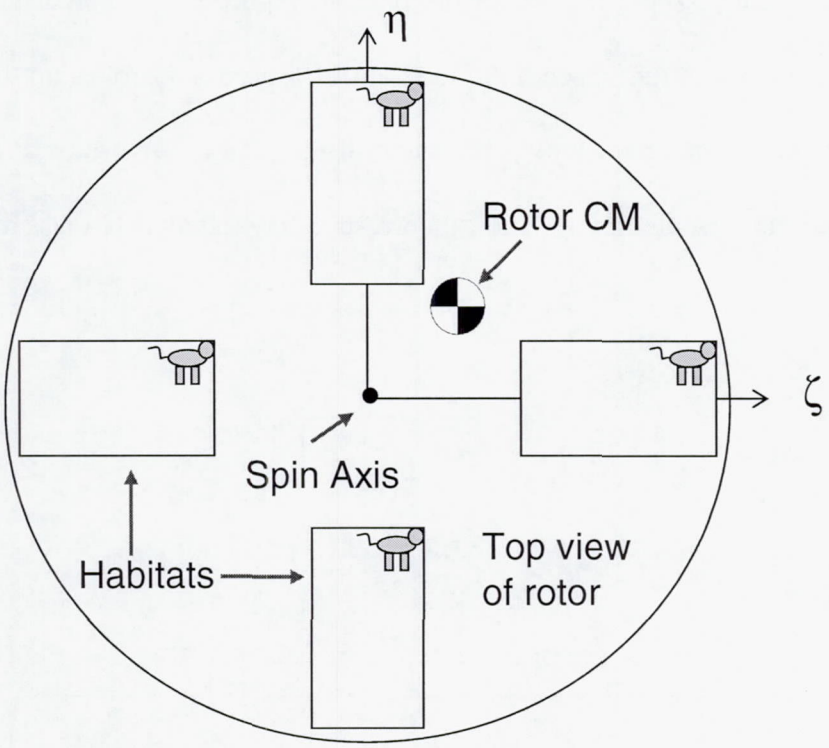

Figure 2-5. Maximum Rodent Imbalance Imposed on the Rotor

In this case all of the rodents are positioned in the upper-right corner of their respective habitats. Equally large imbalances occur if all of the rodents move to any other corner of their habitats at the same time. This maximum imbalance is used to evaluate controller performance in Chapter 4 and Chapter 5.

Note that there are two separate coordinate frames used with respect to the centrifuge rotor. They are shown in Figure 2-6. The (x,y) coordinate frame is fixed with respect to the centrifuge base, and the (ζ,η) coordinate frame rotates with the centrifuge

rotor. Both coordinate frames are used since the rotor displacement sensors work in the fixed coordinate frame and the input to the ABC is a measurement in the rotating coordinate frame.

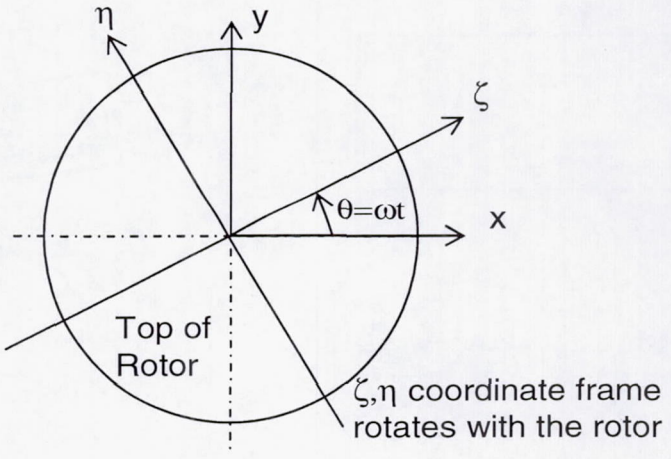

Figure 2-6. Rotor Coordinate Frames

A coordinate transformation as shown in Equation (2) is used to change coordinate frames. Specifically,

$$\begin{bmatrix} \zeta \\ \eta \end{bmatrix} = \begin{bmatrix} \cos(\omega t) & \sin(\omega t) \\ -\sin(\omega t) & \cos(\omega t) \end{bmatrix} \begin{bmatrix} x \\ y \end{bmatrix}. \qquad (2)$$

The ABC system is used to limit the translational response of the rotor due to imbalances imposed by the position of the rodents within the habitats. The input to the controller is an absolute measurement of the rotor displacement (translation and tilt) as shown in Figure 2-7. The centrifuge rotor sensors measure relative displacement between the rotor and the International Space Station. With this relative measurement,

the absolute rotor displacement can be estimated using a Kalman filtering technique [17]. In this thesis it is assumed that these absolute rotor measurements are already available.

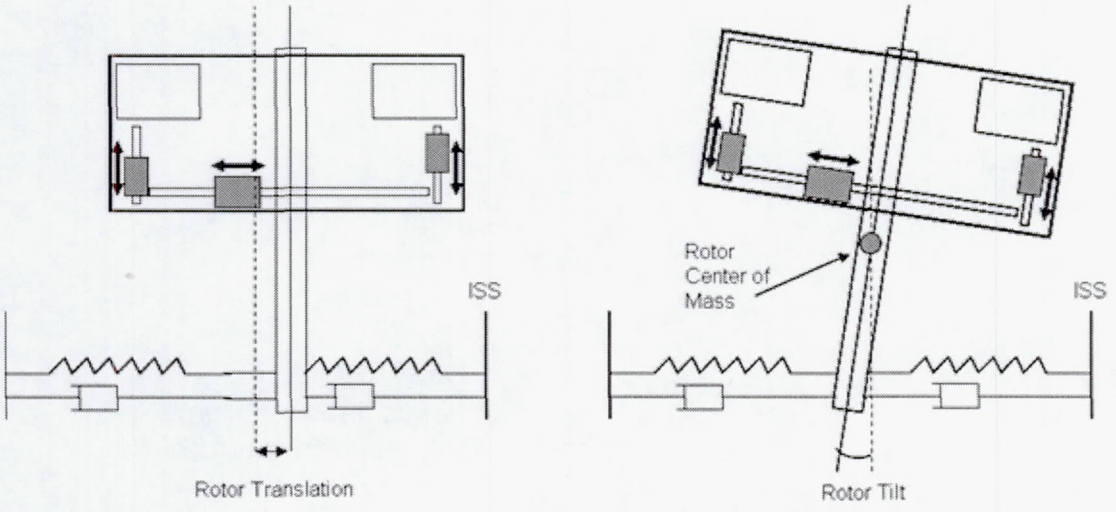

Figure 2-7. Rotor Translation and Tilt

The equations of motion for the centrifuge rotor in the fixed frame coordinate system (x,y coordinate system) are derived below. First, the equations of motion in the translational direction are derived for the system in Figure 2-8. Then, the equations of motion in the tilting direction are derived for the system in Figure 2-9.

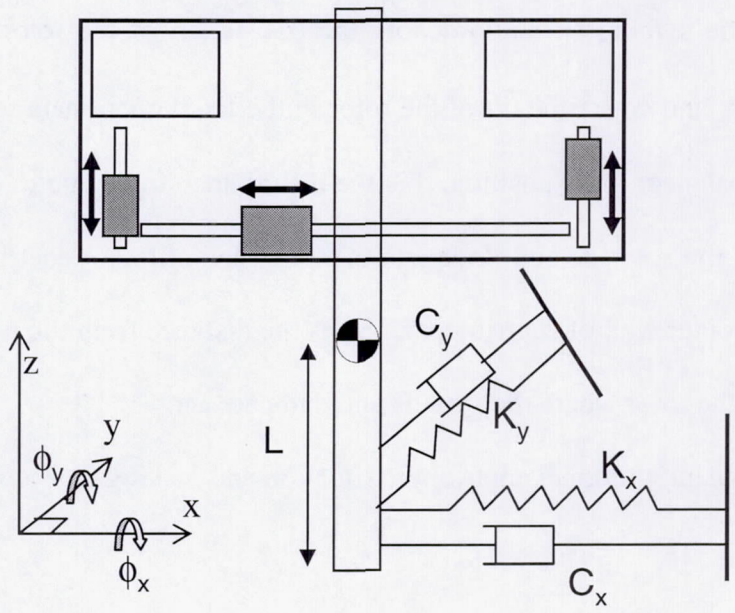

Figure 2-8. Model for Derivation of Equations of Motion in Translational Direction

The equations of motion in the translational direction [17] can be written in each axis as

$$F_x = M\ddot{x} \tag{3}$$

and

$$F_y = M\ddot{y}. \tag{4}$$

The symbol F denotes the external force on the rotor due to springs, dampers, control inputs, and external disturbances. The equations of motion can thus be written

$$F_x = -C_x(\dot{x} - L\sin\dot{\phi}_y) - K_x(x - L\sin\phi_y) + u_x + d_x \tag{5}$$

and

$$F_y = -C_y(\dot{y} + L\sin\dot{\phi}_x) - K_y(y + L\sin\phi_x) + u_y + d_y. \tag{6}$$

where the symbols x and y denote the translation of the rotor in the fixed coordinate frame, ϕ_x and ϕ_y are the tilt of the rotor in the fixed coordinate frame, u is the input force due to balancer mass position, d is the disturbance force due to rodent position, M is the mass of the rotor, C and K denote damping and stiffness coefficients between the rotor and the outer wall of centrifuge, and L is the distance from the rotor center of mass to the base of the rotor where the springs and dampers act.

Using the small angle approximation and making the substitutions

$$C_{11} = C_x = C_y, \tag{7}$$

$$K_{11} = K_x = K_y, \tag{8}$$

$$C_{11} = -C_x L = -C_y L, \tag{9}$$

and

$$K_{11} = -K_x L = -K_y L, \tag{10}$$

the equations of motion in the translational direction can be written in the form

$$M\ddot{x} + C_{11}\dot{x} + C_{12}\dot{\phi}_y + K_{11}x + K_{12}\phi_y = u_x + d_x \tag{11}$$

and

$$M\ddot{y} + C_{11}\dot{y} - C_{12}\dot{\phi}_x + K_{11}y - K_{12}\phi_x = u_y + d_y. \tag{12}$$

To derive the equations of motion in the tilting direction, the model in Figure 2-9 is considered. The symbols K_{ry} and C_{ry} denote rotational stiffness and rotational damping, respectively, about the y-axis. The translational springs/dampers in the y-axis and the rotational springs/dampers about the x-axis are not shown in the figure.

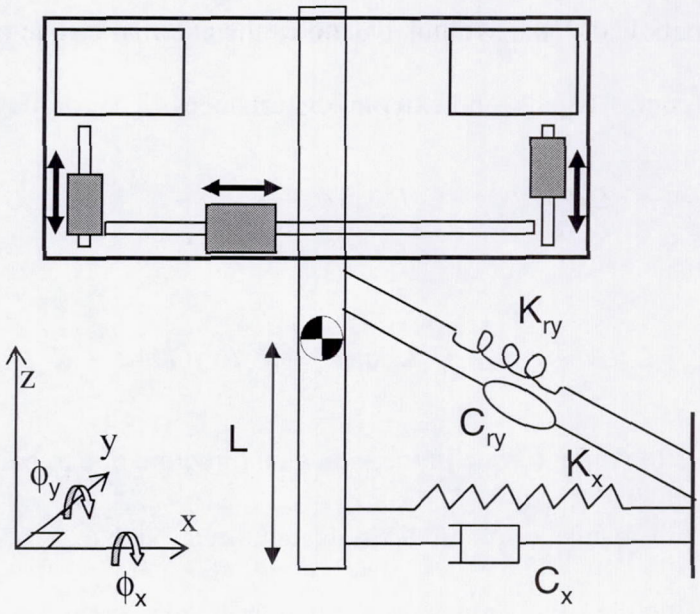

Figure 2-9. Model for Derivation of Equations of Motion in Tilting Direction

With the small angle approximation, the equations of motion in the tilting direction can be written in the form [19]

$$\begin{pmatrix} I_d\ddot{\phi}_x + I_z\omega\dot{\phi}_y \\ I_d\ddot{\phi}_y - I_z\omega\dot{\phi}_x \end{pmatrix} = T \ , \qquad (13)$$

where ω is the spin rate of the rotor, I_d is the transverse moment of inertia of the rotor, I_z is the polar moment of inertia of the rotor, and T is the external torque applied to the rotor.

Specifically, the symbol T denotes the external torque on the rotor due to springs, dampers, control inputs, and external disturbances. The torque can be written as

$$T_{\phi x} = -C_y L\dot{y} - C_{rx}\dot{\phi}_x - C_y L^2 \sin\dot{\phi}_x - K_y Ly - K_{rx}\phi_x - K_y L^2 \sin\phi_x + u_{\phi x} + d_{\phi x} \quad (14)$$

and

$$T_{\phi y} = C_x L\dot{x} - C_{ry}\dot{\phi}_y - C_x L^2 \sin\dot{\phi}_y + K_x Lx - K_{ry}\phi_x - K_x L^2 \sin\phi_y + u_{\phi y} + d_{\phi y}, \quad (15)$$

where u_ϕ is the input torque in the indicated direction due to balancer mass position and d_ϕ is the disturbance torque in the indicated direction due to rodent position.

Using the small angle approximation the torque can be written as

$$T_{\phi x} = -C_y L\dot{y} - C_{rx}\dot{\phi}_x - C_y L^2\dot{\phi}_x - K_y Ly - K_{rx}\phi_x - K_y L^2\phi_x + u_{\phi x} + d_{\phi x} \quad (16)$$

and

$$T_{\phi y} = C_x L\dot{x} - C_{ry}\dot{\phi}_y - C_x L^2\dot{\phi}_y + K_x Lx - K_{ry}\phi_x - K_x L^2\phi_y + u_{\phi y} + d_{\phi y}. \quad (17)$$

Make the substitutions

$$C_{22} = C_{rx} + C_y L^2 = C_{ry} + C_x L^2, \quad (18)$$

$$K_{22} = K_{rx} + K_y L^2 = K_{ry} + K_x L^2, \quad (19)$$

$$C_{12} = -C_x L = -C_y L, \quad (20)$$

and

$$K_{12} = -K_x L = -K_y L. \quad (21)$$

Then, the equations of motion in the tilting direction can be written in the form

$$I_d\ddot{\phi}_x - C_{12}\dot{y} + C_{22}\dot{\phi}_x + \omega I_z\dot{\phi}_y - K_{12}y + K_{22}\phi_x = u_{\phi x} + d_{\phi x} \qquad (22)$$

and

$$I_d\ddot{\phi}_y + C_{12}\dot{x} + C_{22}\dot{\phi}_y - \omega I_z\dot{\phi}_x + K_{12}x + K_{22}\phi_y = u_{\phi y} + d_{\phi y}. \qquad (23)$$

Now, the full equations of motion can be written

$$M\ddot{x} + C_{11}\dot{x} + C_{12}\dot{\phi}_y + K_{11}x + K_{12}\phi_y = u_x + d_x, \qquad (24)$$

$$M\ddot{y} + C_{11}\dot{y} - C_{12}\dot{\phi}_x + K_{11}y - K_{12}\phi_x = u_y + d_y, \qquad (25)$$

$$I_d\ddot{\phi}_x - C_{12}\dot{y} + C_{22}\dot{\phi}_x + \omega I_z\dot{\phi}_y - K_{12}y + K_{22}\phi_x = u_{\phi x} + d_{\phi x}, \qquad (26)$$

and

$$I_d\ddot{\phi}_y + C_{12}\dot{x} + C_{22}\dot{\phi}_y - \omega I_z\dot{\phi}_x + K_{12}x + K_{22}\phi_y = u_{\phi y} + d_{\phi y}. \qquad (27)$$

The equations of motion in the rotating coordinate frame (see Figure 2-6) can be derived from the equations of motion in the fixed frame given in Equations (24), (25), (26), and (27). The importance of deriving the equations of motion in the rotating coordinate frame is emphasized in Section 2.2.

Begin with the equations of motion in the fixed frame (Equations (24), (25), (26), and (27)) and apply the coordinate transformations

$$\begin{bmatrix} x \\ y \end{bmatrix} = R\begin{bmatrix} \zeta \\ \eta \end{bmatrix} \qquad (28)$$

and

$$\begin{bmatrix} \phi_x \\ \phi_y \end{bmatrix} = R\begin{bmatrix} \phi_\zeta \\ \phi_\eta \end{bmatrix}, \qquad (29)$$

where

$$R = \begin{bmatrix} \cos(\omega t) & -\sin(\omega t) \\ \sin(\omega t) & \cos(\omega t) \end{bmatrix}. \tag{30}$$

Also, introduce $\bar{R}$ in the transformations

$$\begin{bmatrix} y \\ -x \end{bmatrix} = \bar{R} \begin{bmatrix} \zeta \\ \eta \end{bmatrix} \tag{31}$$

and

$$\begin{bmatrix} \phi_y \\ -\phi_x \end{bmatrix} = \bar{R} \begin{bmatrix} \phi_\zeta \\ \phi_\eta \end{bmatrix}, \tag{32}$$

where

$$\bar{R} = R\bar{I} = \begin{bmatrix} \sin(\omega t) & \cos(\omega t) \\ -\cos(\omega t) & \sin(\omega t) \end{bmatrix} \tag{33}$$

and

$$\bar{I} = \begin{bmatrix} 0 & 1 \\ -1 & 0 \end{bmatrix}. \tag{34}$$

Differentiation in time of Equation (28) and Equation (29) yields

$$\begin{bmatrix} \dot{x} \\ \dot{y} \end{bmatrix} = \dot{R} \begin{bmatrix} \zeta \\ \eta \end{bmatrix} + R \begin{bmatrix} \dot{\zeta} \\ \dot{\eta} \end{bmatrix} \tag{35}$$

and

$$\begin{bmatrix} \dot{\phi}_x \\ \dot{\phi}_y \end{bmatrix} = \dot{R} \begin{bmatrix} \phi_\zeta \\ \phi_\eta \end{bmatrix} + R \begin{bmatrix} \dot{\phi}_\zeta \\ \dot{\phi}_\eta \end{bmatrix}. \tag{36}$$

Differentiation in time of Equation (35) and Equation (36) yields

$$\begin{bmatrix} \ddot{x} \\ \ddot{y} \end{bmatrix} = \ddot{R}\begin{bmatrix} \zeta \\ \eta \end{bmatrix} + 2\dot{R}\begin{bmatrix} \dot{\zeta} \\ \dot{\eta} \end{bmatrix} + R\begin{bmatrix} \ddot{\zeta} \\ \ddot{\eta} \end{bmatrix} \tag{37}$$

and

$$\begin{bmatrix} \ddot{\phi}_x \\ \ddot{\phi}_y \end{bmatrix} = \ddot{R}\begin{bmatrix} \phi_\zeta \\ \phi_\eta \end{bmatrix} + 2\dot{R}\begin{bmatrix} \dot{\phi}_\zeta \\ \dot{\phi}_\eta \end{bmatrix} + R\begin{bmatrix} \ddot{\phi}_\zeta \\ \ddot{\phi}_\eta \end{bmatrix}. \tag{38}$$

Differentiation in time of R from Equation (30) yields

$$\dot{R} = \begin{bmatrix} -\omega\sin(\omega t) & -\omega\cos(\omega t) \\ \omega\cos(\omega t) & -\omega\sin(\omega t) \end{bmatrix} = -\omega R\bar{I}\,. \tag{39}$$

Differentiating in time of Equation (39) yields

$$\ddot{R} = \begin{bmatrix} -\omega^2\cos(\omega t) & \omega^2\sin(\omega t) \\ -\omega^2\sin(\omega t) & -\omega^2\cos(\omega t) \end{bmatrix} = -\omega^2 R. \tag{40}$$

Also, $\bar{\dot{R}}$ is defined in the same manner as $\bar{R}$ where

$$\bar{\dot{R}} = \dot{R}\bar{I} = -(\omega R\bar{I})\bar{I} = \omega R = \begin{bmatrix} \omega\cos(\omega t) & -\omega\sin(\omega t) \\ \omega\sin(\omega t) & \omega\cos(\omega t) \end{bmatrix}. \tag{41}$$

Then, Equations (24)–(27) can be recast in the form

$$M\left(R\begin{bmatrix}\ddot{\zeta}\\ \ddot{\eta}\end{bmatrix}+2\dot{R}\begin{bmatrix}\dot{\zeta}\\ \dot{\eta}\end{bmatrix}+\ddot{R}\begin{bmatrix}\zeta\\ \eta\end{bmatrix}\right)+C_{11}\left(R\begin{bmatrix}\dot{\zeta}\\ \dot{\eta}\end{bmatrix}+\ddot{R}\begin{bmatrix}\zeta\\ \eta\end{bmatrix}\right)+C_{12}\left(\overline{R}\begin{bmatrix}\dot{\phi}_\zeta\\ \dot{\phi}_\eta\end{bmatrix}+\dot{\overline{R}}\begin{bmatrix}\phi_\zeta\\ \phi_\eta\end{bmatrix}\right)$$
$$+K_{11}R\begin{bmatrix}\zeta\\ \eta\end{bmatrix}+K_{12}\overline{R}\begin{bmatrix}\phi_\zeta\\ \phi_\eta\end{bmatrix}=R\begin{bmatrix}u_\zeta+d_\zeta\\ u_\eta+d_\eta\end{bmatrix} \qquad (42)$$

and

$$I_d\left(R\begin{bmatrix}\ddot{\phi}_\zeta\\ \ddot{\phi}_\eta\end{bmatrix}+2\dot{R}\begin{bmatrix}\dot{\phi}_\zeta\\ \dot{\phi}_\eta\end{bmatrix}+\ddot{R}\begin{bmatrix}\phi_\zeta\\ \phi_\eta\end{bmatrix}\right)+C_{12}\left(-\overline{R}\begin{bmatrix}\dot{\zeta}\\ \dot{\eta}\end{bmatrix}-\dot{\overline{R}}\begin{bmatrix}\zeta\\ \eta\end{bmatrix}\right)$$
$$+C_{22}\left(R\begin{bmatrix}\dot{\phi}_\zeta\\ \dot{\phi}_\eta\end{bmatrix}+\dot{R}\begin{bmatrix}\phi_\zeta\\ \phi_\eta\end{bmatrix}\right)+\omega I_z\left(\overline{R}\begin{bmatrix}\dot{\phi}_\zeta\\ \dot{\phi}_\eta\end{bmatrix}+\dot{\overline{R}}\begin{bmatrix}\phi_\zeta\\ \phi_\eta\end{bmatrix}\right)+K_{12}\left(-\overline{R}\begin{bmatrix}\zeta\\ \eta\end{bmatrix}\right) \qquad (43)$$
$$+K_{22}R\begin{bmatrix}\phi_\zeta\\ \phi_\eta\end{bmatrix}=R\begin{bmatrix}u_{\phi\zeta}+d_{\phi\zeta}\\ u_{\phi\eta}+d_{\phi\eta}\end{bmatrix}.$$

With a similarity transformation [20]

$$R^{-1}=\begin{bmatrix}\cos(\omega t) & \sin(\omega t)\\ -\sin(\omega t) & \cos(\omega t)\end{bmatrix} \qquad (44)$$

and the identities

$$R^{-1}R=\begin{bmatrix}1 & 0\\ 0 & 1\end{bmatrix}, \qquad (45)$$

$$R^{-1}\dot{R}=R^{-1}\left(-\omega R\bar{I}\right)=-\omega R^{-1}R\bar{I}=-\omega\bar{I}=\begin{bmatrix}0 & -\omega\\ \omega & 0\end{bmatrix}, \qquad (46)$$

$$R^{-1}\ddot{R}=R^{-1}\left(-\omega^2R\right)=\omega^2R^{-1}R=\begin{bmatrix}-\omega^2 & 0\\ 0 & -\omega^2\end{bmatrix}, \qquad (47)$$

$$R^{-1}\overline{R}=R^{-1}R\bar{I}=\bar{I}=\begin{bmatrix}0 & 1\\ -1 & 0\end{bmatrix}, \qquad (48)$$

and

$$R^{-1}\dot{\overline{R}} = R^{-1}(\omega R) = \omega R^{-1}R = \begin{bmatrix} \omega & 0 \\ 0 & \omega \end{bmatrix}, \tag{49}$$

Equations (42) and (43) can be written in the form

$$\begin{aligned} &M\left(\begin{bmatrix} \ddot{\zeta} \\ \ddot{\eta} \end{bmatrix} + \begin{bmatrix} 0 & -2\omega \\ 2\omega & 0 \end{bmatrix}\begin{bmatrix} \dot{\zeta} \\ \dot{\eta} \end{bmatrix} + \begin{bmatrix} -\omega^2 & 0 \\ 0 & -\omega^2 \end{bmatrix}\begin{bmatrix} \zeta \\ \eta \end{bmatrix}\right) + C_{11}\left(\begin{bmatrix} \dot{\zeta} \\ \dot{\eta} \end{bmatrix} + \begin{bmatrix} 0 & -\omega \\ \omega & 0 \end{bmatrix}\begin{bmatrix} \zeta \\ \eta \end{bmatrix}\right) \\ &+ C_{12}\left(\begin{bmatrix} 0 & 1 \\ -1 & 0 \end{bmatrix}\begin{bmatrix} \dot{\phi}_\zeta \\ \dot{\phi}_\eta \end{bmatrix} + \begin{bmatrix} \omega & 0 \\ 0 & \omega \end{bmatrix}\begin{bmatrix} \phi_\zeta \\ \phi_\eta \end{bmatrix}\right) + K_{11}\begin{bmatrix} \zeta \\ \eta \end{bmatrix} + K_{12}\begin{bmatrix} 0 & 1 \\ -1 & 0 \end{bmatrix}\begin{bmatrix} \phi_\zeta \\ \phi_\eta \end{bmatrix} = \begin{bmatrix} u_\zeta + d_\zeta \\ u_\eta + d_\eta \end{bmatrix} \end{aligned} \tag{50}$$

and

$$\begin{aligned} &I_d\left(\begin{bmatrix} \ddot{\phi}_\zeta \\ \ddot{\phi}_\eta \end{bmatrix} + \begin{bmatrix} 0 & -2\omega \\ 2\omega & 0 \end{bmatrix}\begin{bmatrix} \dot{\phi}_\zeta \\ \dot{\phi}_\eta \end{bmatrix} + \begin{bmatrix} -\omega^2 & 0 \\ 0 & -\omega^2 \end{bmatrix}\begin{bmatrix} \phi_\zeta \\ \phi_\eta \end{bmatrix}\right) \\ &+ C_{12}\left(\begin{bmatrix} 0 & -1 \\ 1 & 0 \end{bmatrix}\begin{bmatrix} \dot{\zeta} \\ \dot{\eta} \end{bmatrix} + \begin{bmatrix} -\omega & 0 \\ 0 & -\omega \end{bmatrix}\begin{bmatrix} \zeta \\ \eta \end{bmatrix}\right) + C_{22}\left(\begin{bmatrix} \dot{\phi}_\zeta \\ \dot{\phi}_\eta \end{bmatrix} + \begin{bmatrix} 0 & -\omega \\ \omega & 0 \end{bmatrix}\begin{bmatrix} \phi_\zeta \\ \phi_\eta \end{bmatrix}\right) \\ &+ \omega I_z\left(\begin{bmatrix} 0 & 1 \\ -1 & 0 \end{bmatrix}\begin{bmatrix} \dot{\phi}_\zeta \\ \dot{\phi}_\eta \end{bmatrix} + \begin{bmatrix} \omega & 0 \\ 0 & \omega \end{bmatrix}\begin{bmatrix} \phi_\zeta \\ \phi_\eta \end{bmatrix}\right) + K_{12}\begin{bmatrix} 0 & -1 \\ 1 & 0 \end{bmatrix}\begin{bmatrix} \zeta \\ \eta \end{bmatrix} + K_{22}\begin{bmatrix} \phi_\zeta \\ \phi_\eta \end{bmatrix} = \begin{bmatrix} u_{\phi\zeta} + d_{\phi\zeta} \\ u_{\phi\eta} + d_{\phi\eta} \end{bmatrix}. \end{aligned} \tag{51}$$

Collecting terms, the final coupled equations in the rotating frame become

$$\begin{aligned} &M\begin{bmatrix} \ddot{\zeta} \\ \ddot{\eta} \end{bmatrix} + \begin{bmatrix} C_{11} & -2M\omega \\ 2M\omega & C_{11} \end{bmatrix}\begin{bmatrix} \dot{\zeta} \\ \dot{\eta} \end{bmatrix} + \begin{bmatrix} -M\omega^2 + K_{11} & -C_{11}\omega \\ C_{11}\omega & -M\omega^2 + K_{11} \end{bmatrix}\begin{bmatrix} \zeta \\ \eta \end{bmatrix} \\ &+ \begin{bmatrix} 0 & C_{12} \\ -C_{12} & 0 \end{bmatrix}\begin{bmatrix} \dot{\phi}_\zeta \\ \dot{\phi}_\eta \end{bmatrix} + \begin{bmatrix} C_{12}\omega & K_{12} \\ -K_{12} & C_{12}\omega \end{bmatrix}\begin{bmatrix} \phi_\zeta \\ \phi_\eta \end{bmatrix} = \begin{bmatrix} u_\zeta + d_\zeta \\ u_\eta + d_\eta \end{bmatrix} \end{aligned} \tag{52}$$

and

$$
\begin{aligned}
&I_d\begin{bmatrix}\ddot{\phi}_\zeta\\ \ddot{\phi}_\eta\end{bmatrix}+\begin{bmatrix}C_{22} & -2I_d\omega+\omega I_z\\ 2I_d\omega-\omega I_z & C_{22}\end{bmatrix}\begin{bmatrix}\dot{\phi}_\zeta\\ \dot{\phi}_\eta\end{bmatrix}\\
&+\begin{bmatrix}\omega^2(I_z-I_d)+K_{22} & -C_{22}\omega\\ C_{22}\omega & \omega^2(I_z-I_d)+K_{22}\end{bmatrix}\begin{bmatrix}\phi_\zeta\\ \phi_\eta\end{bmatrix}\\
&+\begin{bmatrix}0 & -C_{12}\\ C_{12} & 0\end{bmatrix}\begin{bmatrix}\dot{\zeta}\\ \dot{\eta}\end{bmatrix}+\begin{bmatrix}-C_{12}\omega & -K_{12}\\ K_{12} & -C_{12}\omega\end{bmatrix}\begin{bmatrix}\zeta\\ \eta\end{bmatrix}=\begin{bmatrix}u_{\phi\zeta}+d_{\phi\zeta}\\ u_{\phi\eta}+d_{\phi\eta}\end{bmatrix}.
\end{aligned}
\tag{53}
$$

If the coupling terms are neglected, the equations become

$$
M\begin{bmatrix}\ddot{\zeta}\\ \ddot{\eta}\end{bmatrix}+\begin{bmatrix}C_{11} & -2M\omega\\ 2M\omega & C_{11}\end{bmatrix}\begin{bmatrix}\dot{\zeta}\\ \dot{\eta}\end{bmatrix}+\begin{bmatrix}-M\omega^2+K_{11} & -C_{11}\omega\\ C_{11}\omega & -M\omega^2+K_{11}\end{bmatrix}\begin{bmatrix}\zeta\\ \eta\end{bmatrix}=\begin{bmatrix}u_\zeta+d_\zeta\\ u_\eta+d_\eta\end{bmatrix} \tag{54}
$$

and

$$
\begin{aligned}
&I_d\begin{bmatrix}\ddot{\phi}_\zeta\\ \ddot{\phi}_\eta\end{bmatrix}+\begin{bmatrix}C_{22} & -2I_d\omega+\omega I_z\\ 2I_d\omega-\omega I_z & C_{22}\end{bmatrix}\begin{bmatrix}\dot{\phi}_\zeta\\ \dot{\phi}_\eta\end{bmatrix}\\
&+\begin{bmatrix}\omega^2(I_z-I_d)+K_{22} & -C_{22}\omega\\ C_{22}\omega & \omega^2(I_z-I_d)+K_{22}\end{bmatrix}\begin{bmatrix}\phi_\zeta\\ \phi_\eta\end{bmatrix}=\begin{bmatrix}u_{\phi\zeta}+d_{\phi\zeta}\\ u_{\phi\eta}+d_{\phi\eta}\end{bmatrix},
\end{aligned}
\tag{55}
$$

where ζ and η represent translation of the rotor in the rotating coordinate frame, ϕ_ζ and ϕ_η represent tilt of the rotor in the rotating coordinate frame, u is the input force/torque due to balancer mass positions (ζ_{b1},η_{b2},ξ_{b3},ξ_{b4}), and d is the disturbance force/torque due to rodent position.

Note that the dynamic behavior depends on the spin rate of the rotor, ω. Since ω can vary in time, the equations of motion represent a linear time-varying system. This requires that any ABC must stabilize the system for the range $0 < \omega < \omega_{max}$.

It can be verified that the system with uncoupled dynamics (Equations (54) and (55)) closely approximates the system with coupled dynamics (Equations (52) and (53)) by comparing the frequency response of each system. A comparison of the frequency response of each system in one of the translational directions (ζ) and one of the tilting directions (ϕ_ζ) is presented in Figure 2-10 and Figure 2-11.

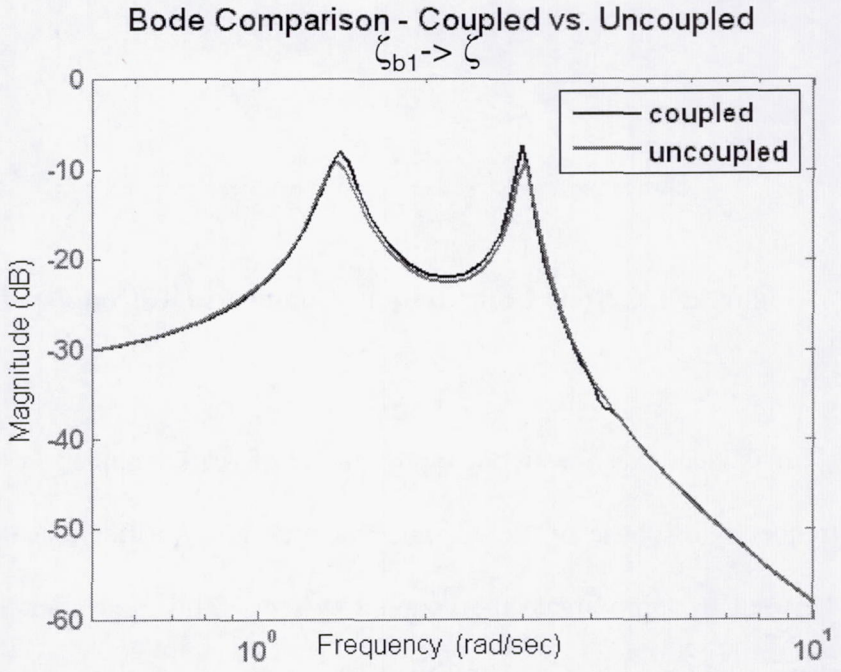

Figure 2-10. Bode Comparison - Coupled vs. Uncoupled Translational Direction

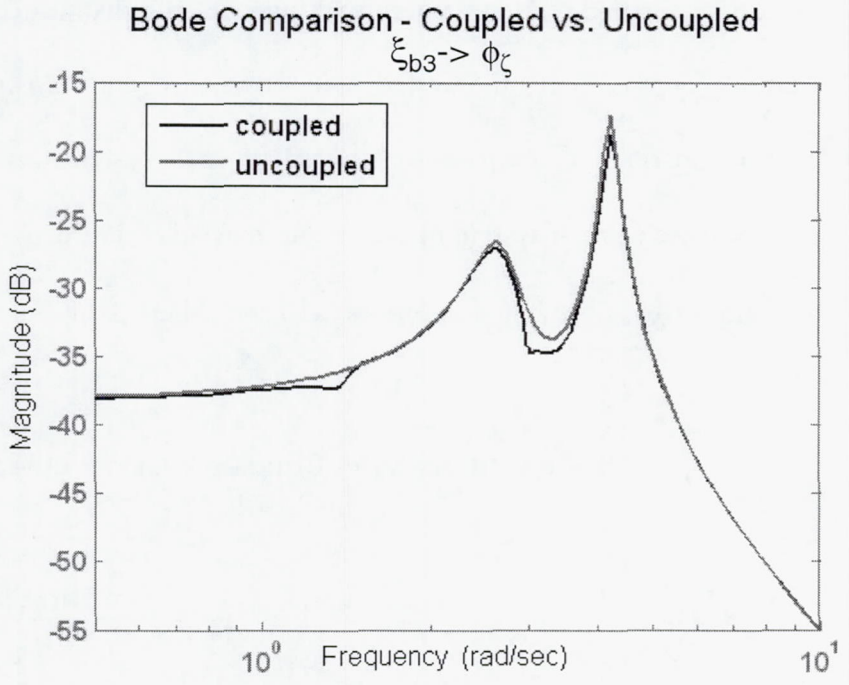

Figure 2-11. Bode Comparison - Coupled vs. Uncoupled Tilt Direction

It is clear that the frequency response of the uncoupled system closely matches the frequency response of the coupled system. This verifies that the uncoupled system can be used to approximate the coupled system. This approximation is utilized in the controller design presented in Chapter 4.

2.2 Auto Balancing Controller

As previously mentioned, the objective of the ABC system is to limit the translation of the rotor due to imbalances imposed by the position of the rodents within the habitats. This includes limiting both the peak translation of the rotor and the steady-state translation of the rotor due to a fixed imbalance. Additionally, the control system should be robust to uncertainty in the rotor spin rate, ω, over the range $0 < \omega < \omega_{max}$, and be robust to other forms of uncertainty in the plant. Finally, the controller should avoid

commanding the balancer masses to change position quickly, causing saturation in the balancer mass speed. By avoiding actuator saturation, the linearity of the control system is preserved.

Based on the rotor displacement, the ABC commands the position of the balancer masses in order to cancel a rodent imbalance and limit the translation of the rotor. A simplified block diagram of the linear system is shown in Figure 2-12.

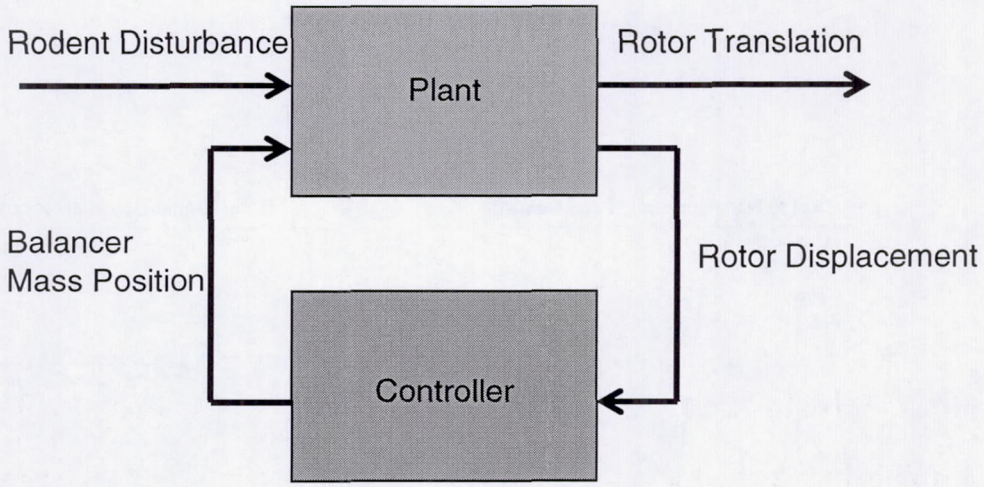

Figure 2-12. Control System Block Diagram

As discussed in Section 2.1, the ABC system operates in the rotational coordinate system. Since the absolute displacement is estimated in the fixed coordinate system [17], a coordinate transformation as shown in Equation (2) is required convert the sensor displacement to the rotating coordinate frame before it is used by the ABC. For the design of the ABC system, the plant dynamics can be formulated in the rotating coordinate frame yielding Equation (52) and Equation (53). While the ABC can be designed using the dynamics in the rotating coordinate frame, the implementation of the

controller is performed on the fixed frame dynamic model with the coordinate transformation.

It is necessary to design the controller using the rotating coordinate frame to effectively cancel imbalances and limit the steady-state translation of the rotor. To illustrate this, it is necessary to see a plot of the rotor translation in each coordinate frame. Plots of the rotor translation in each coordinate system are shown in Figure 2-13 for a stationary rodent imbalance (as described in Figure 2-14) in the open-loop (uncontrolled) system. The rotor is rotating at a constant spin rate.

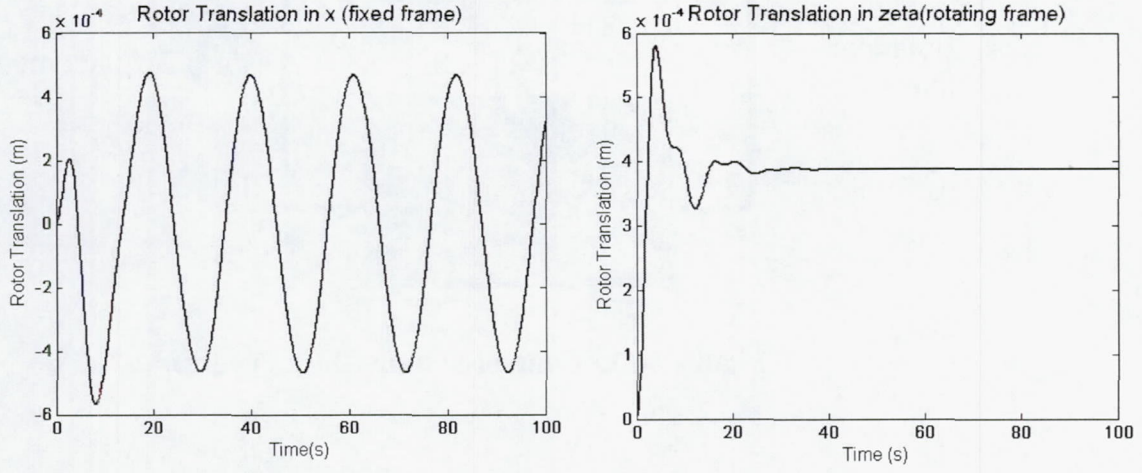

Figure 2-13. Comparison of Rotor Translation in Fixed and Rotating Coordinate Frames

It is worth noting that in the fixed frame coordinate system (x-direction), the response is oscillatory, while in the rotating frame coordinate system (ζ-direction) the response is nearly constant after the transient effects subside. This is a result of the fact that the rotating coordinate system is rotating with the rotor imbalance. The rotor translates in the direction of the imbalance which remains the same in the rotating frame,

but changes in the fixed frame. This effect is illustrated in Figure 2-14 where the imbalance is initially (at time = t1) in both the x-direction and the ζ-direction, but as the rotor rotates through angle ω(t2-t1) the imbalance is no longer in the x-direction but it remains in the ζ-direction.

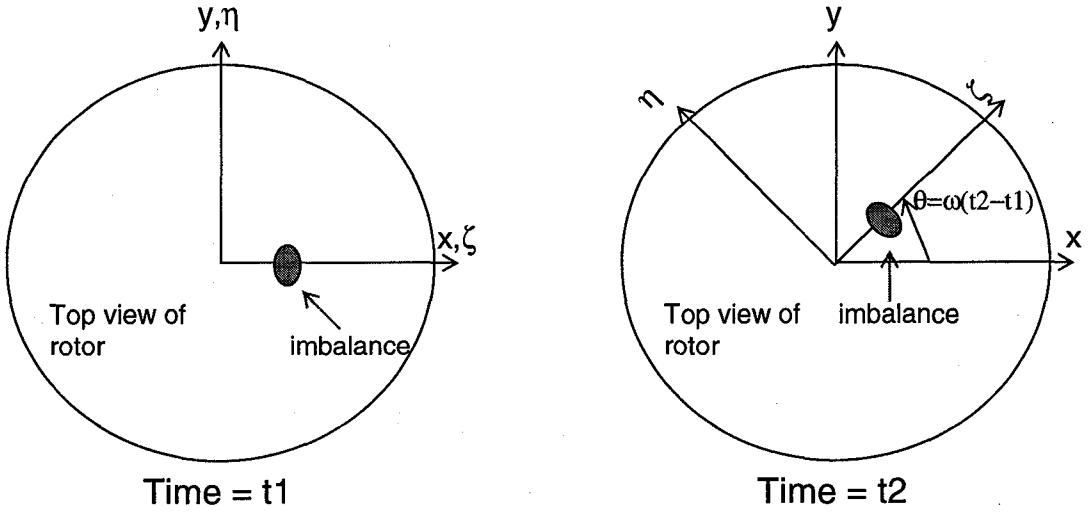

Figure 2-14. Comparison of Imbalance in Fixed and Rotating Coordinate Frames

The importance of this result is that for steady-state error to be limited by the control system, the integral of the rotor displacement must increase as long as the error remains present. Since the response in the fixed frame coordinate system oscillates about 0, the integral is not increasing and the steady-state error cannot be eliminated. The integral of each signal is shown in Figure 2-15. Clearly, the rotating coordinate system must be used to limit steady-state error since the integral of the displacement is not increasing in the fixed frame coordinate system.

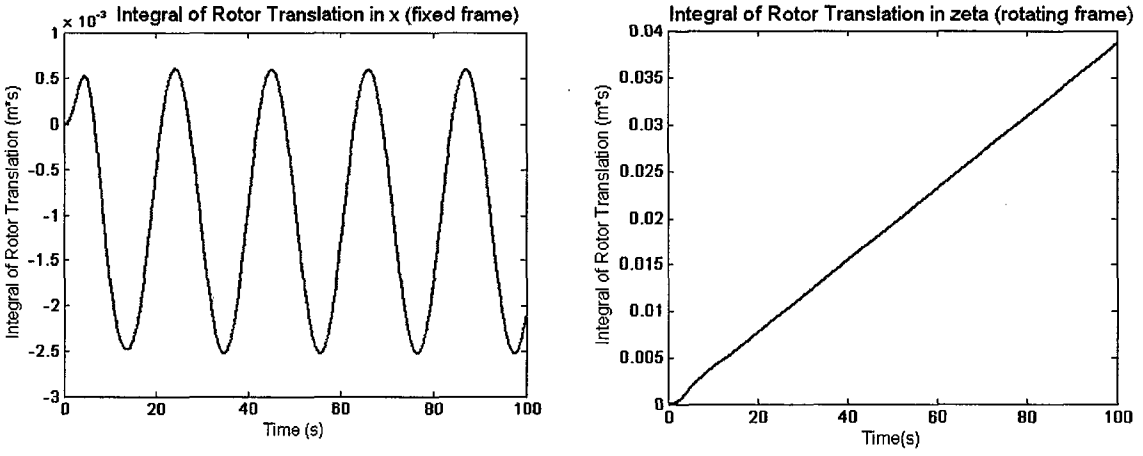

Figure 2-15. Comparison of the Integral of Rotor Translation in Fixed and Rotating Coordinate Frames

Figure 2-16 is a block diagram of the controller. The symbols Kp, Kd, and Ki represent constant gain matrices of size 4x4.

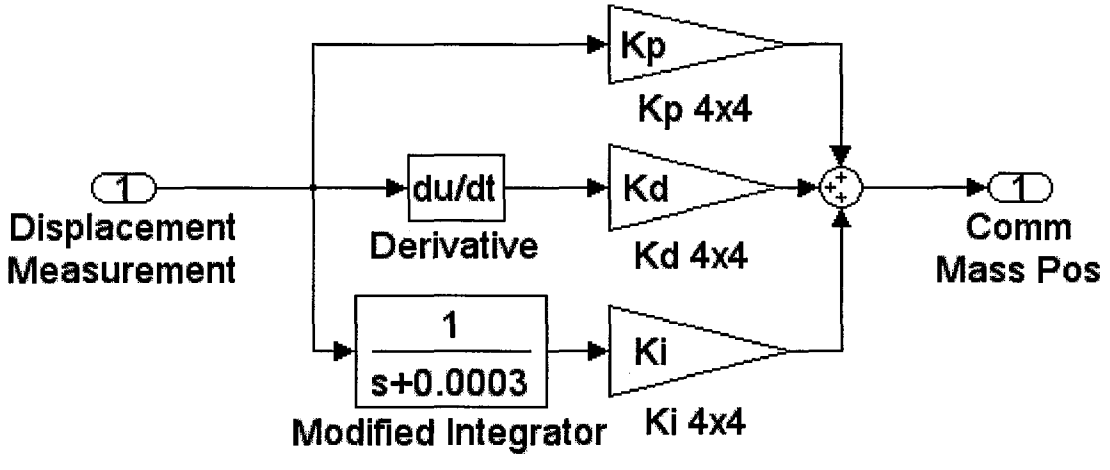

Figure 2-16. Block Diagram of Controller

A modified integrator is used, as opposed to a true integrator (1/s), in order to avoid adding poles on the jω-axis of the complex plane. By adding the poles slightly in

the left-half-plane, the robust stability of the control system is improved. An example of this improvement is presented below.

To illustrate the improvement in robust stability, a single-input, single-output (SISO) system is considered with pure integral control (K/s) and modified integral control (K/(s+p)). Block diagrams of the system in each configuration are shown in Figure 2-17 and Figure 2-18.

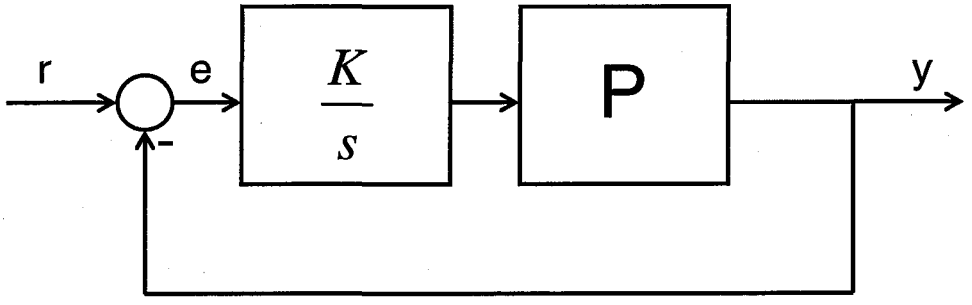

Figure 2-17. System with Pure Integral Control

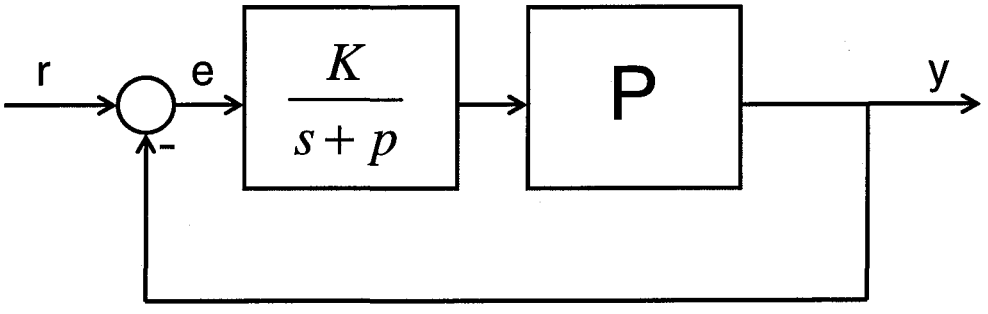

Figure 2-18. System with Modified Integral Control

The symbol P denotes the plant and is specified by the equation

$$P = \frac{1}{s^2 + \frac{c}{m}s + \frac{k}{m}} \tag{56}$$

The system parameters are assumed to be K=1, p=1, m=1, c=2, and k=1. A plot of the poles of the transfer function from r to y for each system is given in Figure 2-19.

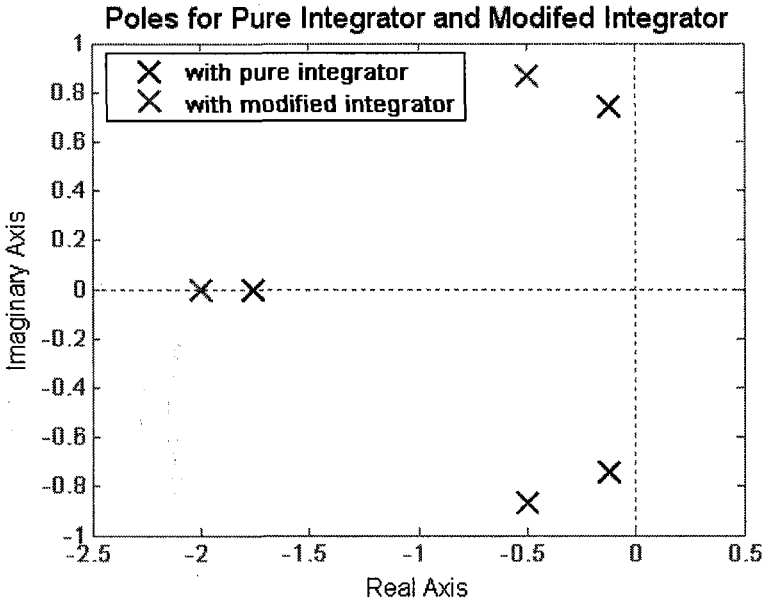

Figure 2-19. Poles for Systems with a Pure Integrator and a Modified Integrator

It is observed from Figure 2-19 that the system with the modified integrator has closed-loop poles farther from the jω-axis than the system with the pure integrator. In general, this corresponds to a system with better robust stability since it will take a larger perturbation for the closed-loop poles to move to the unstable region on the right side of the jω-axis. This is demonstrated by allowing the damping coefficient to decrease until instability is reached. For the system with the pure integrator the pole plot of the closed-

loop system is presented in Figure 2-20. The plot shows the poles for decreasing values of the damping coefficient, c.

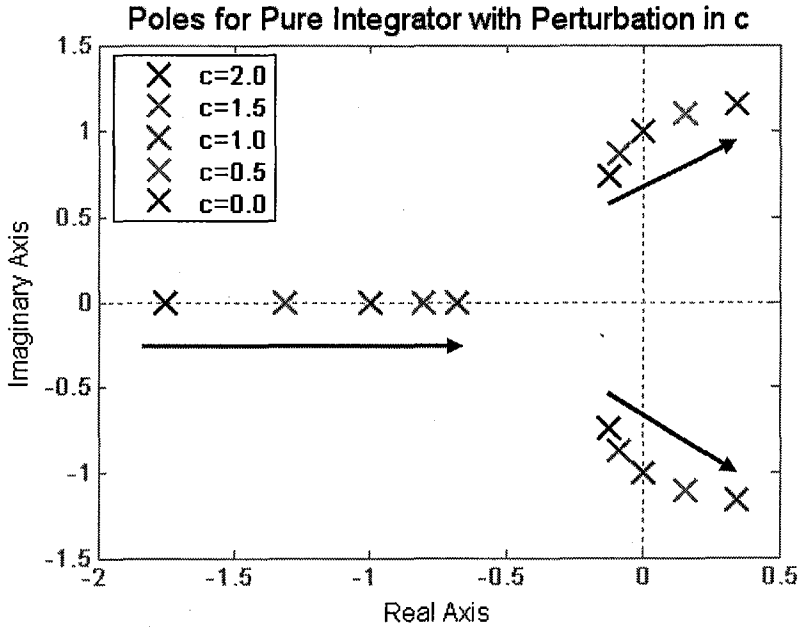

Figure 2-20. Poles for Pure Integrator with Perturbation in c

From Figure 2-20 it is seen that the system poles cross into the unstable region for c = 1.0. Therefore, the pure integral control is able to tolerate a 50% variation in the damping coefficient.

For the system with the modified integrator the pole plot is presented in Figure 2-21 for decreasing values of the damping coefficient, c.

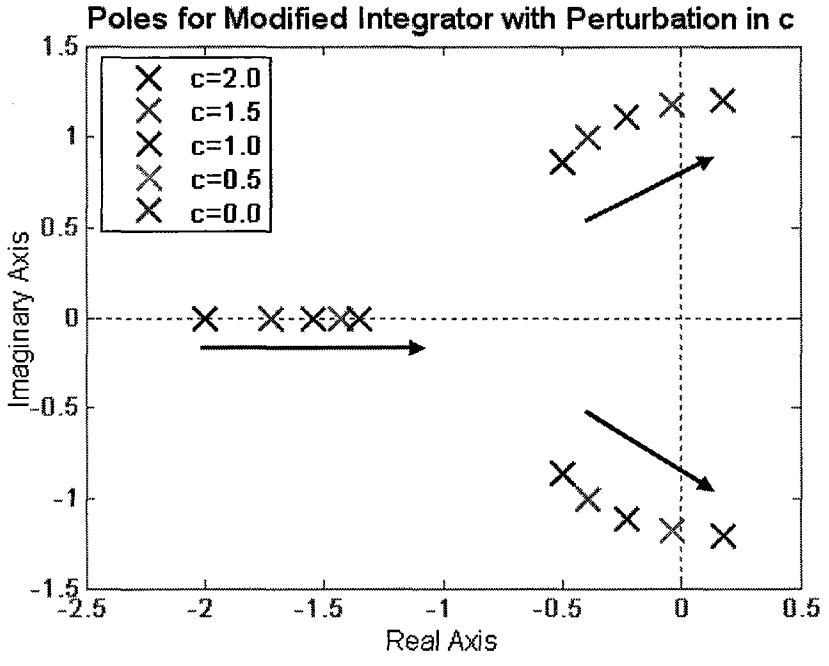

Figure 2-21. Poles for Modified Integrator with Perturbation in c

From Figure 2-21 it is observed that the system poles cross into the unstable region for c = 0.4. Therefore, the modified integral control is able to tolerate an 80% variation in the damping coefficient. This is significantly larger than the system with pure integral control, indicating that the system with modified integral control is more robust to variations in the damping coefficient (as well as other plant parameters). This increase in robust stability comes at the cost of increased steady-state error as discussed in Section 3.5.

Block diagrams of the centrifuge rotor control system are shown in Figure 2-22 and Figure 2-23. Figure 2-22 is the system used to design the controller. The dynamic equations of motion are in the rotating coordinate frame and time delays are neglected.

Since the time delays are small, they are neglected in the linear stability analysis, but they are accounted for in the time domain simulation portion of the design in Chapter 4.

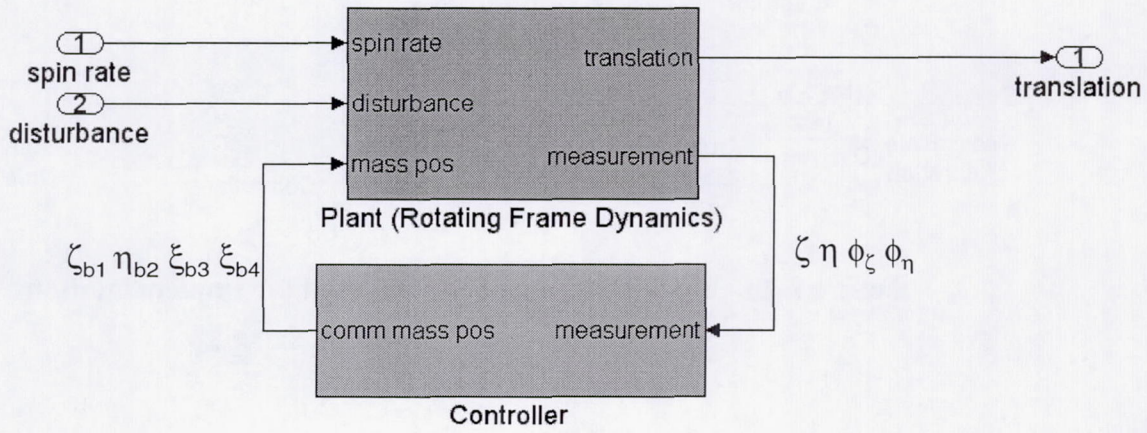

Figure 2-22. Block Diagram of System used for Design

Figure 2-23 shows the system used to implement and test the controller. The system is simulated using a solver based on the Runge-Kutta (4,5) numerical integration scheme [21]. The dynamic equations of motion are in the fixed coordinate frame and time delays are present. A coordinate transform is used to transit from the fixed coordinate frame to the rotating coordinate frame. The symbols (ζ_{b1},η_{b2},ξ_{b3},ξ_{b4}) denote the commanded positions of the balancer masses.

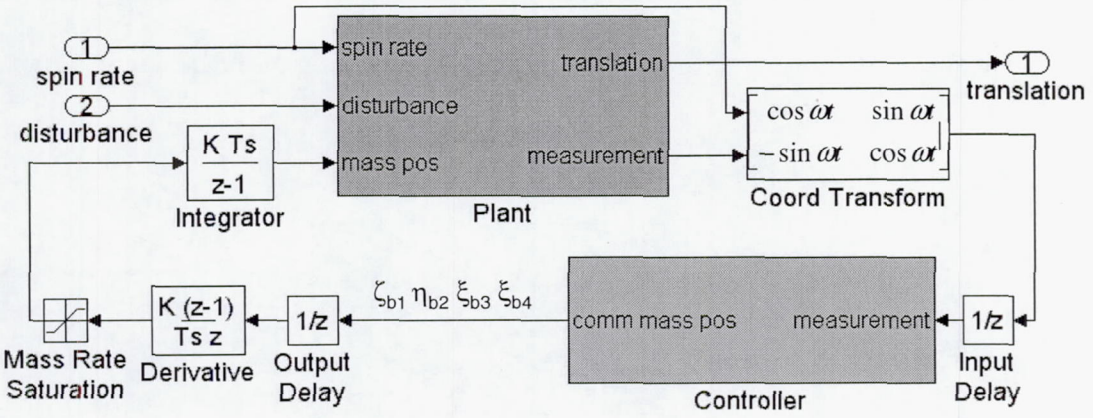

Figure 2-23. Block Diagram of System used for Implementation

2.3 General Problem Statement

It is assumed that the following constraints apply to the ABC:

I. limit the peak translation ($\sqrt{\zeta^2 + \eta^2}$) of the rotor < γ_1 for all rodent disturbances,

II. ensure stability over the range $0 < \omega < \omega_{max}$,

III. be robust in the presence of spin rate(ω), rotor mass (M), and rotor inertia(I_d,I_z) uncertainty,

IV. limit commanded balancer mass speed < γ_2, and

V. limit steady-state rotor translation < γ_3 for a fixed disturbance (rodents are stationary),

where the symbols γ_1,γ_2, and γ_3 represent specific problem constraints to be defined in Section 4.1. Note that the tilt of the rotor is not directly constrained since it contributes to the translation of the rotor (which is constrained).

3 Technical Background

Before introducing the design process of Chapter 4, some background in the technical tools used to analyze the control system is necessary. In this section, background in robust control for multi-input, multi-output (MIMO) systems is presented. Also, steady-state error in control systems is examined. Finally, a robust constrained optimization approach to control design is presented.

3.1 Multi-Input, Multi-Output (MIMO) Control

It is well known from classical control, single-input, single-output (SISO) systems, that the gain of a system can be defined in terms of the frequency response or Bode plot [22]. Defining the gain of a system for the MIMO case is less clear since a Bode plot only represents the frequency response from a single input to a single output.

To describe system gain for the MIMO case, singular values are introduced [23]. Consider the transfer function matrix G with m inputs and n outputs. If G is evaluated at a fixed frequency, ω, $G(j\omega)$ is a constant n x m complex matrix. Any matrix G can be decomposed into its singular value decomposition (SVD) [23]

$$G = U\Sigma V^{H}, \qquad (57)$$

where the symbol Σ is an n x m matrix with non-negative singular values, σ_i, in descending order along the main diagonal, U is an n x n unitary matrix of output singular vectors, and V is an m x m unitary matrix of input singular vectors.

The column vectors of U, u_i, represent the output directions of the plant, while the column vectors of V, v_i, represent the input directions of the plant. That is, if an input in

the direction of v_i is considered, the output will be in the direction u_i and the signals are related by the corresponding singular value. Specifically,

$$Gv_i = \sigma_i u_i \,. \tag{58}$$

It can be shown that the largest gain in any input direction is equal to the largest singular value [24]. The largest singular value of a matrix is denoted by the symbol

$$\overline{\sigma}(G) = \sigma_1(G) \,. \tag{59}$$

To obtain the MIMO frequency response for G(s), G is evaluated at s=jω for the interval ω for which the frequency response is desired. The maximum singular values are then plotted as functions of ω to provide the maximum system gain at any frequency, ω. The peak of this frequency response plot is known as the H-infinity norm of the system[24], defined by the equation

$$\left\| G(s) \right\|_\infty = \max_\omega \overline{\sigma}(G(j\omega)) \,. \tag{60}$$

To illustrate, the system [25] in Figure 3-1 is examined.

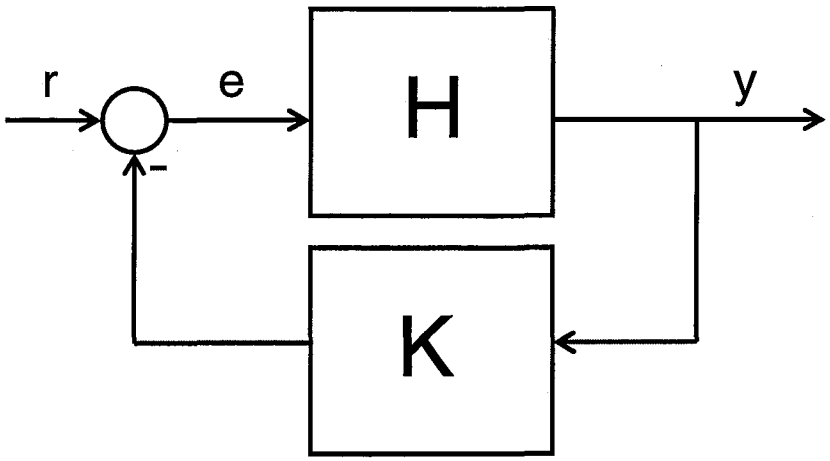

Figure 3-1. Control System Example

In this example, H and K are specified by the equations

$$H(s)=\begin{bmatrix} \dfrac{9}{s+1} & \dfrac{-10}{s+1} \\ \dfrac{-8}{s+2} & \dfrac{9}{s+2} \end{bmatrix} \tag{61}$$

and

$$K=\begin{bmatrix} 2 & 1 \\ 1 & 2 \end{bmatrix}. \tag{62}$$

The transfer function from r to y can be written in the form

$$y=Tr, \tag{63}$$

where

$$T=(I+HK)^{-1}H. \tag{64}$$

This matrix is evaluated at s=jω=0 to find the singular values of the system at ω=0 rad/sec. This yields

$$T(j\omega=0)=\begin{bmatrix} 0.6452 & -0.6774 \\ -0.2903 & 0.3548 \end{bmatrix}. \qquad (65)$$

Using SVD, this matrix can be written in the form

$$\begin{bmatrix} 0.6452 & -0.6774 \\ -0.2903 & 0.3548 \end{bmatrix}=\begin{bmatrix} -0.8983 & 0.4395 \\ 0.4395 & 0.8983 \end{bmatrix}\begin{bmatrix} 1.0413 & \\ & 0.0310 \end{bmatrix}\begin{bmatrix} -0.6790 & 0.7341 \\ 0.7341 & 0.6790 \end{bmatrix}. \qquad (66)$$

It is seen that the singular values at ω=0 are σ_1=1.0413 and σ_2=0.0310. Using SVD for each frequency in a set of desired frequencies and plotting the maximum singular value produces the frequency response plot in Figure 3-2.

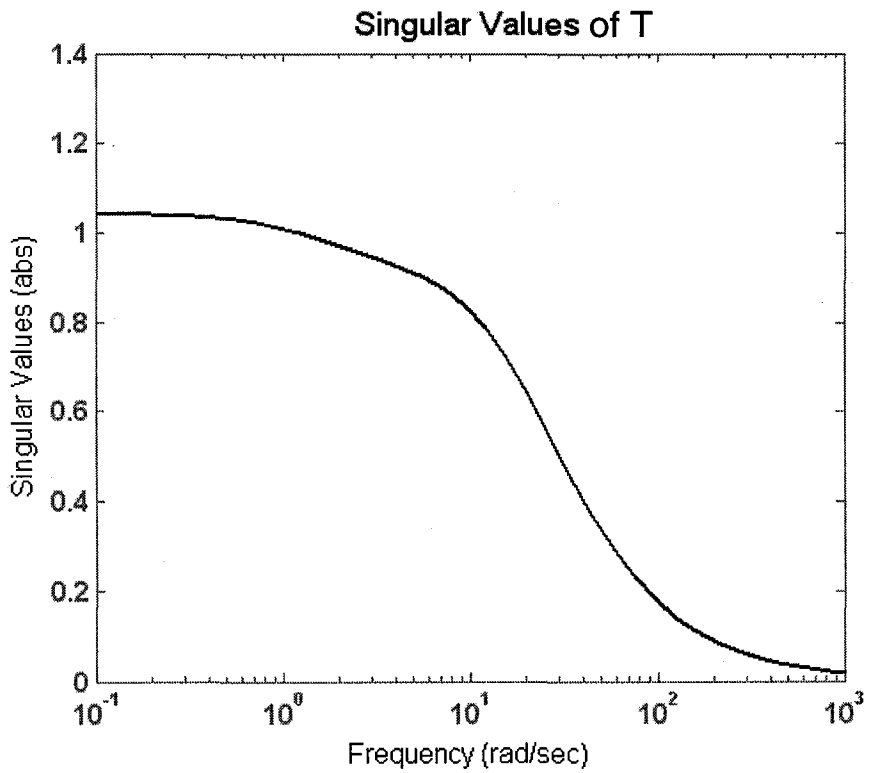

Figure 3-2. Maximum Singular Values

It is verified that the maximum singular value at $\omega=0$ is $\sigma_1=1.0413$. Singular values have two distinct advantages over eigenvalues for MIMO systems; they provide information about the gains of the plant and they can be obtained for non-square plants.

3.2 Uncertain Systems

One of the problem constraints presented in Section 2.3 was that the system with the ABC must be robust to uncertainty in plant parameters. Uncertainty in a control system is the discrepancy between the actual system and the model of the system. Uncertainty can arise from many sources. Some sources of uncertainty are [25]:

I. approximate or erroneously valued parameters in the plant,

II. ignored complexities (nonlinearities, time delays, etc.),

III. imperfections in sensors/actuators,

IV. unmodeled dynamics, and

V. model order reduction of the plant.

In general, uncertainty appears in two basic forms: parametric uncertainty and unmodeled dynamics [28]. Parametric uncertainty will be the form of uncertainty primarily examined in the design process for this thesis.

Uncertainty can be easily modeled in a feedback manner known as a linear fractional transformation (LFT) [24][28][29]. Using LFTs it is possible to separate what is known (model of the system (M)) from what is unknown (the bounded uncertainty (Δ)) in a feedback interconnection [28] as shown in Figure 3-3.

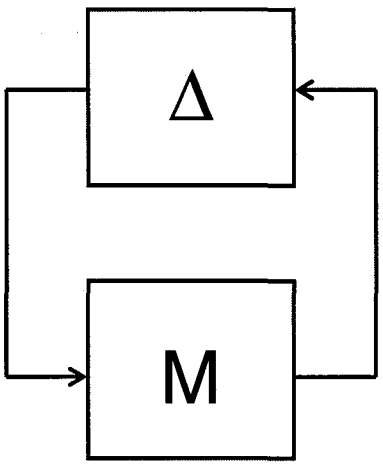

Figure 3-3. Linear Fractional Transformation

In the case of unmodeled dynamics, Δ is any fully populated transfer function matrix where

$$\|\Delta\|_\infty \leq 1. \tag{67}$$

This is known as unstructured uncertainty.

In the case of parametric uncertainty, Δ generally has a diagonal structure of the form

$$\Delta = \begin{bmatrix} \delta_1 & & & \\ & \delta_2 & & \\ & & \ddots & \\ & & & \delta_n \end{bmatrix}. \tag{68}$$

Equation (67) still applies to the case of parametric uncertainty, but the structure of the uncertainty is constrained to the form in Equation (68). This is known as structured uncertainty. Generally, weighting functions are added to the plant so that Equation (67) is satisfied.

To illustrate how system uncertainty can be formulated in an LFT framework, the system in Figure 3-4 is considered. This is the same system considered in Section 3.1 with an uncertainty added in the input to the plant (or the actuator signal).

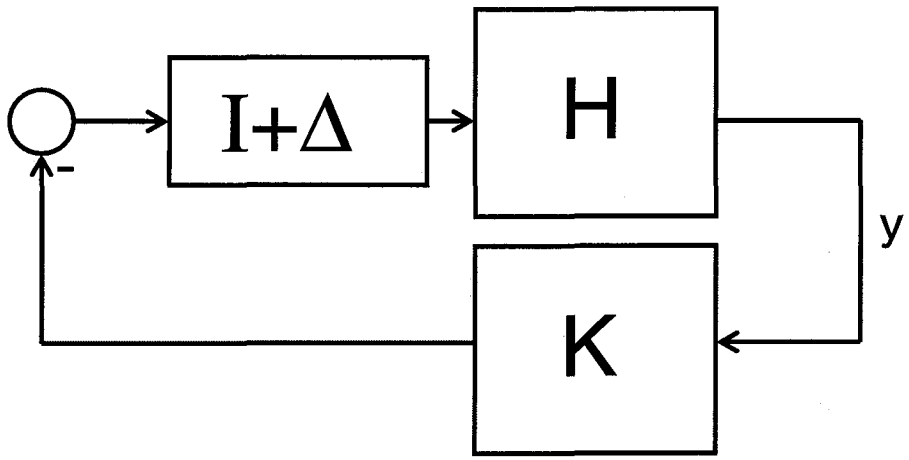

Figure 3-4. Uncertain System Example

The symbols H and K are as defined in Section 3.1 and Δ has a diagonal structure. Specifically,

$$\Delta = \begin{bmatrix} \delta_1 & \\ & \delta_2 \end{bmatrix}. \tag{69}$$

and δ_1 and δ_2 are allowed to vary on the interval [-0.8,0.8], allowing for 80% uncertainty in each actuator signal. The uncertainties can be "pulled out" and the system and can be re-arranged as in Figure 3-5.

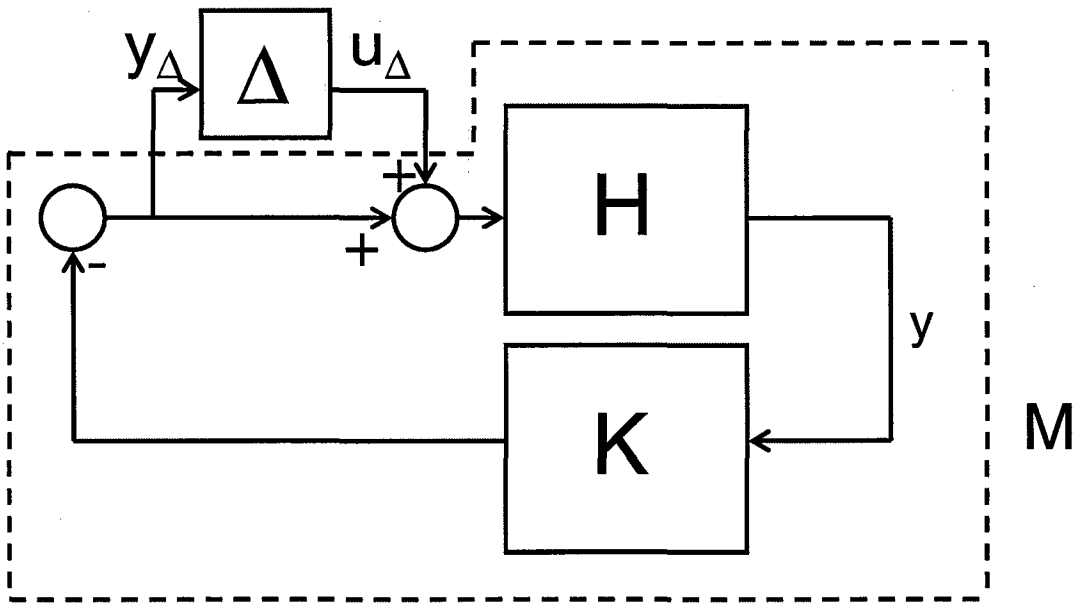

Figure 3-5. Pulling out the Uncertainty

The symbol M represents the transfer function from u_Δ to y_Δ. Using block diagram algebra, an expression for M is derived. Specifically,

$$y_\Delta = -Ky \ , \tag{70}$$

$$y_\Delta = -KH(u_\Delta + y_\Delta) \ , \tag{71}$$

$$y_\Delta = -KHu_\Delta - KHy_\Delta \ , \tag{72}$$

$$(I + KH)y_\Delta = -KHu_\Delta \ , \tag{73}$$

$$y_\Delta = -(I + KH)^{-1} KHu_\Delta \ , \tag{74}$$

and

$$M = -(I + KH)^{-1} KH \ . \tag{75}$$

Now, the system can be written as an LFT as in Figure 3-3. However, Δ must still be normalized so that the norm bound on Δ is 1. Weighting functions, W_1 and W_2, as shown in Figure 3-6, are used to accomplish this scaling.

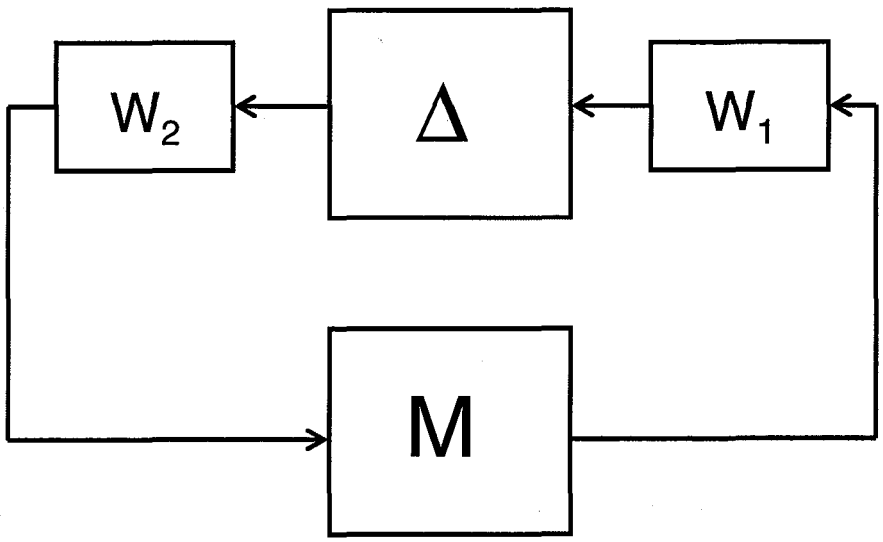

Figure 3-6. Normalizing the Uncertainty

In this case, the weighting functions

$$W_1 = \begin{bmatrix} 0.8 & 0 \\ 0 & 0.8 \end{bmatrix} \tag{76}$$

and

$$W_2 = \begin{bmatrix} 1 & 0 \\ 0 & 1 \end{bmatrix} \tag{77}$$

normalize the uncertainty while allowing the actuator gain 80% uncertainty. The weighting functions are appended to M to recast the system in the form of Figure 3-3 with Δ normalized to 1.

3.3 Small Gain Theorem

The small gain theorem ties together the concepts of singular values and system uncertainty to form the basis of the robust stability problem for MIMO systems. Robust stability is achieved when all plants in a given uncertainty set are stable for all possible perturbations [24]. Consider the system shown in Figure 3-7 where M(s) and Δ(s) are strictly stable transfer function matrices.

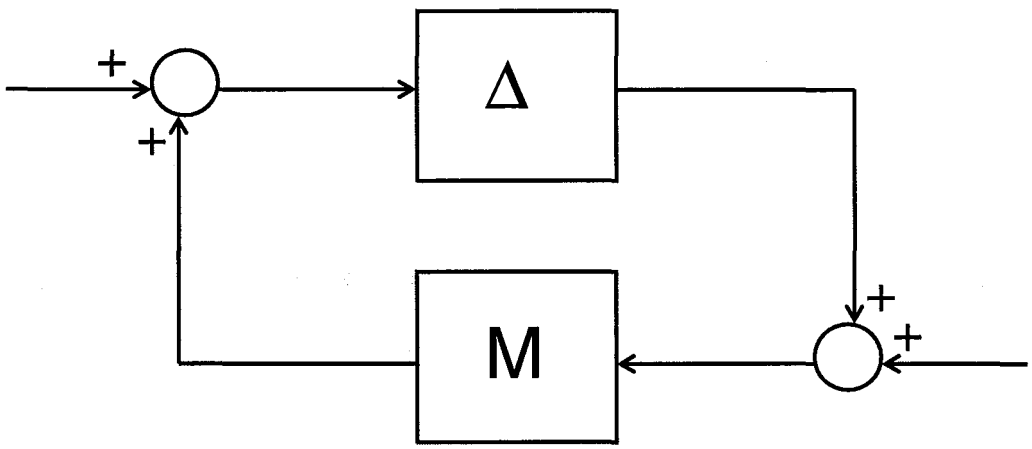

Figure 3-7. Small Gain Theorem

The small gain theorem [29] states that for $\gamma>0$ the interconnected system in Figure 3-7 is well-posed and internally stable for all Δ(s) with

$$\|\Delta\|_\infty \le 1/\gamma \text{ if and only if } \|M\|_\infty < \gamma. \quad (78)$$

This condition can be re-written as

$$\bar{\sigma}(M(j\omega))\bar{\sigma}(\Delta(j\omega)) < 1 \ \forall\omega. \quad (79)$$

Commonly, the problem is posed such that Δ is norm-bounded by 1. In this case, the robust stability (RS) condition based on the small gain theorem can be written as

$$\text{RS} \Leftrightarrow \bar{\sigma}(M(j\omega)) < 1 \; \forall \omega. \tag{80}$$

Alternatively, the condition can be written as

$$\text{RS} \Leftrightarrow \|M\|_{\infty} < 1. \tag{81}$$

3.4 The Structured Singular Value

The small gain theorem provides the foundation for answering the problem of robust stability. However, the small gain theorem is conservative for the case of structured uncertainty, or parametric uncertainty, since it assumes an unstructured perturbation. The structured singular value is an expansion of the small gain theorem used to provide a less conservative answer to the question of robust stability (or robust performance) subject to structured uncertainty. The structured singular value was first introduced by Doyle in 1982 [26][27].

3.4.1 Robust Stability with the Structured Singular Value

The small gain theorem gives a condition for robust stability in Equation (80). While this condition provides a method for evaluating robust stability, it is known to be conservative for the case of structured uncertainty [25]. The structured singular value (μ) is introduced to provide a less conservative answer for the case of structured uncertainty.

The structured singular value, μ, is defined as

$$\mu_{\Delta}(M) = \frac{1}{\min\{\bar{\sigma}(\Delta) \; s.t. \; \det(I - M\Delta) = 0\}} , \qquad (82)$$

where the denominator is the maximum singular value of the smallest Δ that is able to destabilize the system. While it is quite difficult to compute μ directly, advanced algorithms exist [28] to compute upper and lower bounds on μ. This thesis will be primarily concerned with the upper bound since it provides a slightly conservative answer, while the lower bound often provides an answer that is not conservative enough. From the small gain theorem, an initial upper bound on μ can be formulated. Specifically,

$$\mu_{\Delta}(M) \leq \bar{\sigma}(M(j\omega)) . \qquad (83)$$

As previously stated, the bound in Equation (83) is known to be conservative for the case of structured uncertainty. To reduce conservatism, scaling matrices, D and D^{-1}, are introduced as shown in Figure 3-8. Figure 3-7 is replaced with Figure 3-8 for evaluating robust stability with μ.

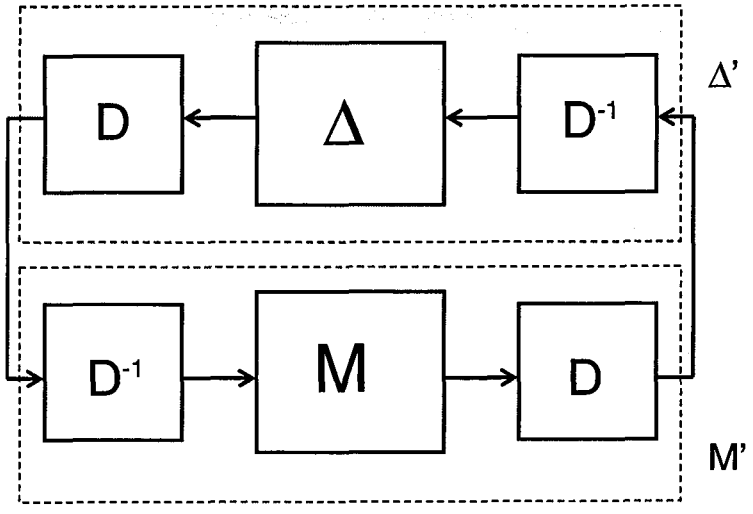

Figure 3-8. Robust Stability with Scaling Matrices

Since Δ has a diagonal structure for the case of structured uncertainty and D is a block diagonal scaling matrix,

$$D\Delta D^{-1} = \Delta \ . \tag{84}$$

The block diagram can now be drawn as in Figure 3-9.

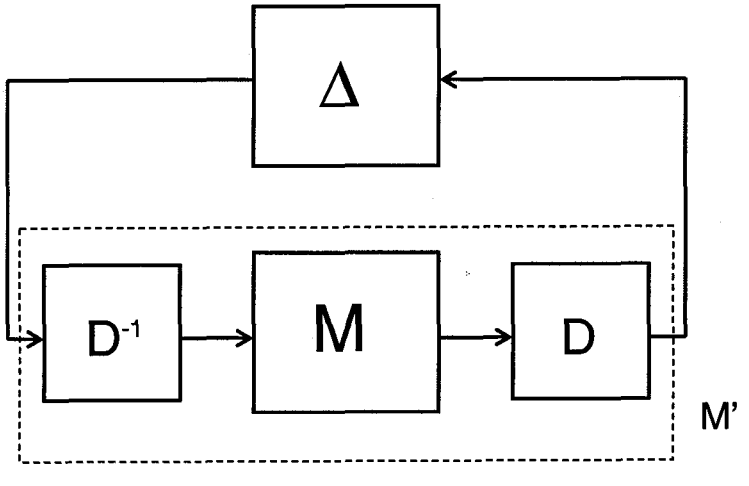

Figure 3-9. Simplified Robust Stability with Scaling

The small gain theorem now provides the upper bound on μ

$$\mu(M) \le \bar{\sigma}\left(DMD^{-1}\right), \tag{85}$$

where D is a free parameter that can be used to get a less conservative upper bound on μ. It follows that an optimal D can be found to find the least conservative upper bound on μ, which provides a new, less conservative condition for robust stability. That is,

$$RS \Leftrightarrow \min_{D} \left\| DMD^{-1} \right\|_{\infty} < 1. \tag{86}$$

To illustrate the advantage of using the structured singular value to determine robust stability, the example from Section 3.2 is again considered. The system with weighting functions as specified in Section 3.2 is presented in Figure 3-10. The system, M, is taken to be the closed-loop transfer function, T, as defined in Section 3.1.

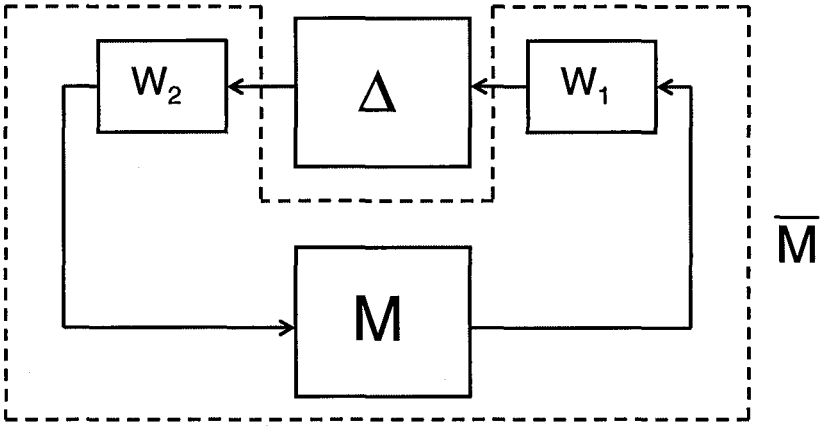

Figure 3-10. System with Weighting Functions

For evaluating robust stability, there are two conditions. Both provide an upper bound on μ. Specifically,

$$RS \Leftrightarrow \bar{\sigma}\left(\overline{M}(j\omega)\right) < 1 \quad \forall \omega \qquad \text{Small Gain Theorem} \tag{87}$$

and

$$RS \Leftrightarrow \min_{D} \left\| D\overline{M}D^{-1} \right\|_{\infty} < 1 \qquad \text{Structured Singular Value} \; . \tag{88}$$

The upper bounds on μ for each case are plotted in Figure 3-11. In this case the small gain theorem does not guarantee robust stability for the system since the peak value is greater than 1. However, the structured singular value does guarantee robust stability since the peak is below 1. Clearly, the small gain theorem is conservative in this case. The structured singular value allows for a less conservative answer to the question of robust stability through the use of the scaling matrices, D and D^{-1}.

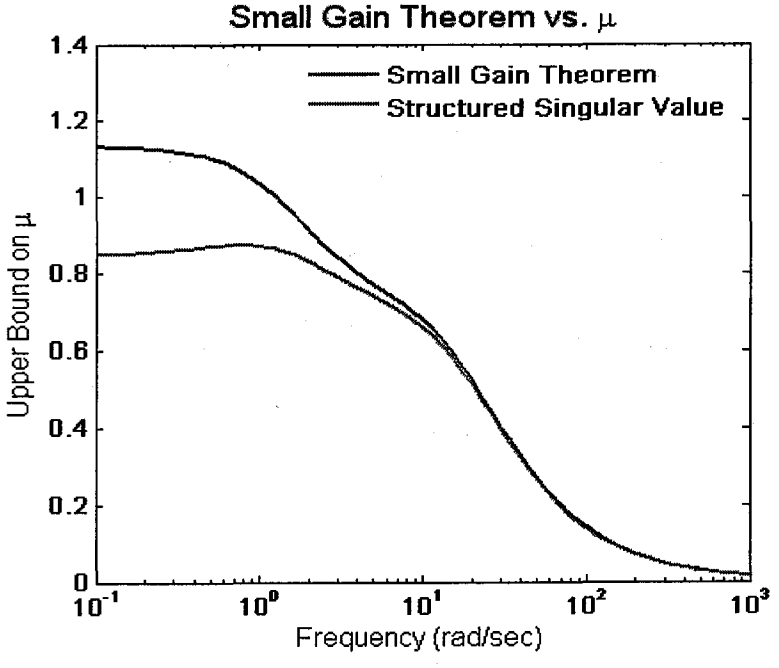

Figure 3-11. Small Gain Theorem vs. μ

3.4.2 Robust Performance with the Structured Singular Value

Robust performance is achieved when a given performance objective is achieved for all plants in a given uncertainty set. More specifically, for the system in Figure 3-12, robust performance is defined as

$$RP \Leftrightarrow \|F\|_{\infty} < \alpha \ . \qquad (89)$$

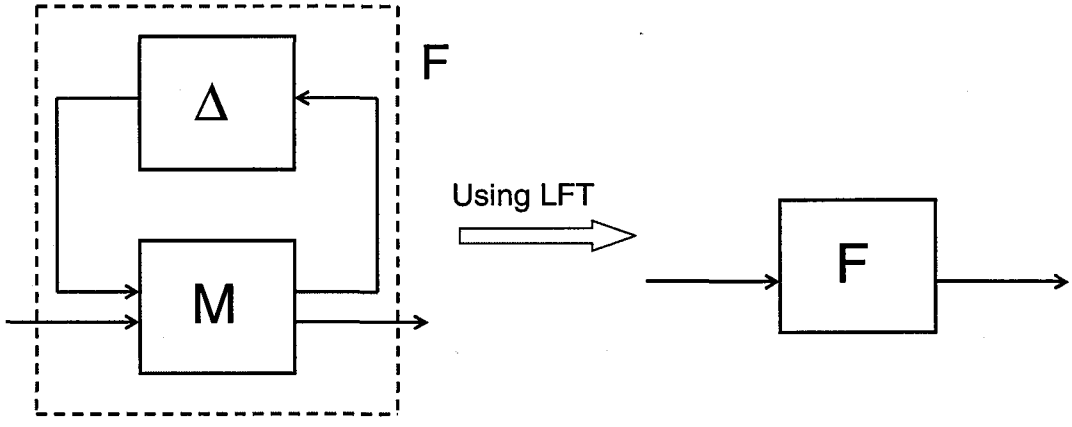

Figure 3-12. Definition of Robust Performance

Generally, weighting functions are added to F so that the problem can be written

$$RP \Leftrightarrow \|F\|_{\infty} < 1. \qquad (90)$$

The problem of robust performance can be treated in the framework of the structured singular value by using the small gain theorem to convert the problem to a robust stability problem. Since the requirement for robust performance in Equation (90) is the same as the small gain requirement for robust stability in Equation (81) where M is replaced by F, the robust performance problem can be posed as a robust stability

problem. Figure 3-13 is a pictorial representation of a robust performance problem being converted to a robust stability problem through the use of a fictitious uncertainty block Δ_P [24].

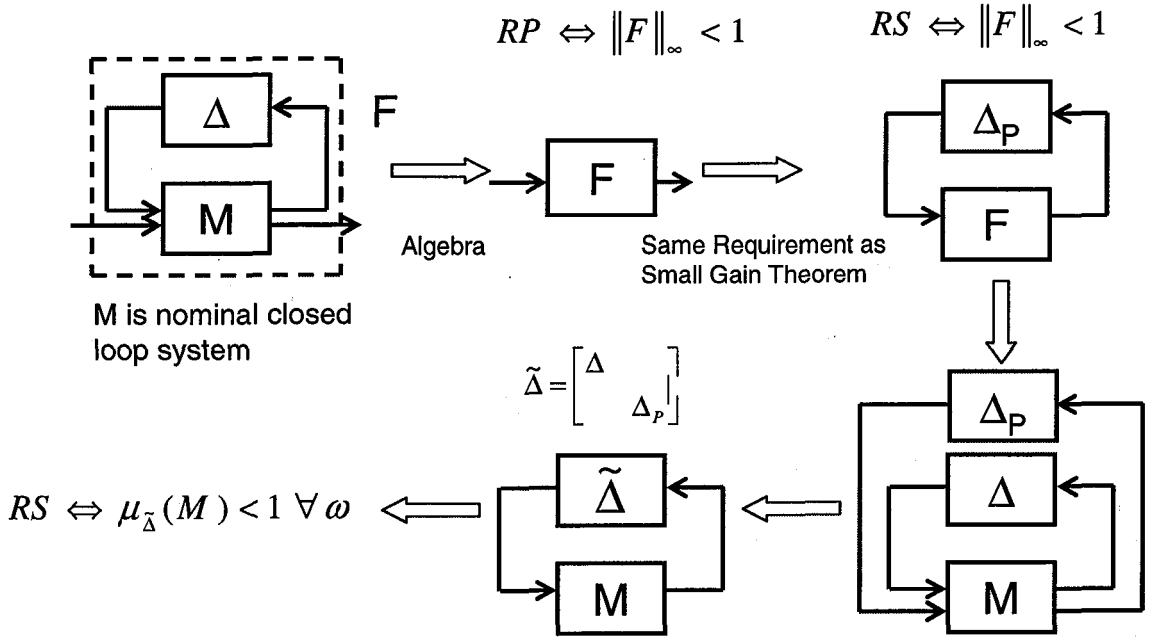

Figure 3-13. Converting a RP Problem to a RS Problem

Now, if the robust stability requirement

$$RS \Leftrightarrow \mu_{\tilde{\Delta}}(M) < 1 \ \forall \omega \qquad (91)$$

is satisfied, robust performance is guaranteed. To illustrate how robust performance is evaluated with the structured singular value, the example from Section 3.2 is again examined. The system in Figure 3-14 is considered.

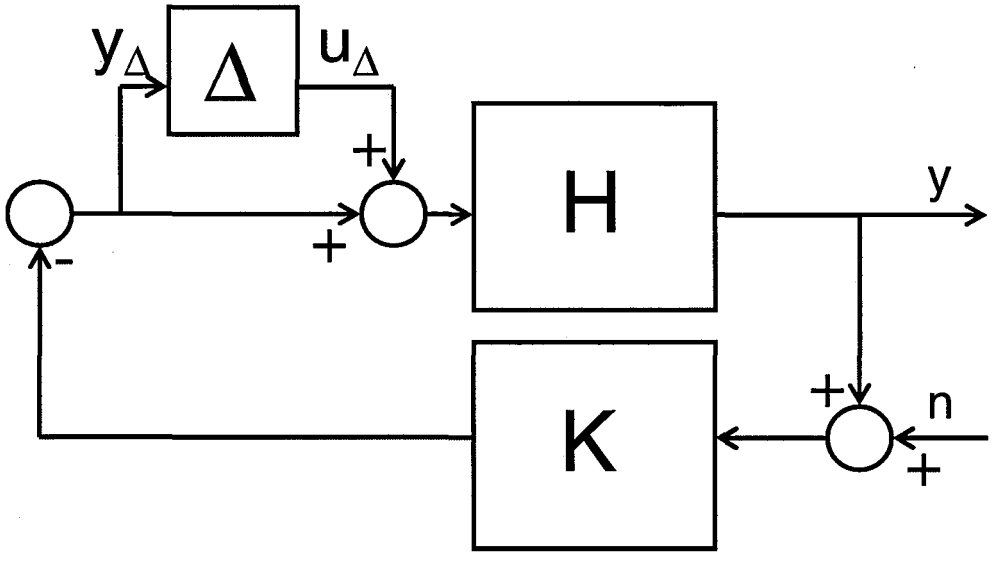

Figure 3-14. System for Robust Performance Problem

The symbol n represents the system input, sensor noise, and the symbol y represents the variable to be regulated. It is assumed that for the system with 80% actuator uncertainty, the performance objective is to limit the output, y, to 10% of the sensor noise, n, at high frequencies (where sensor noise is most likely). This performance objective requires that the system is robust to the sensor noise. To normalize the performance objective to 1, weighting functions are added to the system as shown in Figure 3-15.

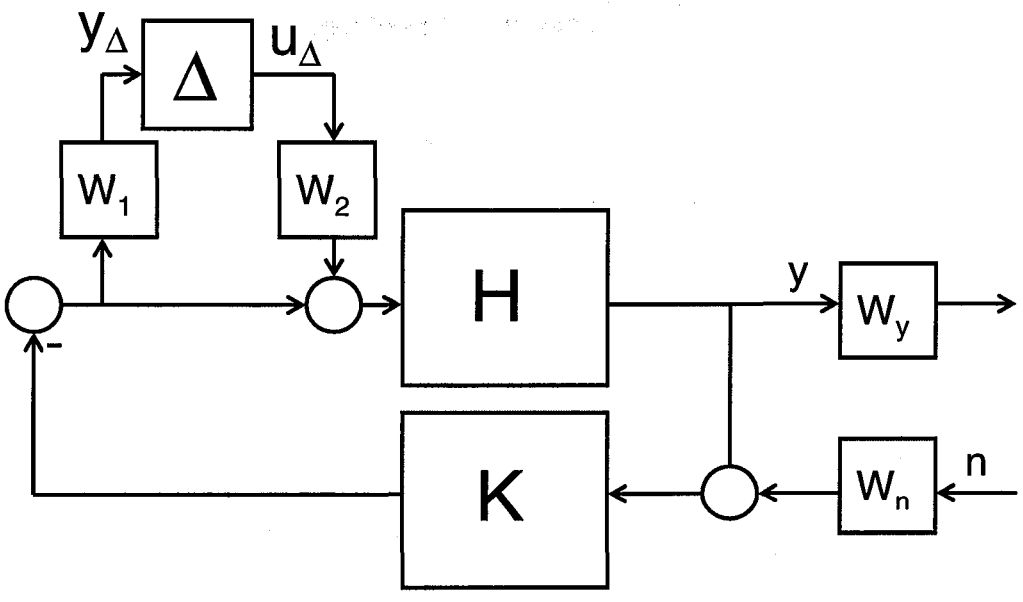

Figure 3-15. System with Weighting Functions

The symbols W_1 and W_2 are as described in Section 3.2. The matrix

$$W_y = \begin{bmatrix} 10 & \\ & 10 \end{bmatrix} \tag{92}$$

serves to impose the 10% limit on the output of the system. Further, W_n serves to impose the robust performance requirement at high frequencies only. In this case the output is required to be less than 10% of the sensor noise at frequencies above 100 rad/sec (roughly where the plot of W_n' (shown in Figure 3-16) nears 1). Specifically,

$$W_n = \begin{bmatrix} W_n' & \\ & W_n' \end{bmatrix} \tag{93}$$

and

$$W_n' = \frac{s+1.73}{s+173}. \tag{94}$$

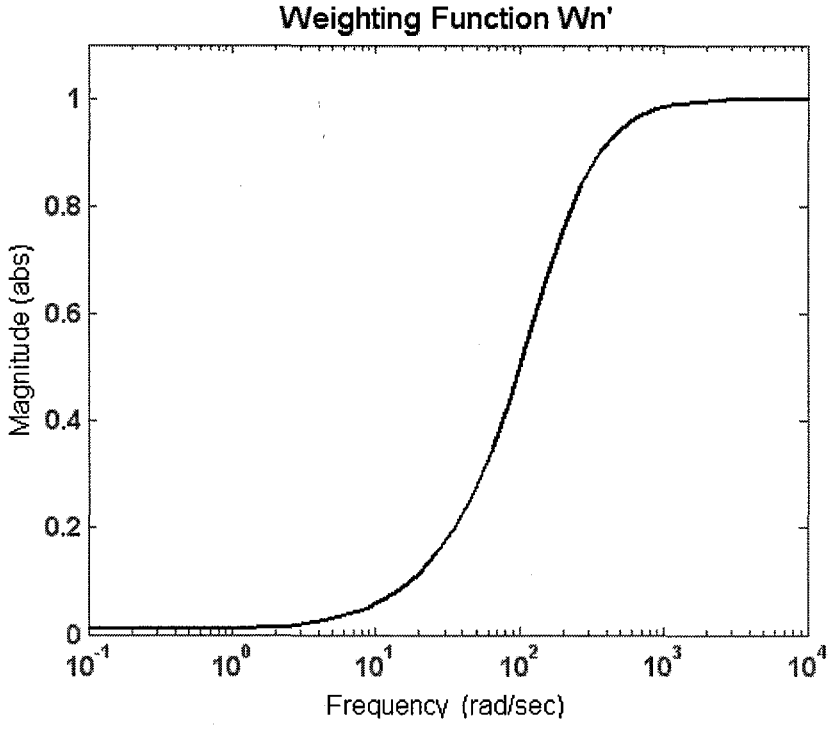

Figure 3-16. Weighting Function W_n'

This performance objective is evaluated using μ. The upper bound of μ is plotted for the 10% requirement in Figure 3-17.

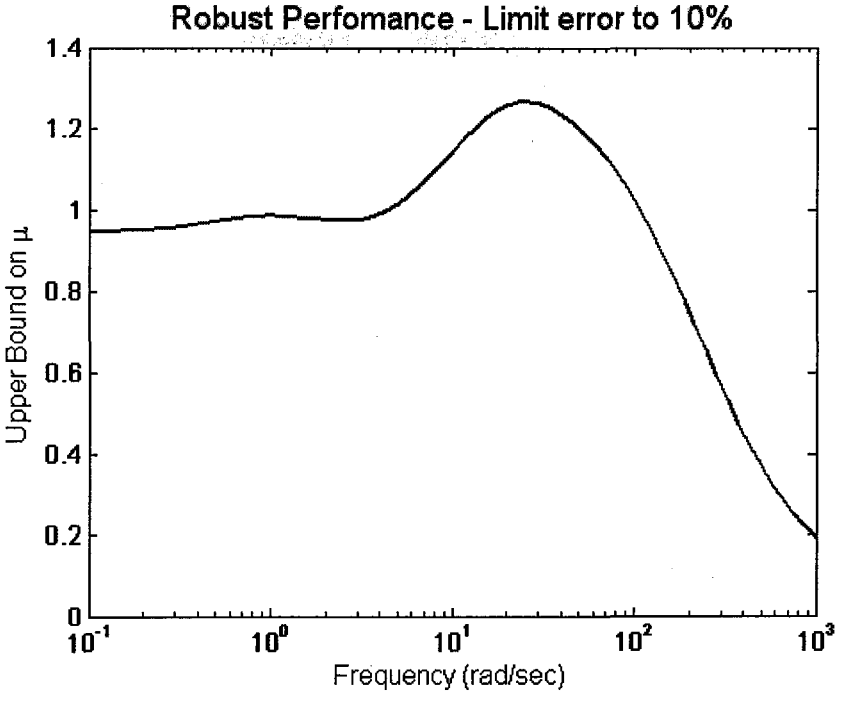

Figure 3-17. Robust Performance Plot for 10% Requirement

Since the peak of the robust performance plot is greater than 1, the conditions for robust performance are not satisfied. However, if the performance requirement is relaxed to limit the output to 20% of the input signal over the same frequency range, robust performance is achieved. The results are shown in Figure 3-18.

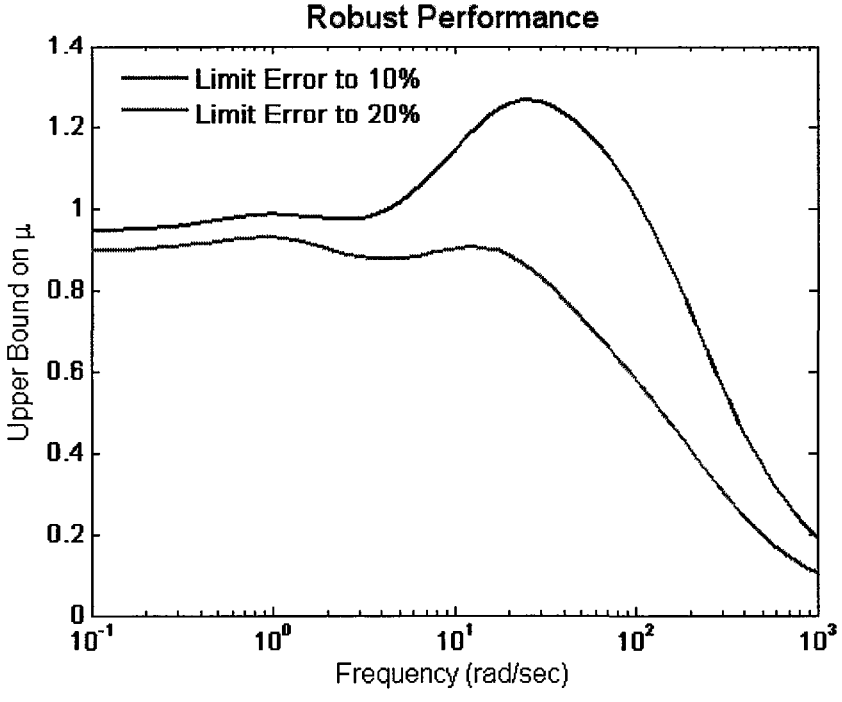

Figure 3-18. Comparison of 10% and 20% Requirements for Robust Performance

3.4.3 Real Parametric Uncertainty to Complex Uncertainty

For a complex uncertainty (unmodeled dynamics or complex parameter uncertainty) μ is a continuous function. However, μ is not necessarily a continuous function when all perturbation blocks are real, as is often the case for parametric uncertainty [30]. This discontinuity can cause problems in the convergence of the bounds on μ [28].

In fact, in order to derive a more reliable bound for the design of the ABC, the parametric uncertainty in the spin rate was treated as an uncertain complex parameter. The interval for spin rate was then divided into several smaller complex intervals and each interval was tested for robust stability and performance [31]. An illustration of how the uncertainty in the spin rate was treated is shown in Figure 3-19.

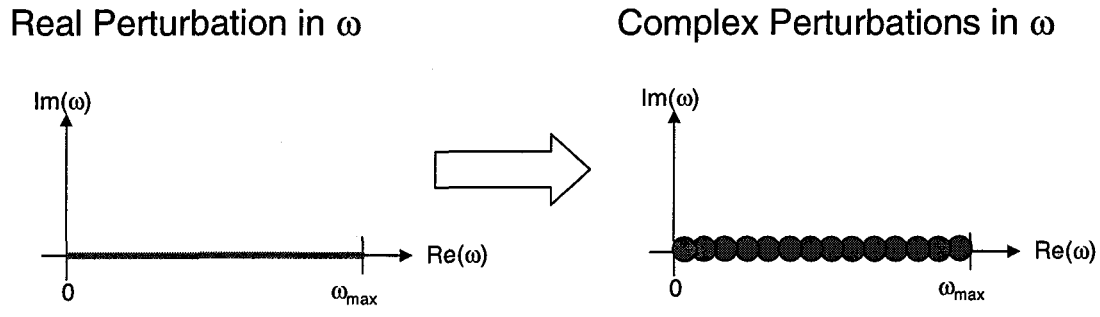

Figure 3-19. Real to Complex Uncertainty

The complex uncertainty representation is somewhat conservative since it allows for a small complex contribution in the spin rate, which is not possible. However, the complex representation contains the entire interval in the real uncertainty representation and it allows for a more reliable computation of the bound on the structured singular value.

3.4.4 Centrifuge Rotor System in μ-analysis Framework

Figure 3-20 presents a pictorial representation of an uncertain centrifuge rotor system formulated into a robust stability problem using the structured singular value. The diagram describes the steps necessary to put the uncertain centrifuge rotor system in the μ-analysis framework.

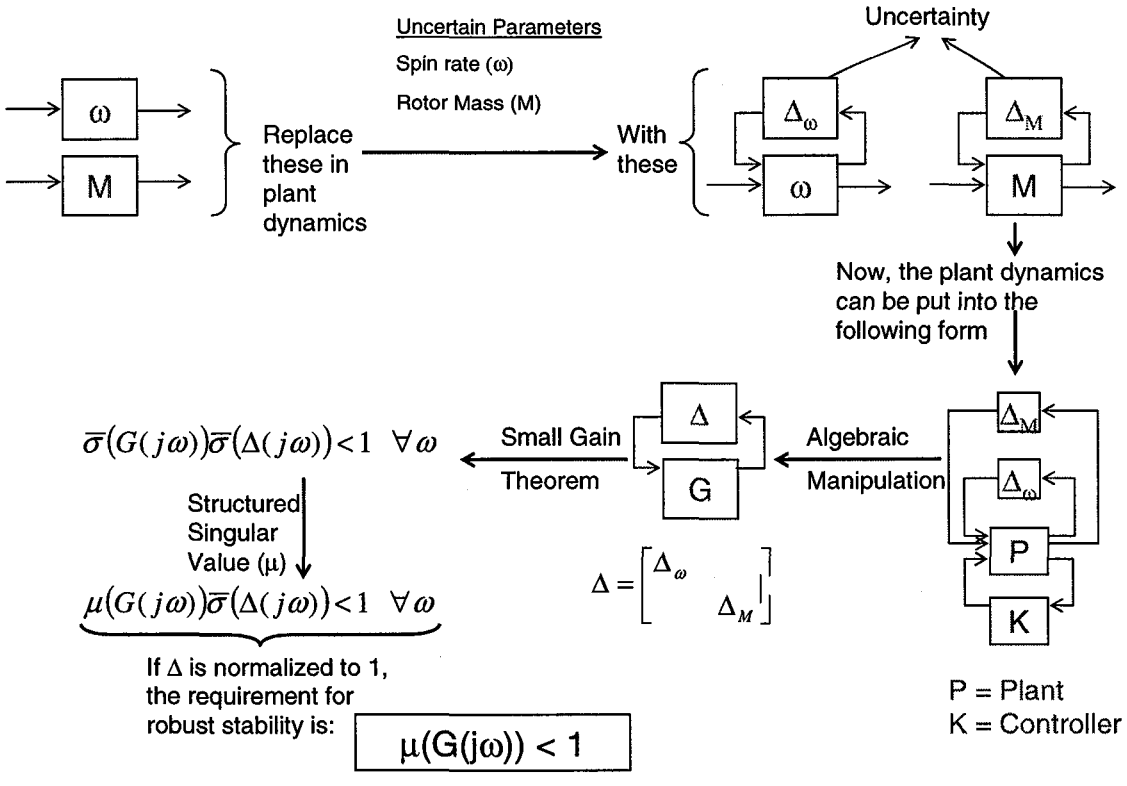

$$\bar{\sigma}(G(j\omega))\bar{\sigma}(\Delta(j\omega)) < 1 \quad \forall\omega$$

$$\mu(G(j\omega))\bar{\sigma}(\Delta(j\omega)) < 1 \quad \forall\omega$$

$$\Delta = \begin{bmatrix} \Delta_\omega & \\ & \Delta_M \end{bmatrix}$$

Figure 3-20. Evaluating System Robustness with the Structured Singular Value

3.5 Steady-State Error in Control Systems

One of the problem constraints as presented in Section 2.3 is to limit the steady-state error in the centrifuge rotor system. It is common practice in control design to introduce an integral term into the controller to eliminate steady-state error. This integral term increases the system type. The system type is defined as the number of poles the open-loop system (the transfer function from e to y in Figure 3-21) has at s = 0 [22]. Adding an integral term in the controller introduces a single pole at s = 0. The steady-state error of a system can be expressed with respect to the system type and the input to the system. For example, the steady-state error due to a step input for a type 0 system and type 1 systems and higher is shown in Table 3-1.

System Type	Steady-State Error
Type 0 System	e_{ss} = constant
Type 1 (or higher) System	$e_{ss} = 0$

Table 3-1. Steady-State Error due to Step Input

A controller utilizing only an integral term has the structure shown in Figure 3-21. P is a type 0 system. Since an integral term has been added via the controller to a type 0 system, the system is now a type 1 system. It should have steady-state error of 0 for a step input.

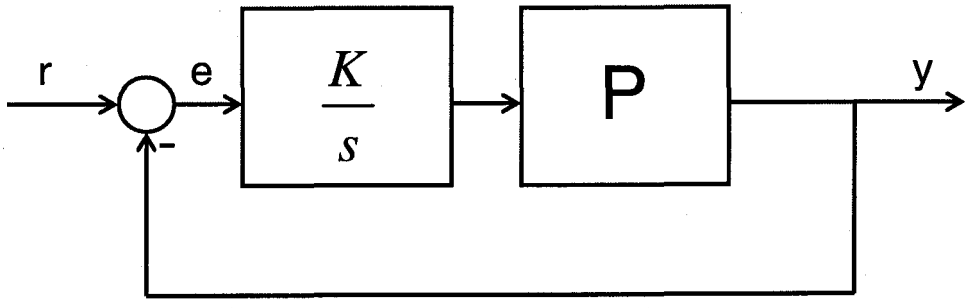

Figure 3-21. System with Pure Integral Control

If K is chosen so that the system is stable, the integral controller in Figure 3-21 will eliminate steady-state error. However, adding an integral term to the controller adds a pole of the open-loop system on the jω-axis. Although this pole can be moved off the axis for the closed-loop system, K is often constrained to be small to satisfy other problem constraints. In this case, the pole is not moved far off of the jω-axis and this close proximity to the unstable region can lead to poor system robustness. For this

reason, it is often advantageous to use a modified integrator, such as in Figure 3-22, to move the pole away from the jω-axis when p is a positive real number. The system is a type 0 system and steady-state error is expected for a step input.

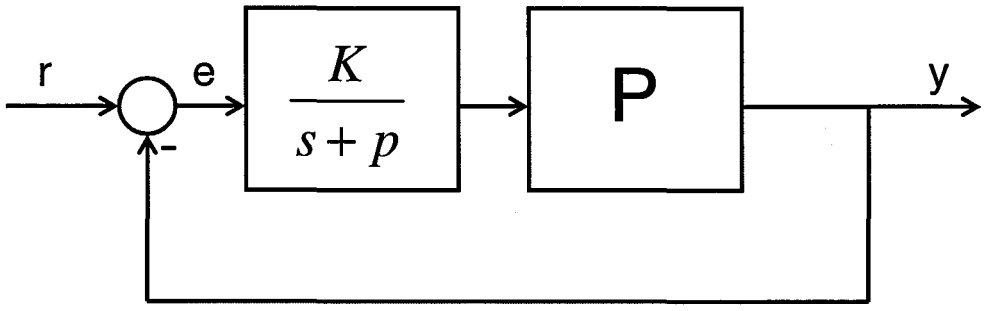

Figure 3-22. System with Modified Integral Control

The increase in system robustness for modified integral control comes at the cost of allowing some steady-state error for a step input. This relationship is derived through use of the final value theorem [22] which provides the relationship

$$\lim_{t\to\infty} f(t) = \lim_{s\to 0} sF(s) \quad . \tag{95}$$

The final value theorem relates the final value, or steady-state value in the time domain, to the Laplace transform of a system evaluated at s=0. As an example, consider the system presented in Figure 3-22 where the plant is defined by the equation

$$P = \frac{1}{s^2 + \frac{c}{m}s + \frac{k}{m}} \quad . \tag{96}$$

Since the steady-state error is of interest, the transfer function from r to e will be evaluated. The closed-loop transfer function from r to e can be written in the form

$$\frac{e}{r} = \frac{1}{1 + P\left(\frac{K}{s+p}\right)} . \tag{97}$$

Evaluating this transfer function with the final value theorem yields a measure of steady-state error as the ratio of the magnitude of the steady-state error to the magnitude of the reference input signal.

First, make the substitutions

$$a_3 = 1, \tag{98}$$

$$a_2 = \frac{c}{m} + p, \tag{99}$$

$$a_1 = \frac{c}{m} p + \frac{k}{m}, \tag{100}$$

and

$$a_0 = \frac{k}{m} p . \tag{101}$$

The transfer function from r to e can be written in the form

$$F(s) = \frac{a_3 s^3 + a_2 s^2 + a_1 s + a_0}{a_3 s^3 + a_2 s^2 + a_1 s + a_0 + K} . \tag{102}$$

To evaluate the steady-state error for a unit step input from r, the term (1/s) must be added to account for the step input. Thus,

$$e(s) = F(s)r(s) = \frac{a_3 s^3 + a_2 s^2 + a_1 s + a_0}{a_3 s + a_2 s^2 + a_1 s + a_0 + K} \frac{1}{s}. \qquad (103)$$

Now the term on the right side of Equation (95) is evaluated. That is,

$$e_{ss} = sF(s)r(s)\Big|_{s=0} = \frac{a_0}{a_0 + K} = \frac{\frac{k}{m} p}{\frac{k}{m} p + K}. \qquad (104)$$

where e_{ss} is the steady-state error with a reference input of a unit step. It is seen that for p=0, there is no steady-state error. Also, the steady-state error increases as p increases for a given value of K. This is verified through time domain simulation for the case where c=10, k=1, m=1, K=1, and p=0.1. Based on Equation (104), a steady-state error of 0.091 is expected for a unit step input in r. The step response is shown in Figure 3-23 for the system with a pure integrator and the system with a modified integrator.

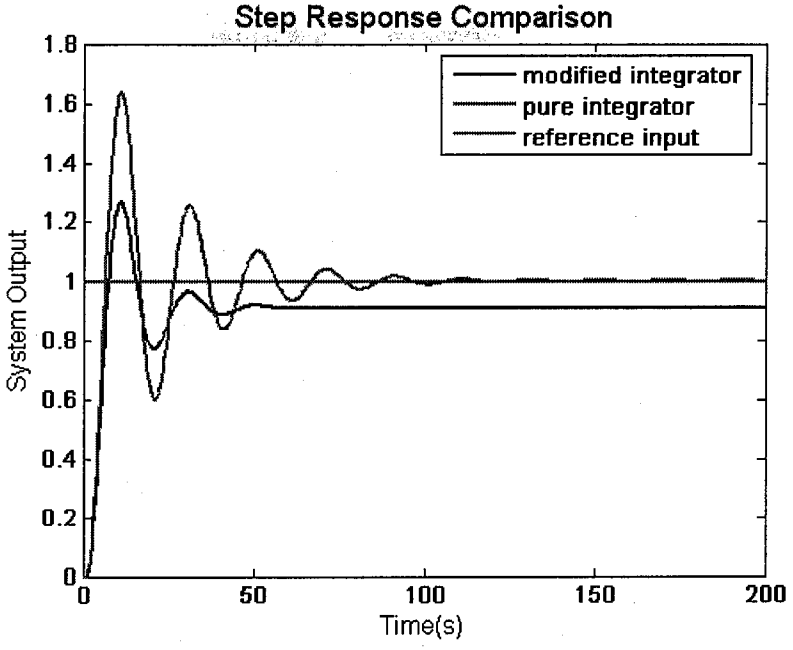

Figure 3-23. Step Response Comparison for Pure and Modified Integrator

It is seen from Figure 3-23 that the system with the pure integrator does not have steady-state error, while the system with the modified integrator has steady-state error of 0.091 as expected. However the system with the pure integrator sacrifices system robustness when compared to this system with the pure integrator. It is demonstrated in this section that the system with the modified integrator is significantly more robust to error in the sensor measurement. Sensor error is introduced as shown in the block diagram in Figure 3-24.

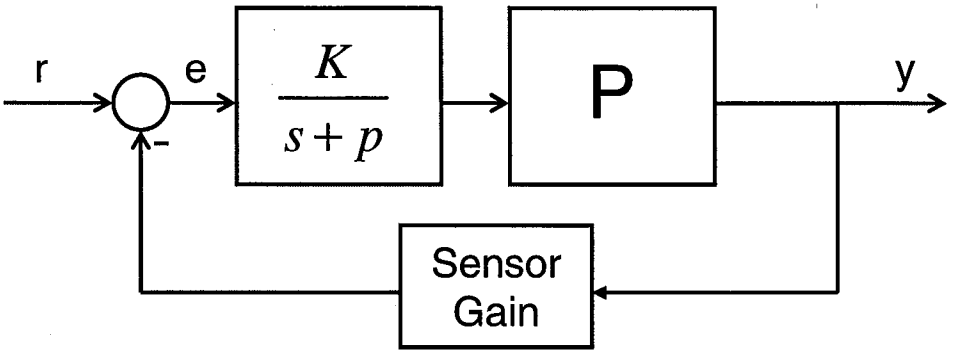

Figure 3-24. System with Sensor Error

Applying a sensor gain of 15, the systems are compared. The response of the variable y is shown in Figure 3-25 for each system when r is a unit step input.

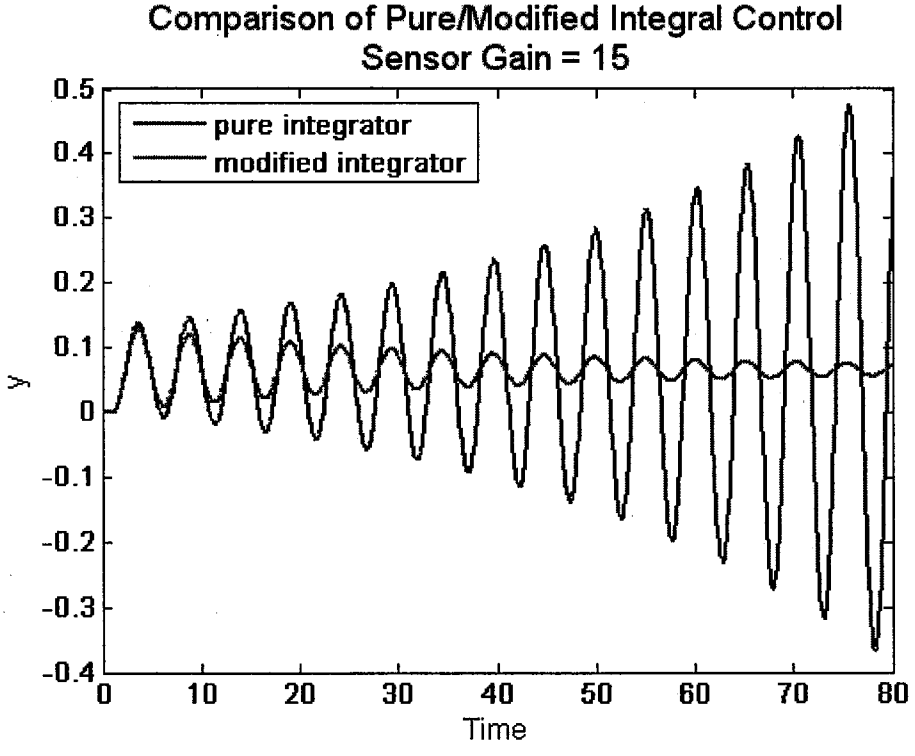

Figure 3-25. Comparison of Pure/Modified Integral Control

While neither system follows the step input very well, it is clear that the system with pure integral control is unstable, while the system with modified integral control is stable. In fact, the gain margin for the system with pure integral control is 10 (20 dB), while the gain margin for the system with modified integral control is 20.1 (26 dB). It is notable that the system with the modified integrator has a gain margin twice as large as the system with pure integral control while sacrificing steady-state error of 9.1%.

In the case of the centrifuge rotor, the steady-state error analysis is modified to treat the MIMO case. If the step input $r = r_{amp} * (1/s)$, then $e = F * (1/s) * r_{amp}$. Using the induced 2-norm (denoted as i2) to define performance, the steady-state error can be expressed as

$$\|e_{ss}\|_2 \leq \|F(s=0)\|_{i2} \|r_{amp}\|_2, \qquad (105)$$

where the symbol F denotes the closed-loop transfer function from r (or the disturbance in the case of the centrifuge rotor) to e (the translation in the case of the centrifuge rotor). This equation is valid for the case where r is a signal with finite area under the curve. In the case where r is a step input, the relationship is written using the induced 1-norm (denoted as i1) [32] as

$$\|e_{ss}\|_\infty \leq \|F(s=0)\|_{i1} \|r_{amp}\|_\infty. \qquad (106)$$

The steady-state error of the centrifuge rotor with a controller is analyzed in Section 4.3.1.2.

3.6 A Constrained Optimization Approach to Control Design

To design the ABC a procedure is proposed to combine both time domain and frequency domain constraints [33][34]. The ABC design problem is first converted into a constrained optimization problem where the translation of the rotor due to a fixed worst-case imbalance during "spin-up" is minimized subject to problem constraints. A constrained optimization approach is then applied to solve the problem.

A flow chart of the process used in a robust constrained optimization approach to control design is shown in Figure 3-26. This process is applied to the mathematical formulation of the control problem presented in Section 4.2 to generate an ABC. The optimization problem is solved using a gradient-descent method [38][39][40].

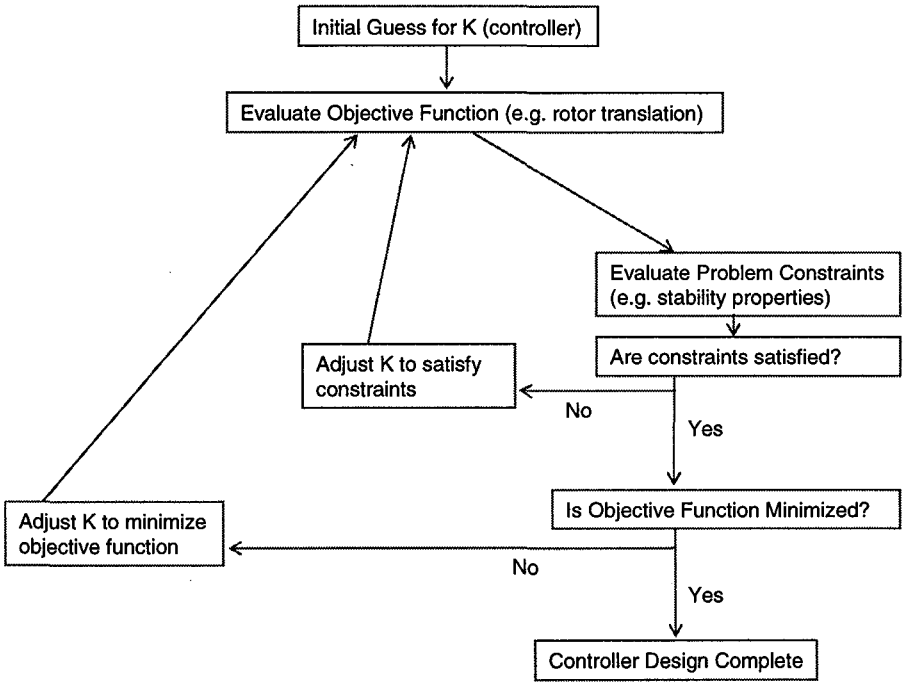

Figure 3-26. Flow of Robust Constrained Optimization Approach to Control Design

This approach has also been used to design control systems for the International Space Station Momentum Manager, an active vibration isolation system, and the Control Momentum Gyroscope Flex Filter for the International Space Station [35][36][37]. A major advantage of this approach is the capacity to deal with both time domain constraints (such as rotor translation constraints) and frequency domain constraints (such as robust stability specifications) simultaneously.

4 Solution Method

To solve the ABC design problem, a robust constrained optimization approach to control design is implemented. The problem to be solved is re-stated more specifically in Section 4.1 and Section 4.2. A three stage design procedure is implemented and the intermediate design results are presented in Section 4.3.

4.1 Problem Setup

It is assumed that the following specific constraints apply to the ABC:

I. limit the peak translation ($\sqrt{\zeta^2 + \eta^2}$) of the rotor < 3.5mm for all rodent disturbances,

II. stability is required over the range $0 < \omega < \omega_{max}$,

III. be robust to uncertainty in:

   a. spin rate (ω) of 100%,

   b. rotor mass (M) of 60%, and

   c. rotor inertia (I_d,I_z) of 45%,

IV. limit commanded balancer mass speed < 1mm/sec, and

V. limit steady-state rotor translation < 0.1mm for a fixed disturbance (rodents are stationary).

Note that the tilt of the rotor is not directly constrained since it contributes to the translation of the rotor (which is constrained). The above formulation is a specific statement of the problem to be solved from the more general problem statement presented in Section 2.3.

4.2 Mathematical Problem Formulation

The mathematical formulation of the optimization problem can then be posed as:

$$\text{Minimize} \quad \max\|r\|_2 \qquad \text{(Objective Function)} \qquad (107)$$

subject to

$$\lambda(A-BK)<0 \qquad \text{(Nominal Stability)}, \qquad (108)$$

$$\max\|r\|_2 < 3.5mm \qquad \text{(Nominal Performance)}, \qquad (109)$$

$$\left|r(t_{final})\right| < 0.1mm \qquad \text{(Nominal Performance)}, \qquad (110)$$

$$\mu_{rs}(G(j\omega))<1 \qquad \text{(Robust Stability)}, \qquad (111)$$

$$\mu_{rp}(G(j\omega))<1 \qquad \text{(Robust Performance)}, \qquad (112)$$

and

$$\frac{db}{dt} < 1\frac{mm}{\sec} \qquad \text{(Actuator Limits)}, \qquad (113)$$

where $r(t)=[\zeta(t) \quad \eta(t)]^T$ and $b=[\zeta_{b1} \quad \eta_{b2} \quad \xi_{b3} \quad \xi_{b4}]^T$. The symbols A and B denote the state-space matrices of the coupled plant dynamics of Equations (52) and (53). The symbol G is defined as the closed-loop centrifuge rotor system as shown in Figure 3-20 where the uncertainty is in the spin rate, rotor mass, and rotor inertia as defined in Section 4.1. In this formulation, the peak of the translational response of the rotor is minimized.

4.3 Three Stage Solution Procedure

The controller design task is broken into three separate stages. This is done to reduce the number of degrees-of-freedom and constraints in the optimization problem. This approach is called "constraint relaxation" in the literature [41]. Since the equations of motion of the plant can be easily decoupled (see Section 2.1), it is possible to design a controller for the translational equations of motion (Equation (54)) and a controller for the tilting equations of motion (Equation (55)) separately, making up the first two stages of the design. The third stage then involves designing a controller for the coupled dynamics (Equations (52) and (53)), using the controllers resulting from stage 1 and stage 2 as a starting point. Stage 3 is used to fill in the cross terms of the controller as shown in Equation (117).

The final controller has the structure

$$b = Kx \tag{114}$$

where

$$b = [\zeta_{b1} \quad \eta_{b2} \quad \xi_{b3} \quad \xi_{b4}]^T, \tag{115}$$

$$x = [\zeta \quad \eta \quad \phi_\zeta \quad \phi_\zeta \quad \dot{\zeta} \quad \dot{\eta} \quad \dot{\phi}_\zeta \quad \dot{\phi}_\eta \quad \int\zeta \quad \int\eta \quad \int\phi_\zeta \quad \int\phi_\eta]^T, \tag{116}$$

and

$$K = \begin{bmatrix} K\_tran_{2x6} & K\_cross1_{2x6} \\ K\_cross2_{2x6} & K\_tilt_{2x6} \end{bmatrix}. \tag{117}$$

K_tran is designed in stage 1, K_tilt is designed in stage 2, and K_cross1 and K_cross2 are designed in stage 3. Overall, the controller design has 48 degrees of freedom (the control gains of the K matrix), however, breaking the design task into three stages, it is re-formulated as three separate optimization problems having 12, 12, and 24 degrees of freedom, respectively. This reduction of the problem size allows the optimization routine to converge more quickly and reliably.

4.3.1 Stage 1

As mentioned in Section 4.3, stage 1 involves the design of K_tran. After stage 1 is complete, the controller has the structure

$$K = \begin{bmatrix} K\_tran_{2x6} & 0_{2x6} \\ 0_{2x6} & 0_{2x6} \end{bmatrix}. \qquad (118)$$

The objective of stage 1 is to find K_tran such that the peak translation of the rotor is minimized, while ensuring that the problem constraints are met. The peak translation is defined by the maximum translation of the rotor during time domain simulation. The scenario simulated includes a spin-up from 0 to the maximum spin rate. The maximum spin rate is reached in 1800 seconds and the rotor continues to spin at this rate until the simulation ends at 2500 seconds. The disturbance acting on the plant is the disturbance resulting from the rodents being stationary in positions causing the largest imbalance in the rotor (see Section 2.1). In addition to minimizing the translation, the constraints in Equations (108) – (113) must be met as well. The mathematical formulation is presented in Section 4.3.1.1.

4.3.1.1 Stage 1 Problem Formulation

$$\text{Minimize} \quad \max\|r\|_2 \qquad \text{(Objective Function)} \qquad (119)$$

subject to

$$\lambda(A-BK)<0 \qquad \text{(Nominal Stability)}, \qquad (120)$$

$$\max\|r\|_2 < 3.5mm \qquad \text{(Nominal Performance)}, \qquad (121)$$

$$\left|r(t_{final})\right| < 0.1mm \qquad \text{(Nominal Performance)}, \qquad (122)$$

$$\mu_{rs}(G(j\omega))<1 \qquad \text{(Robust Stability)}, \qquad (123)$$

$$\mu_{rp}(G(j\omega))<1 \qquad \text{(Robust Performance)}, \qquad (124)$$

and

$$\frac{db}{dt} < 1\frac{mm}{\sec} \qquad \text{(Actuator Limits)}, \qquad (125)$$

where $r(t)=[\zeta(t) \quad \eta(t)]^T$ and $b = [\zeta_{b1} \quad \eta_{b2}]^T$. The symbols A and B denote the state-space matrices of the full coupled dynamics in Equations (52) and (53). The coupled dynamic equations are used to check nominal stability to ensure that the controller will not be unstable for the coupled system when stage 3 of the design process is reached. The robust stability and robust performance measures must be met for the range $0 < \omega < \omega_{max}$ and 60% rotor mass uncertainty from the nominal value. G is defined as the closed-loop centrifuge rotor system as shown in Figure 3-20 where the uncertainty is in the spin rate and rotor mass as defined above.

4.3.1.2 Stage 1 Design Loop Results

The constrained optimization problem was solved using the Matlab function *fmincon* [38]. The initial guess to start the optimization process is K_tran = 0_{2x6}. The optimization took over 1000 iterations to yield the final solution which is presented in this section.

From Figure 4-1, it is apparent that the closed-loop system achieves nominal stability since all of the poles lie to the left of the jω-axis. The poles that appear to lie near the jω-axis are the result of the modified integrators that were appended to the system. Since the modified integrators add poles at s = -0.0003 to the open-loop system, these poles appear to be quite near the imaginary-axis, but are in the left half plane (LHP).

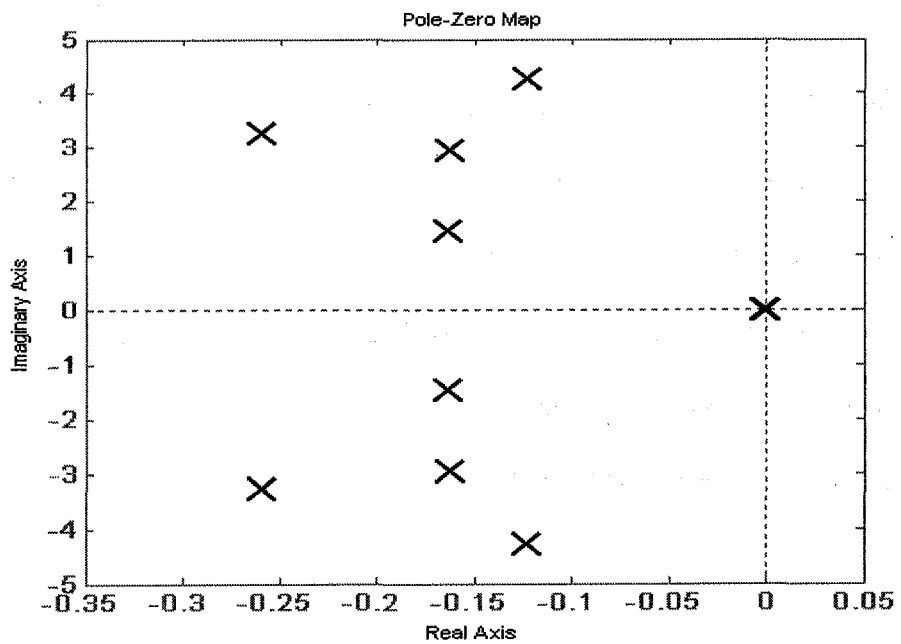

Figure 4-1. Stage 1 - Nominal Stability

Figure 4-2 shows the translation of the rotor when simulated under the conditions described in Section 4.3.1. The peak translation of the rotor is well under the maximum allowable translation 3.5mm. In fact, the peak translation is 2.52mm. Further, the steady-state translation of the rotor is less than 0.10mm satisfying the requirement for steady-state error (the constraint imposed on the final value of rotor translation).

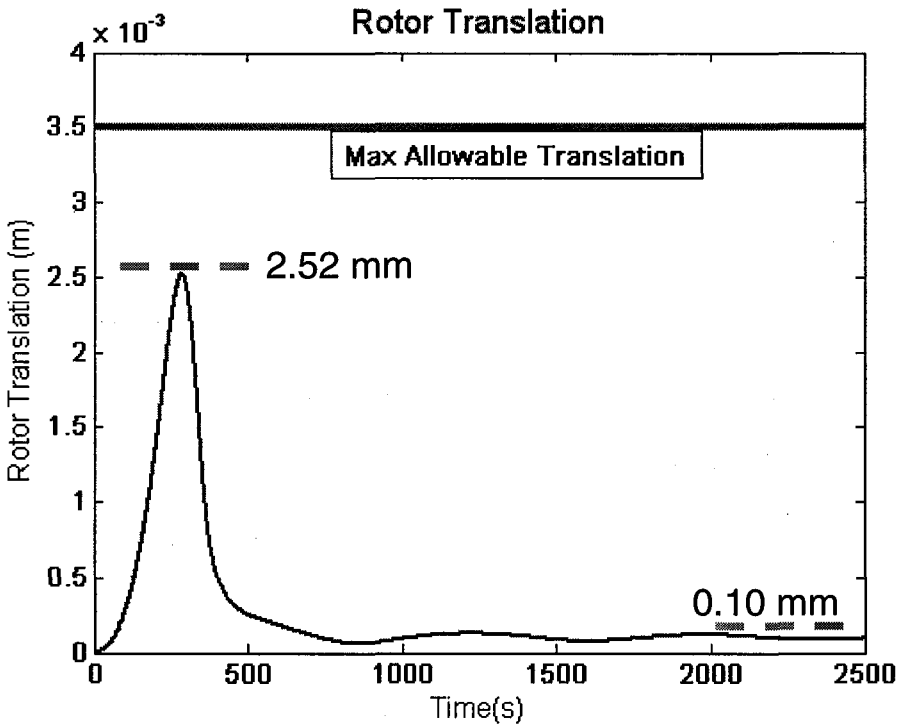

Figure 4-2. Stage 1 - Rotor Translation

The steady-state error that is present in the response is due to the modified integrators being used in the controller (see Section 3.5). Recall that in the MIMO case steady-state error for a step input can be expressed as

$$\|e_{ss}\|_{\infty} \leq \|F(s=0)\|_{i1} \|r_{amp}\|_{\infty}. \qquad (126)$$

In the case of the centrifuge rotor, the symbol F denotes the closed-loop transfer function from the rodent disturbance to rotor translation. The closed-loop centrifuge rotor system for stage 1 yields

$$\|e_{ss}\|_{\infty} \leq \left\| \begin{matrix} -0.00002 & -0.00023 \\ 0.00021 & -0.00003 \end{matrix} \right\|_{i1} \left\| \begin{matrix} 0.3 \\ 0.3 \end{matrix} \right\|_{\infty} = 0.000078\ m\ , \qquad (127)$$

where the maximum size of the elements in the vector r is 0.3. Since the maximum size of the steady-state error is 0.000078 m in each direction (ζ and η), the upper bound on the translation is $(0.000078^2 + 0.000078^2)^{1/2} = 0.0001103$m. From Figure 4-2, it is seen that this relationship provides a good upper bound. The actual steady-state error is slightly less than 0.0001m.

Figure 4-3 indicates that the closed-loop system maintains stability for 60% mass uncertainty over the range $0 < \omega < \omega_{max}$ since the upper bound of $\mu < 1$ at all frequencies. The interval for ω was divided into several intervals to evaluate robust stability as shown in Section 3.4.3. The plot of robust stability presented is the interval with the highest peak for the upper bound of μ.

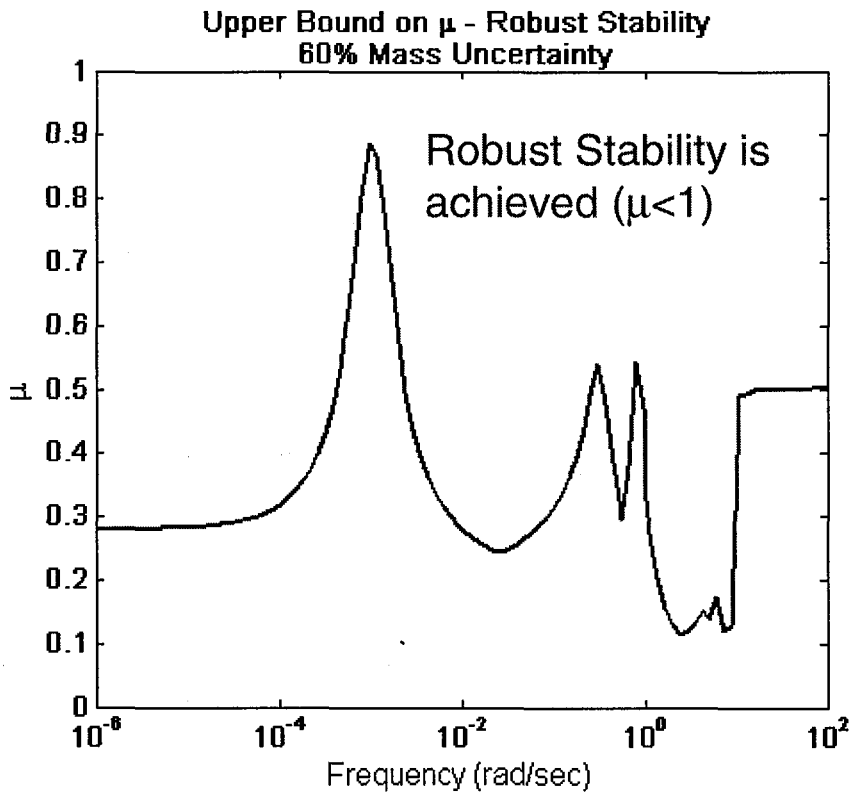

Figure 4-3. Stage 1 - Robust Stability

The transfer function evaluated to analyze robust stability is the transfer function from u_Δ to y_Δ shown in Figure 4-4. The uncertainty Δ is normalized to 1, and it represents the uncertainty present in the rotor mass and rotor spin rate. The symbols D and D^{-1} are as specified in Section 3.4 and represent scaling matrices used by the structured singular value.

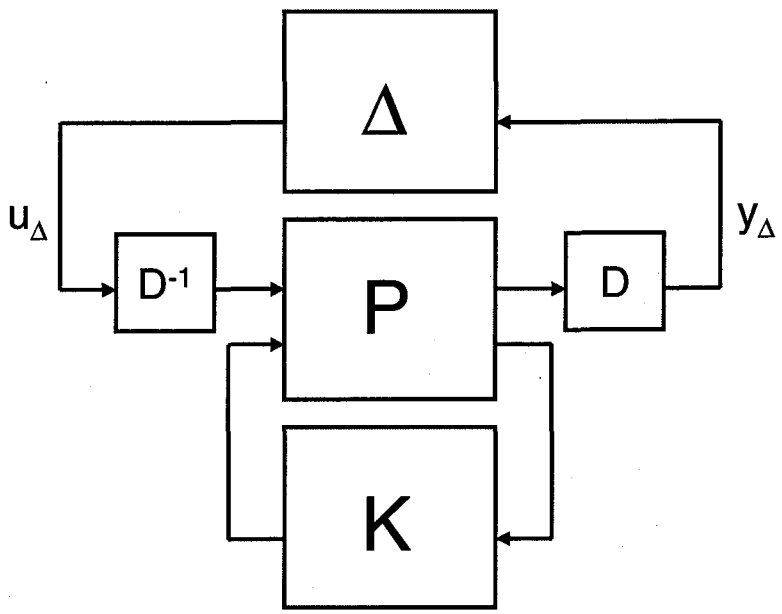

Figure 4-4. Block Diagram for Evaluating Robust Stability

Figure 4-5 indicates that the closed-loop system achieves the performance objective for 60% mass uncertainty over the range $0 < \omega < \omega_{max}$ since the upper bound of $\mu < 1$ at all frequencies. The interval for ω was again divided into several intervals. The plot of robust performance presented is for the ω interval with the highest peak for μ.

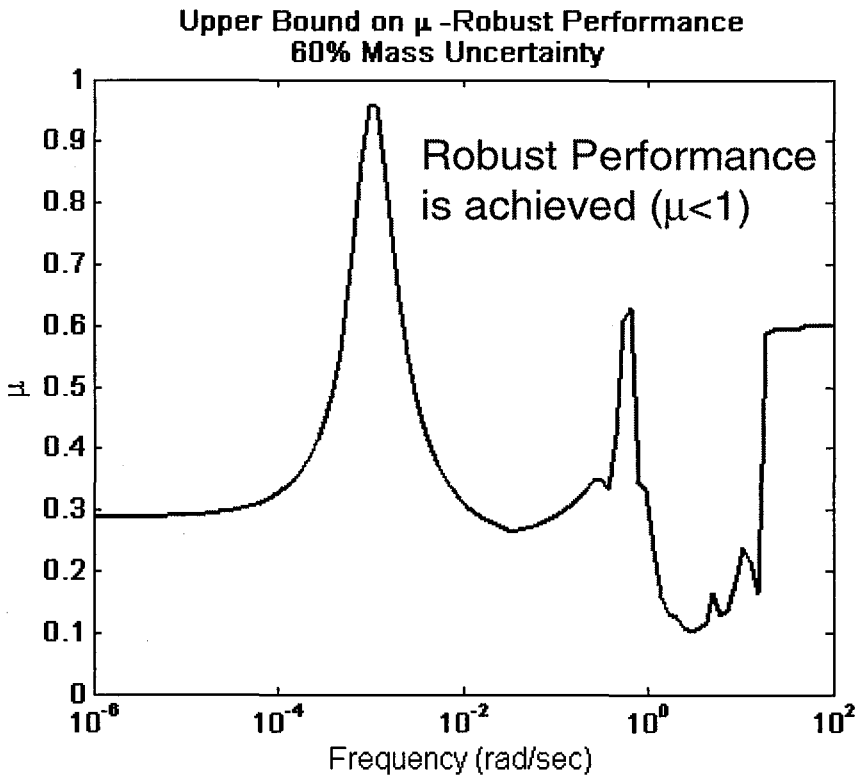

Figure 4-5. Stage 1 - Robust Performance

The robust performance objective was to limit rotor translation < 3.5mm for a disturbance of maximum amplitude (as in the time domain simulation) and frequency content from DC to 0.0001 Hz (0.000628 rad/sec). This performance objective is formulated by appending weighting functions to the unweighted plant as in Section 3.4.2.

The weighting functions are appended to the plant as shown in Figure 4-6 to normalize the performance objective as stated above from d to e to a performance objective from d' to e' as shown in Figure 4-6. The transfer function evaluated for robust performance is $[u_\Delta\ d']^T \rightarrow [y_\Delta\ e']^T$.

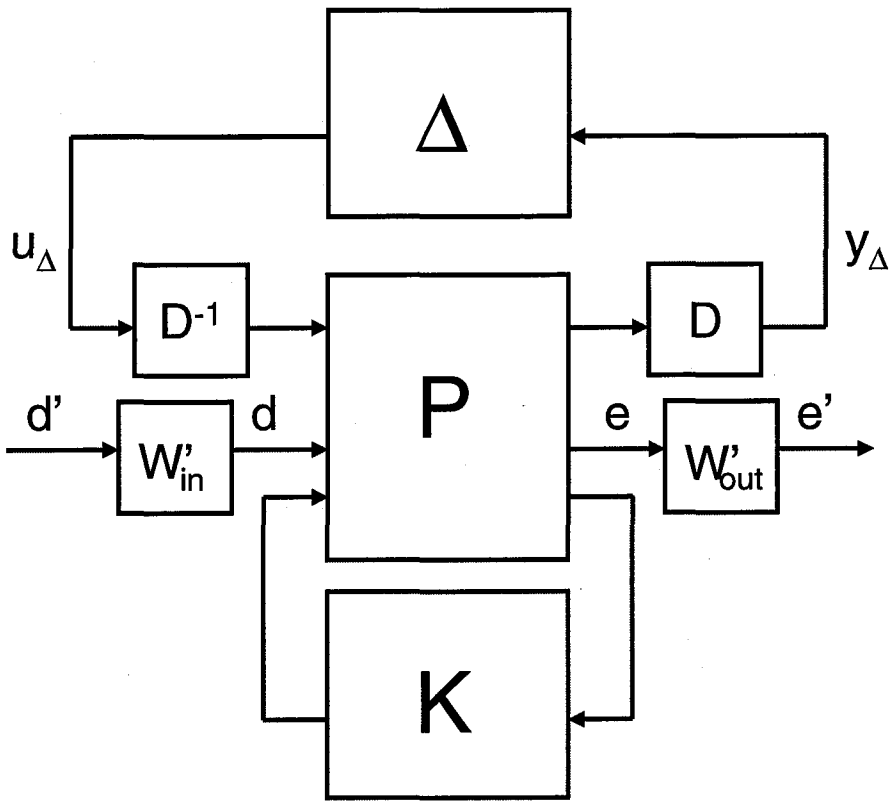

Figure 4-6. Weighting Functions for Robust Performance

The weighting functions used to normalize the performance objective are presented in Figure 4-7 and Figure 4-8 where

$$W'_{in} = \begin{bmatrix} W_{in} & \\ & W_{in} \end{bmatrix} \quad (128)$$

and

$$W'_{out} = \begin{bmatrix} W_{out} & \\ & W_{out} \end{bmatrix}. \quad (129)$$

The weighting function rolls off near 0.000628 rad/sec since the performance objective is to reject disturbances with frequency content less than 0.0001 Hz (0.000628 rad/sec). The magnitude of the weighting function is 0.3 is since the largest expected disturbance has a magnitude of 0.3.

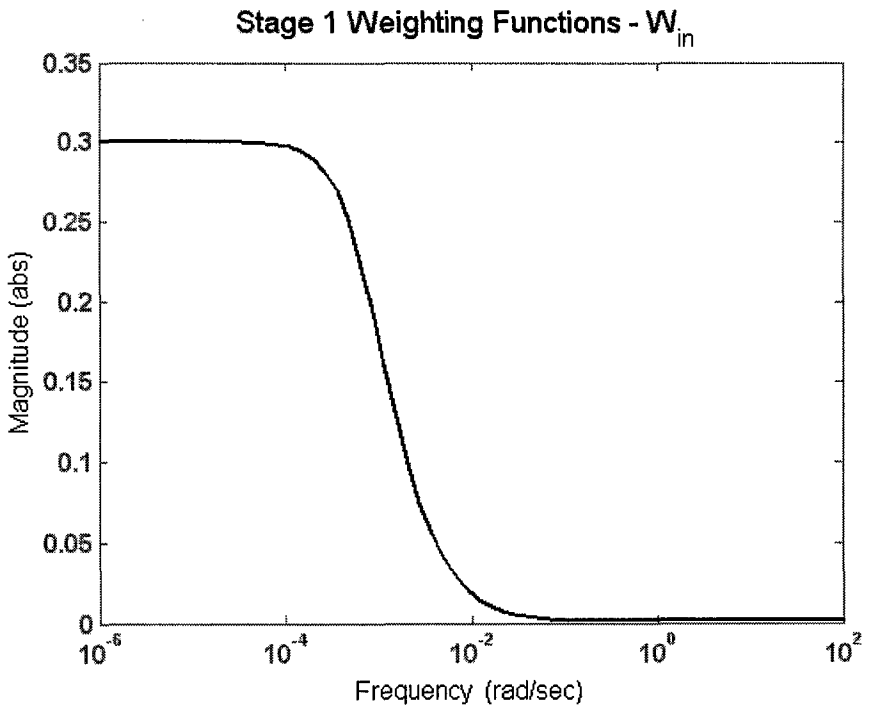

Figure 4-7. Stage 1 Weighting Functions - Input Weight

Figure 4-8 shows the weighting function used to normalize the output to 1. Since the largest allowable rotor translation is 3.5mm or 0.0035m at all frequencies, the weighting function has the magnitude 285.7.

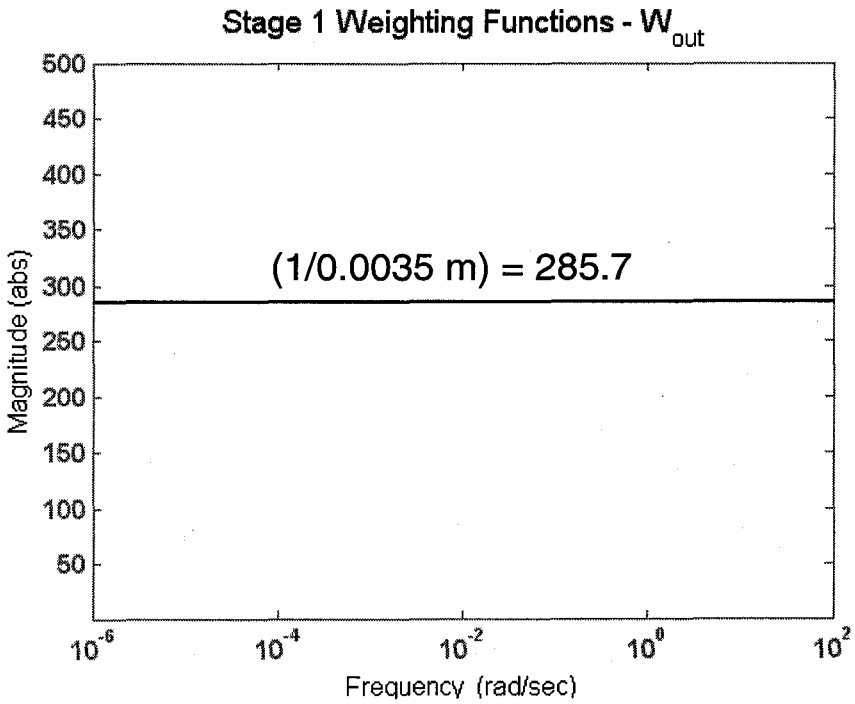

Figure 4-8. Stage 1 Weighting Functions - Output Weight

Figure 4-9 shows that in the time domain simulation the actuator saturation constraints of 1mm/s (0.001m/s) are not exceeded. By avoiding actuator saturation, the linearity of the system is preserved. This is important because linear analysis results (such as robust stability and robust performance) are not valid if the actuator constraints are saturated since a system with saturation is not linear.

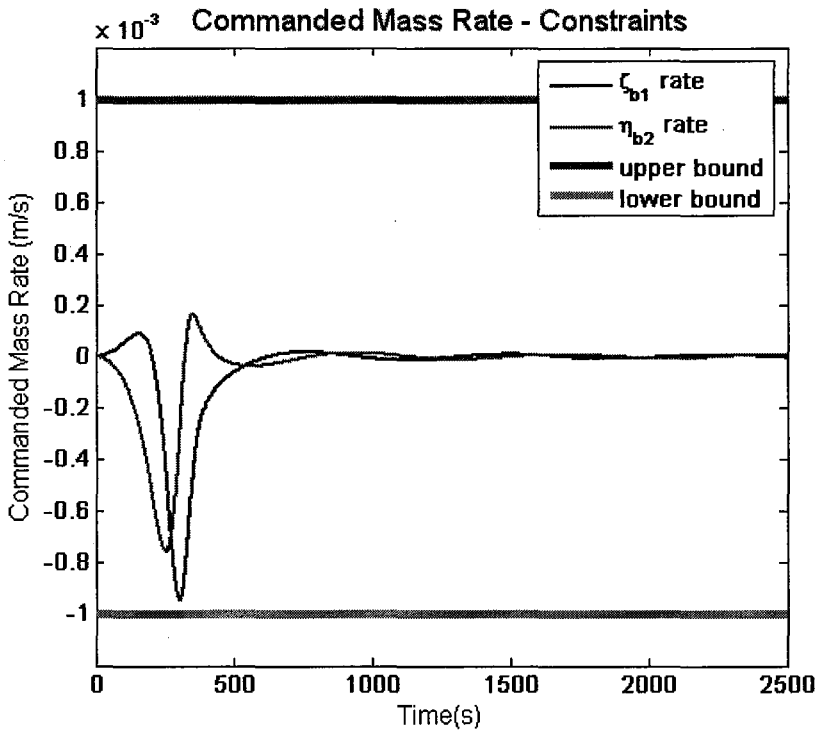

Figure 4-9. Stage 1 - Actuator Constraints

It is seen that all of the constraints are met in stage 1 and the peak rotor translation is minimized.

4.3.2 Stage 2

As stated in Section 4.3, stage 2 involves the design of K_tilt. After stage 2 is complete, the controller has the form

$$K = \begin{bmatrix} K\_tran_{2x6} & 0_{2x6} \\ 0_{2x6} & K\_tilt_{2x6} \end{bmatrix}. \qquad (130)$$

The objective of stage 2 is to find K_tilt such that the peak tilt of the rotor is minimized, while ensuring that the problem constraints are met. The peak tilt is defined by the maximum tilt of the rotor during time domain simulation. The scenario simulated is the same as that in stage 1. In addition to minimizing the tilt, the stability, robustness, steady-state error, and actuator constraints must be met as well. The mathematical formulation is presented in Section 4.3.2.1.

4.3.2.1 Stage 2 Problem Formulation

$$\text{Minimize} \quad \max\|\phi\|_2 \qquad \text{(Objective Function)} \qquad (131)$$

subject to

$$\lambda(A - BK) < 0 \qquad \text{(Nominal Stability)}, \qquad (132)$$

$$\max\|\phi\|_2 < 0.6mrad \qquad \text{(Nominal Performance)}, \qquad (133)$$

$$\left|\phi(t_{final})\right| < 0.1mrad \qquad \text{(Nominal Performance)}, \qquad (134)$$

$$\mu_{rs}(G(j\omega)) < 1 \qquad \text{(Robust Stability)}, \qquad (135)$$

$$\mu_{rp}(G(j\omega)) < 1 \qquad \text{(Robust Performance)}, \qquad (136)$$

and

$$\frac{db}{dt} < 1\frac{mm}{\text{sec}} \qquad \text{(Actuator Limits)}, \qquad (137)$$

where $\phi(t) = [\phi_\zeta(t) \quad \phi_\eta(t)]^T$ and $b = [\xi_{b3} \quad \xi_{b4}]^T$. The symbols A and B denote the state-space matrices of the full coupled dynamics in Equations (52) and (53). The robust stability and robust performance measures must be met for the range of $0 < \omega < \omega_{max}$ and 30% independent inertia uncertainty in I_d and I_z. This inertia uncertainty will be increased to 45% in stage 3. G is defined as the closed-loop centrifuge rotor system as shown in Figure 3-20 where the uncertainty is in the spin rate and rotor inertia as defined above. The tilt of the rotor is not constrained in Equations (108) – (113) since in the coupled system it contributes a small amount to the translation. However, that is not the case in the uncoupled system used for stage 2 of the controller design, so the tilt is

constrained to be < 0.6 mrad (which would contribute 0.35mm of translation in the coupled system or 10% of the maximum allowable translation).

4.3.2.2 Stage 2 Design Loop Results

The constrained optimization problem was solved using the Matlab function *fmincon* [38]. The initial guess to start the optimization process is K_tilt = 0_{2x6}. The optimization took over 1000 iterations to yield the final solution which will be presented in this section.

From Figure 4-10, it is apparent that the closed-loop system achieves nominal stability since all of the poles lie to the left of the jω-axis. As in Figure 4-1 the poles that appear to lie near the jω-axis are in the LHP and are the result of the modified integrators that were appended to the system.

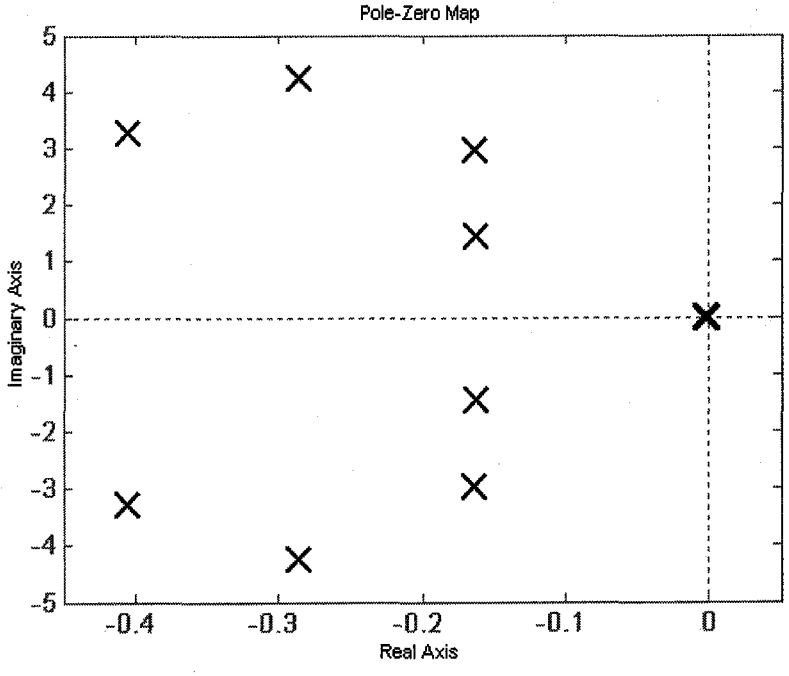

Figure 4-10. Stage 2 - Nominal Stability

Figure 4-11 shows the tilt of the rotor when simulated under the conditions described in Section 4.3.1. The peak tilt of the rotor is less than the maximum allowable tilt of 0.6mrad. In fact, the peak tilt is 0.54mrad. Further, the steady-state tilt of the rotor is less than 0.10mrad, satisfying the requirement for steady-state error (the constraint imposed on the final value of rotor tilt).

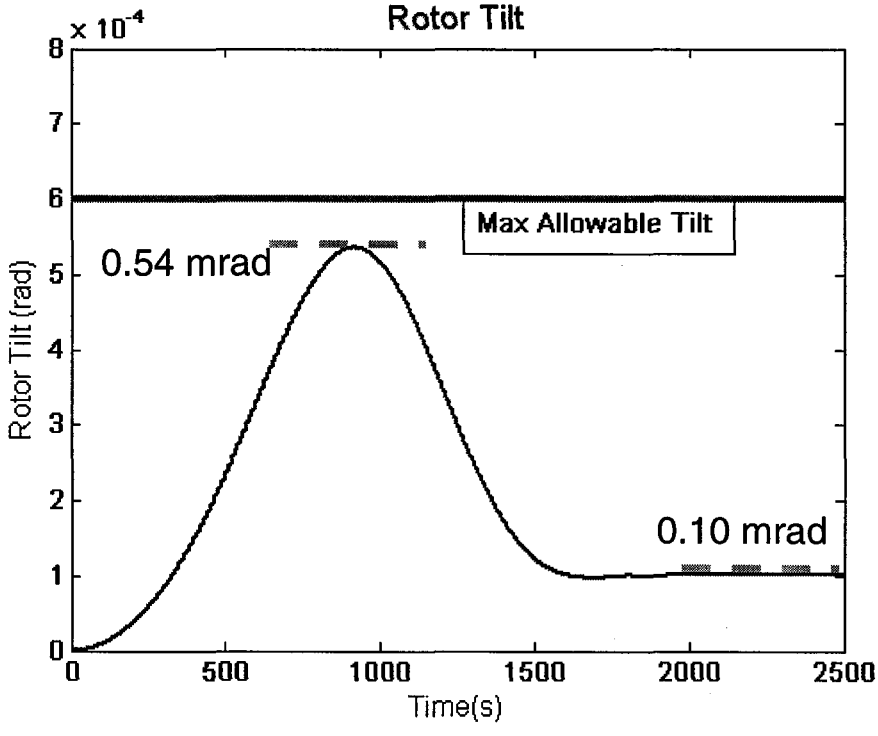

Figure 4-11. Stage 2 - Rotor Tilt

Figure 4-12 indicates that the closed-loop system maintains stability for 30% inertia uncertainty over the range $0 < \omega < \omega_{max}$ since the upper bound of $\mu < 1$ at all frequencies. Again, the interval for ω was divided into several intervals to evaluate robust stability as shown in Section 3.4.3. The plot of robust stability presented is the interval with the highest peak for the upper bound of μ. The transfer function evaluated to analyze robust stability is the same as that in Figure 4-4, but the uncertainty block Δ represents uncertainty in the rotor inertia and rotor spin rate. The plant is the tilting dynamics in Equation (55) and the controller is K_tilt.

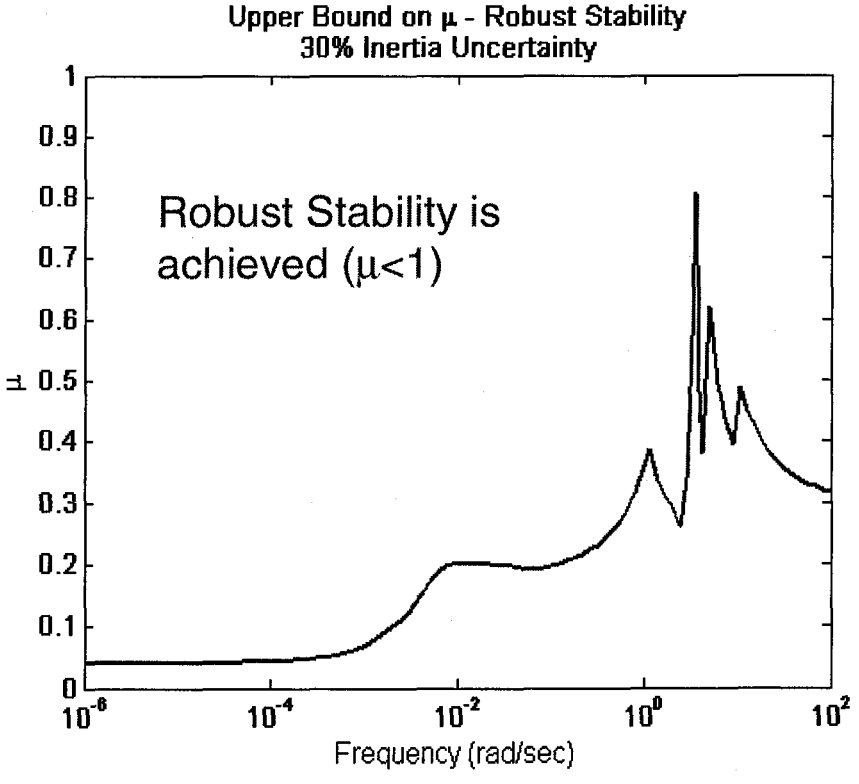

Figure 4-12. Stage 2 - Robust Stability

Figure 4-13 shows that the closed-loop system achieves the performance objective for 30% inertia uncertainty over the range $0 < \omega < \omega_{max}$ since the upper bound of $\mu < 1$ at all frequencies. The interval for ω was again divided into several intervals. The plot of robust performance presented is for the ω interval with the highest peak for the upper bound of μ.

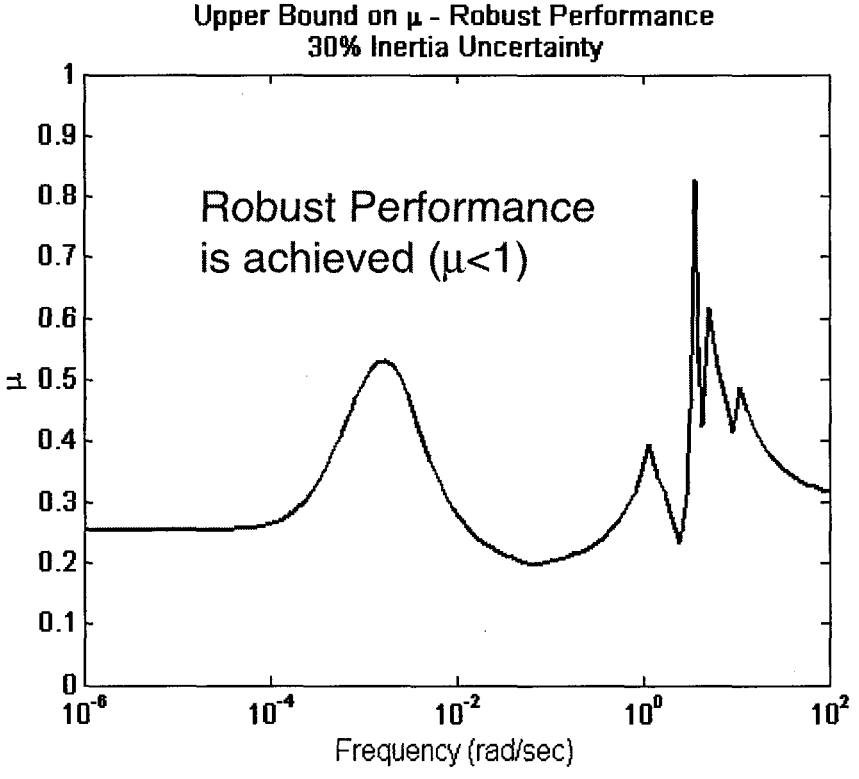

Figure 4-13. Stage 2 - Robust Performance

The robust performance objective in stage 2 was to limit the tilt of the rotor < 0.6mrad for a disturbance of maximum amplitude (as in the time domain simulation) and frequency content from DC to 0.0001 Hz (0.000628 rad/sec). This performance objective is formulated by appending weighting functions to the unweighted plant.

The weighting functions are appended to the plant as shown in Figure 4-6. Again the transfer function evaluated is $[u_\Delta\ d']^T \rightarrow [y_\Delta\ e']^T$ from Figure 4-6. The weighting functions used to normalize the performance objective for stage 2 are presented in Figure 4-14 and Figure 4-15 where

$$W'_{in} = \begin{bmatrix} W_{in} & \\ & W_{in} \end{bmatrix} \tag{138}$$

and

$$W'_{out} = \begin{bmatrix} W_{out} & \\ & W_{out} \end{bmatrix}. \tag{139}$$

The weighting function for the input to the system rolls off near 0.000628 rad/sec since the performance objective is to reject disturbances with frequency content less than that. The magnitude of the weighting functions at low frequencies is 0.00033 since that is the magnitude of the largest expected disturbance in the frequency range.

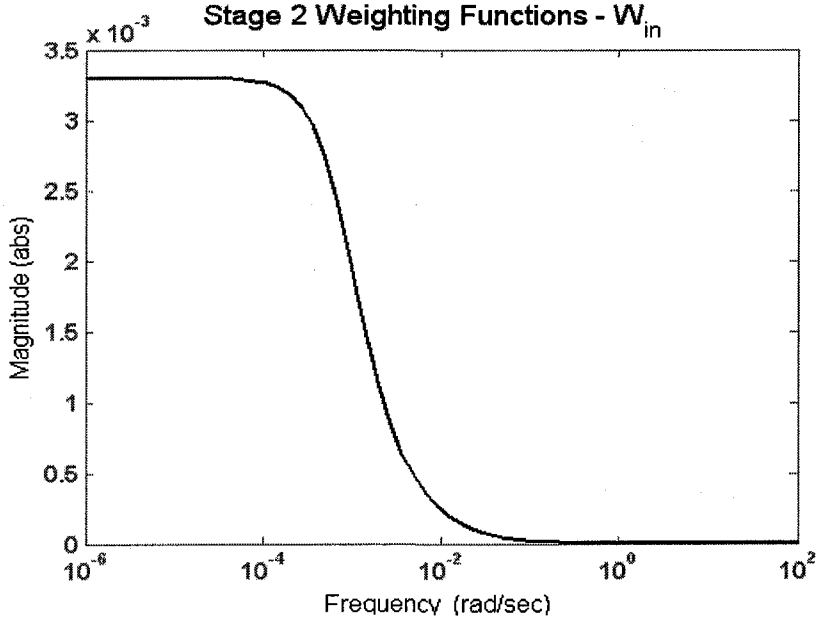

Figure 4-14. Stage 2 Weighting Functions - Input Weight

Figure 4-15 shows the weighting function used to normalize the output to 1. Since the largest allowable rotor tilt is 0.6mrad or 0.0006rad at all frequencies, the weighting function has the magnitude 1666.7.

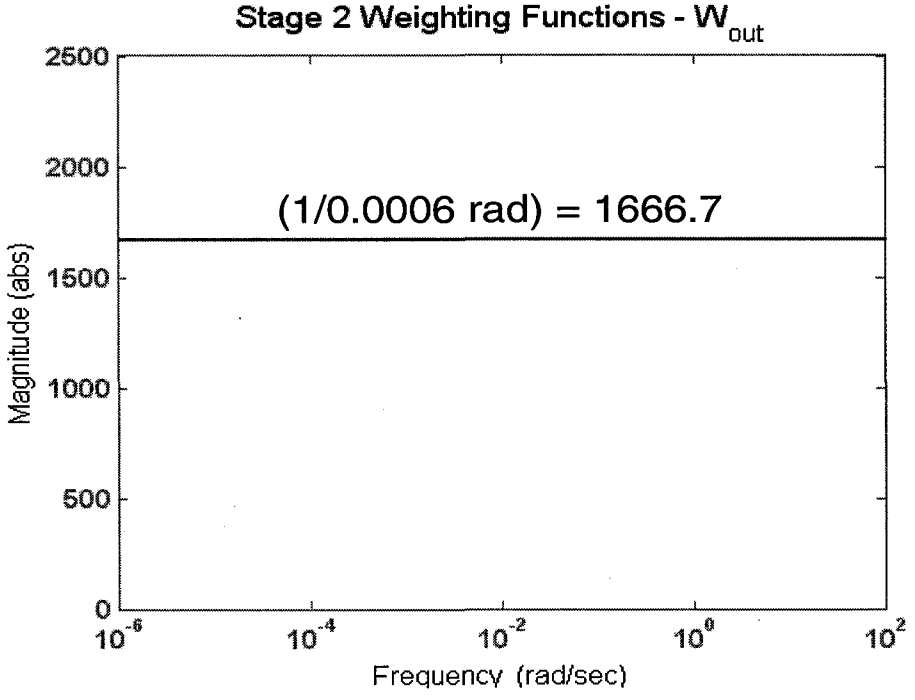

Figure 4-15. Stage 2 Weighting Function - Output Weight

Figure 4-16 shows that in the time domain simulation, the actuator saturation constraints of 1mm/sec or 0.001m/sec are not exceeded. In fact, the mass rates are far from the saturation limits. The lower plot is a closer view of the mass rates. By avoiding actuator saturation, the linearity of the system is preserved.

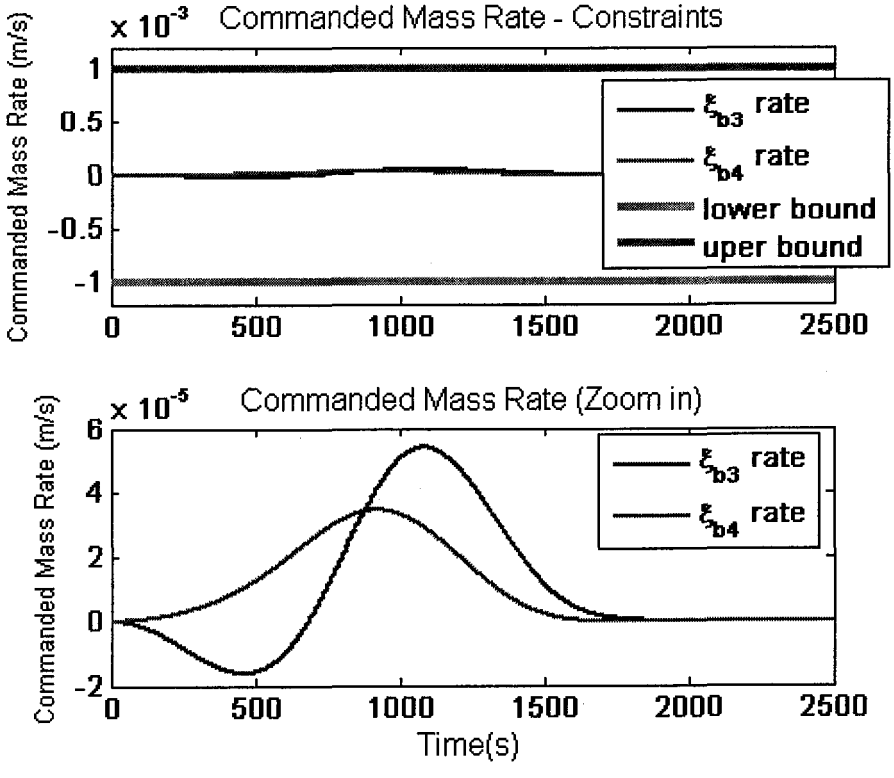

Figure 4-16. Stage 2 - Actuator Constraints

It is seen that all of the constraints are met in stage 2 and the peak rotor tilt is minimized.

4.3.3 Stage 3

As mentioned in Section 4.3, stage 3 involves the design of K_cross1 and K_cross2. These sub-matrices are designed simultaneously allowing for 24 degrees of freedom (12 for each K_cross matrix) in the stage 3 problem formulation After stage 3 is complete, the controller has the form

$$K = \begin{bmatrix} K\_tran_{2x6} & K\_cross1_{2x6} \\ K\_cross2_{2x6} & K\_tilt_{2x6} \end{bmatrix}. \qquad (140)$$

The objective of stage 3 is to find K_cross1 and K_cross2 such that the peak translation of the rotor is minimized, while ensuring that the problem constraints are met. Further, it is desirable to increase the amount of inertia uncertainty that the system can tolerate. The requirement for inertia uncertainty is increased to 45% uncertainty in both I_d and I_z. In addition to minimizing the translation, the constraints in Equations (108) – (113) must be met as well. The mathematical formulation is presented in Section 4.3.3.1. This formulation is the same as formulation in Section 4.2 since stage 3 is the last stage in the design process and all problem constraints must be met for the system with coupled dynamics.

4.3.3.1 Stage 3 Problem Formulation

$$\text{Minimize}_{\max\|r\|_2} \quad \text{(Objective Function)} \qquad (141)$$

subject to

$$\lambda(A-BK)<0 \quad \text{(Nominal Stability)}, \qquad (142)$$

$$\max\|r\|_2 < 3.5mm \quad \text{(Nominal Performance)}, \qquad (143)$$

$$\left|r(t_{final})\right| < 0.1mm \quad \text{(Nominal Performance)}, \qquad (144)$$

$$\mu_{rs}(G(j\omega))<1 \quad \text{(Robust Stability)}, \qquad (145)$$

$$\mu_{rp}(G(j\omega))<1 \quad \text{(Robust Performance)}, \qquad (146)$$

and

$$\frac{db}{dt} < 1\frac{mm}{\sec} \quad \text{(Actuator Limits)}, \qquad (147)$$

where $r(t)=[\zeta(t) \quad \eta(t)]^T$ and $b=[\zeta_{b1} \quad \eta_{b2} \quad \xi_{b3} \quad \xi_{b4}]^T$. The symbols A and B denote the state-space matrices of the full coupled dynamics in Equations (52) and (53). The robust stability and robust performance measures must be met for the range of $0 < \omega < \omega_{max}$, 45% of rotor inertia uncertainty in both I_z and I_d, and 60% rotor mass uncertainty from the nominal value. G is defined as the closed-loop centrifuge rotor system as shown in Figure 3-20 where the uncertainty is in the spin rate, rotor mass, and rotor inertia as defined above.

4.3.3.2 Stage 3 Design Loop Results

The constrained optimization problem was solved using the Matlab function *fmincon* [38]. The initial guess to start the optimization process is K_cross1 = K_cross2 = 0_{2x6}. The optimization took over 1000 iterations to yield the final solution which will be presented in this section.

From Figure 4-17, it is apparent that the closed-loop system achieves nominal stability since all of the poles lie to the left of the jω-axis. As in Figure 4-1 and Figure 4-10 the poles that appear to lie near the jω-axis are in the LHP and are the result of the modified integrators that were appended to the system.

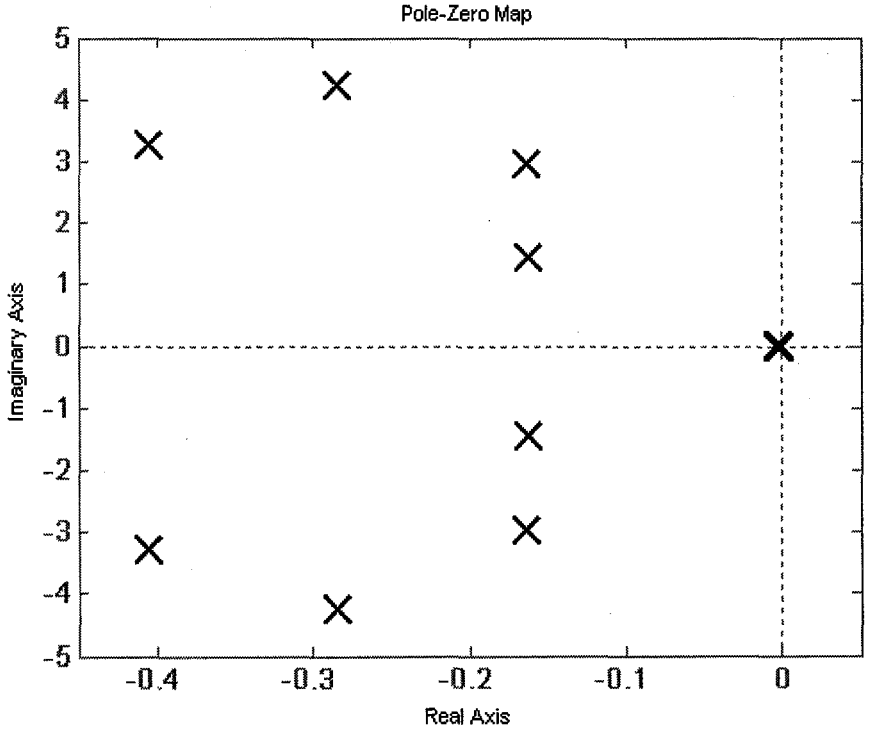

Figure 4-17. Stage 3 - Nominal Stability

Figure 4-18 shows the translation of the rotor when simulated under the conditions described in Section 4.3.1. The peak translation of the rotor is well under the maximum allowable translation of 3.5mm. In fact, the peak translation is 2.54mm. It is seen that the peak translation is slightly higher than the final result of stage 1. This is due to the fact that the coupled dynamic equations of motion include the contribution from the tilt in the rotor translation. Further, the steady-state translation of the rotor is less than 0.10mm satisfying the requirement for steady-state error (the constraint imposed on the final value of rotor translation).

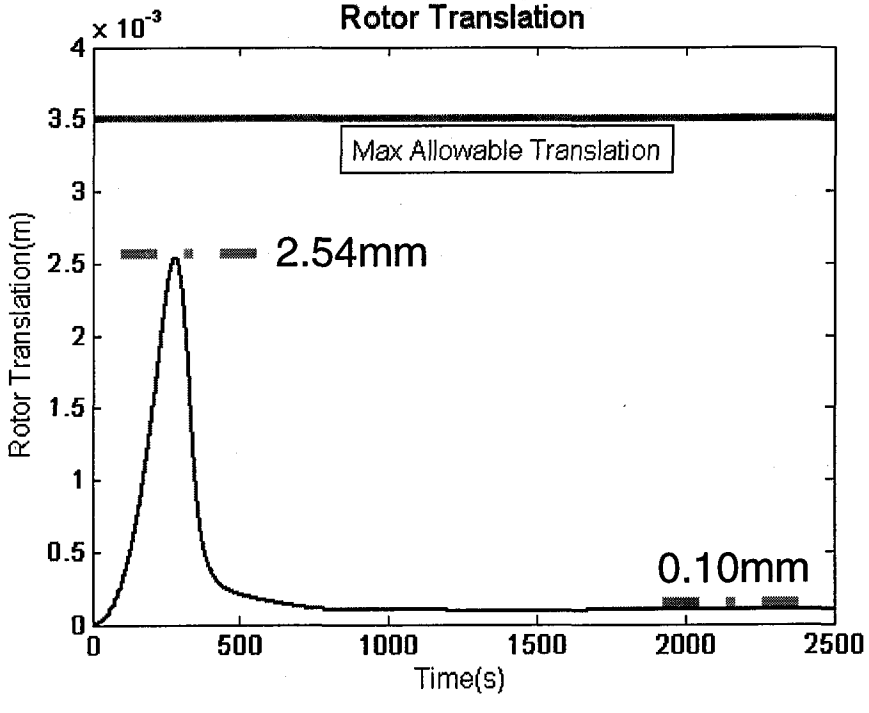

Figure 4-18. Stage 3 - Rotor Translation

Figure 4-19 indicates that the closed-loop system maintains stability for 60% rotor mass uncertainty and 45% rotor inertia uncertainty over the range $0 < \omega < \omega_{max}$ since the upper bound of $\mu < 1$ at all frequencies. The interval for ω was again divided into several intervals to evaluate robust. The plot of robust stability presented is the interval with the highest peak for the upper bound of μ. The transfer function evaluated is the same as that evaluated in stage 1 and stage 2 of the design process, but the plant includes the full coupled dynamics and the uncertainty is in the rotor mass, rotor inertia, and rotor spin rate.

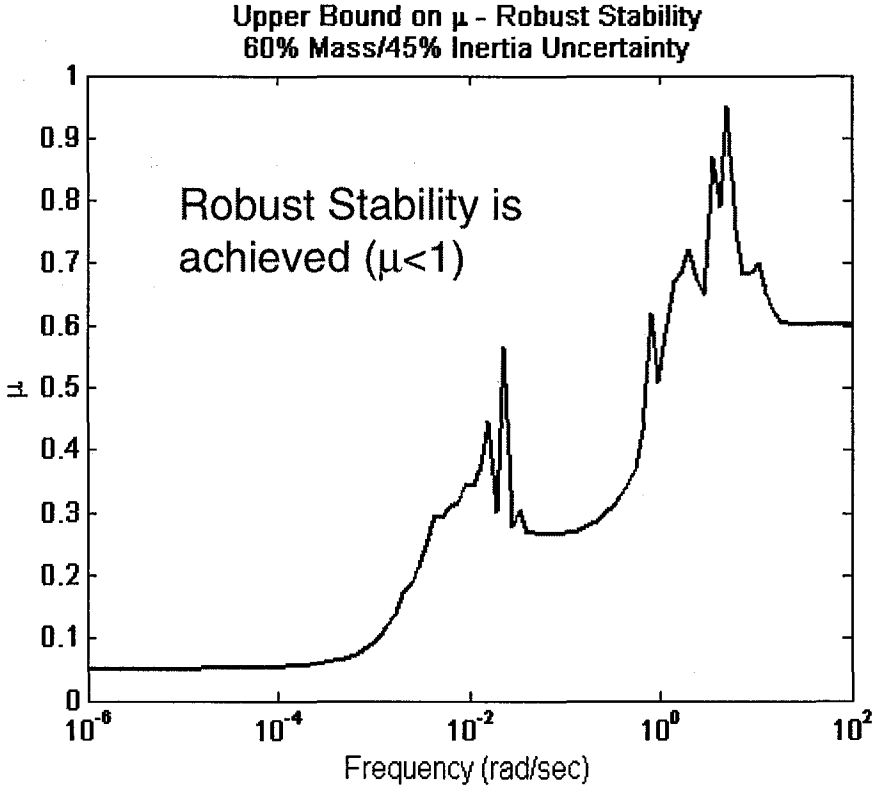

Figure 4-19. Stage 3 - Robust Stability

Figure 4-20 shows that the closed-loop system achieves the performance objective for 60% rotor mass uncertainty and 45% rotor inertia over the range $0 < \omega < \omega_{max}$ since the upper bound of $\mu < 1$ at all frequencies. Again, the interval for ω was again divided into several intervals. The plot of robust performance presented is for the ω interval with the highest peak for the upper bound on μ. The transfer function evaluated is the same as that in stage 1 and stage 2 of the design process, but the plant includes the full coupled dynamics and the uncertainty is in the rotor mass, rotor inertia, and rotor spin rate.

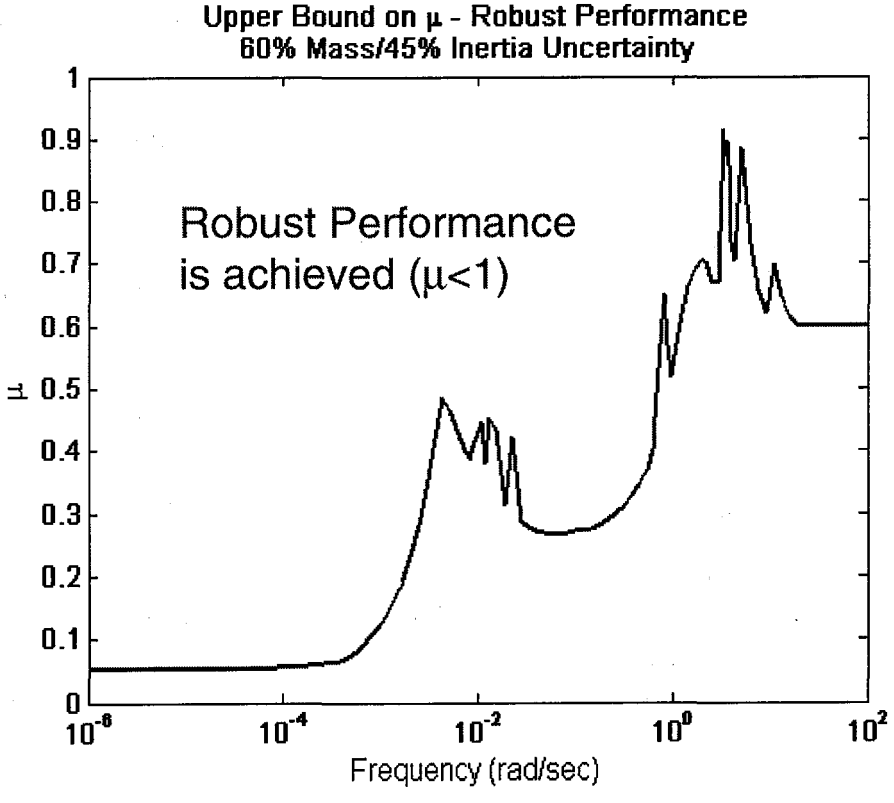

Figure 4-20. Stage 3 - Robust Performance

The robust performance objective was to limit the translation of the rotor < 3.5mm for a disturbance of maximum amplitude (as in the time domain simulation) and frequency content from DC to 0.0001 Hz (0.000628 rad/sec). This performance objective is formulated by appending weighting functions to the unweighted plant.

The weighting functions are appended to the plant as shown in Figure 4-6 in order to normalize the performance objective as stated above from d to e to a performance objective from d' to e'.

The weighting functions used to normalize the performance objective for stage 3 are a combination of the weighting functions for stage 1 and stage 2. Specifically,

$$W_{in\,stage3} = \begin{bmatrix} W_{in\,stage1} & & & \\ & W_{in\,stage1} & & \\ & & W_{in\,stage2} & \\ & & & W_{in\,stage2} \end{bmatrix} \qquad (148)$$

and

$$W_{out\,stage3} = \begin{bmatrix} W_{out\,stage1} & & & \\ & W_{out\,stage1} & & \\ & & W_{out\,stage2} & \\ & & & W_{out\,stage2} \end{bmatrix}. \qquad (149)$$

Figure 4-21 shows that in the time domain simulation the actuator saturation constraints of 1mm/sec or 0.001m/sec are not exceeded. By avoiding actuator saturation the linearity of the system is preserved.

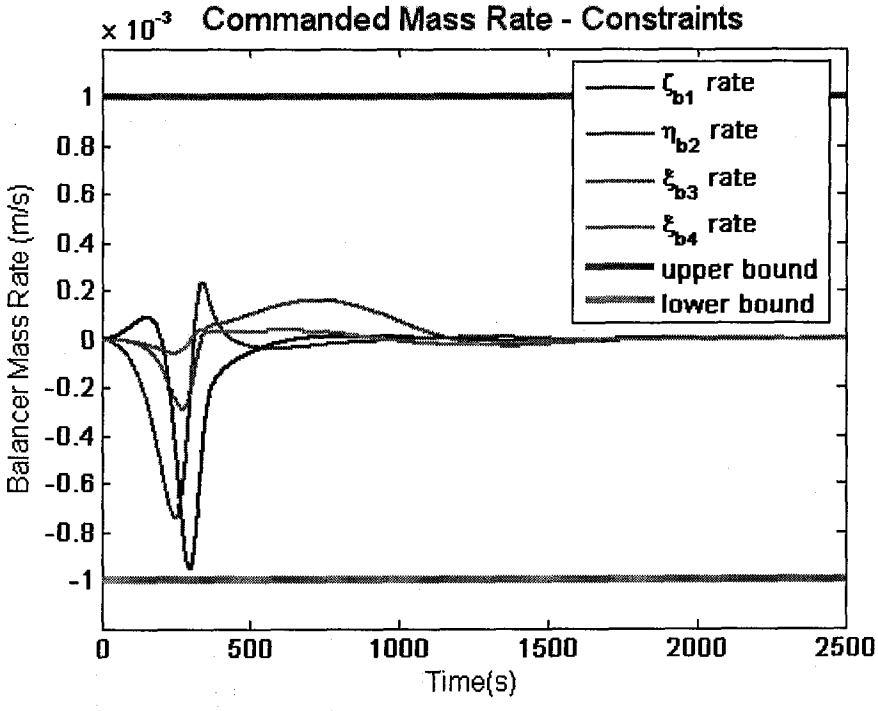

Figure 4-21. Stage 3 - Actuator Constraints

It is seen that all of the problem constraints specified in Equations (108) – (113) are met in stage 3 and the peak translational response of the rotor is minimized resulting in the final design of the ABC.

5 Results

In order to further examine of the effectiveness of the ABC design presented in Chapter 4, analysis was performed using frequency domain techniques to further analyze stability and time domain simulation (including Monte Carlo simulation) to further analyze performance. Much of the needed analysis was done during the design phase in Chapter 4 where nominal stability, nominal performance, robust stability, robust performance, and actuator saturation are analyzed for the linear system in the design phase. In this chapter, both stability margin analysis and nonlinear time domain analysis are performed to further verify the ABC design.

5.1 Stability Margin

Frequency domain stability and performance results are seen in Figure 4-19 and Figure 4-20 in Chapter 4 for the final ABC. These results guarantee the stability and performance of the closed-loop system for the range of possible spin rates and for parametric variations of 60% in the mass of the rotor (M) and 45% in the transverse moment of inertia (I_d) and polar moment of inertia (I_z) values. These requirements were the primary stability constraints of the control design. This section provides further verification of the stability of the system.

As an additional measure of the stability of the closed-loop system, gain margin and phase margin are calculated. Gain margin refers to the amount of gain that could be multiplied by the signal at the point where the loop break is shown while maintaining closed-loop stability. Phase margin refers to the amount phase that could be added to the signal at the point where the loop break is shown while maintaining closed-loop stability.

The control system is analyzed one loop at a time. The loops are shown in Figure 5-1 and Figure 5-2. First, the stability margins are evaluated at the input to the plant (in the actuator signal). Next, the stability margins are evaluated at the output of the plant (in the sensor signal).

The stability margins at the input of the plant as shown in Figure 5-1 are presented in Table 5-1. All stability margins are computed for the plant with a nominal spin rate, $\omega_{max}/2$.

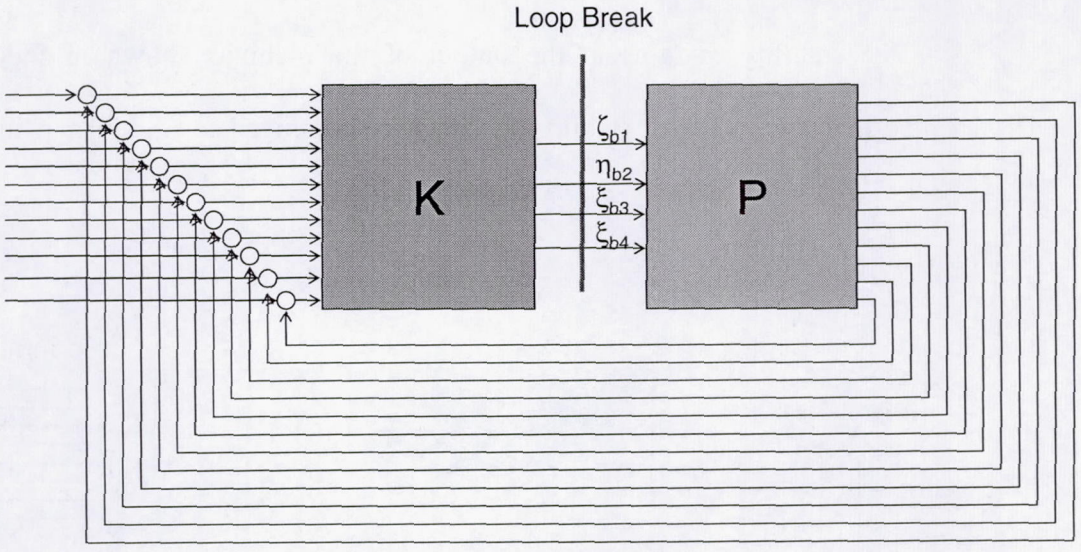

Figure 5-1. Loop Break for SISO Stability Margins at Plant Input

Traditional guidelines for good stability are gain/phase margins of 6dB/30deg or better. From the results in Table 5-1, it is apparent that the gain margins far exceed 6dB, with the smallest gain margin in the $\xi_{b3} \rightarrow \xi_{b3}$ loop being 18.5dB. The smallest phase margin, 28.9 deg occurs in the $\eta_{b2} \rightarrow \eta_{b2}$ loop. While this is slightly less than 30 deg phase margin, it is acceptable.

	Gain Margin(dB)	Phase Margin(deg)
$\zeta_{b1} \rightarrow \zeta_{b1}$	34.7	37.5
$\eta_{b2} \rightarrow \eta_{b2}$	31.0	28.9
$\xi_{b3} \rightarrow \xi_{b3}$	18.5	102.7
$\xi_{b4} \rightarrow \xi_{b4}$	Inf	107.8

Table 5-1. SISO Stability Margins at Plant Input for Nominal Spin Rate

The stability margins at the output of the plant as shown in Figure 5-2 are presented in Table 5-2. All stability margins are computed for the plant with a nominal spin rate, $\omega_{max}/2$.

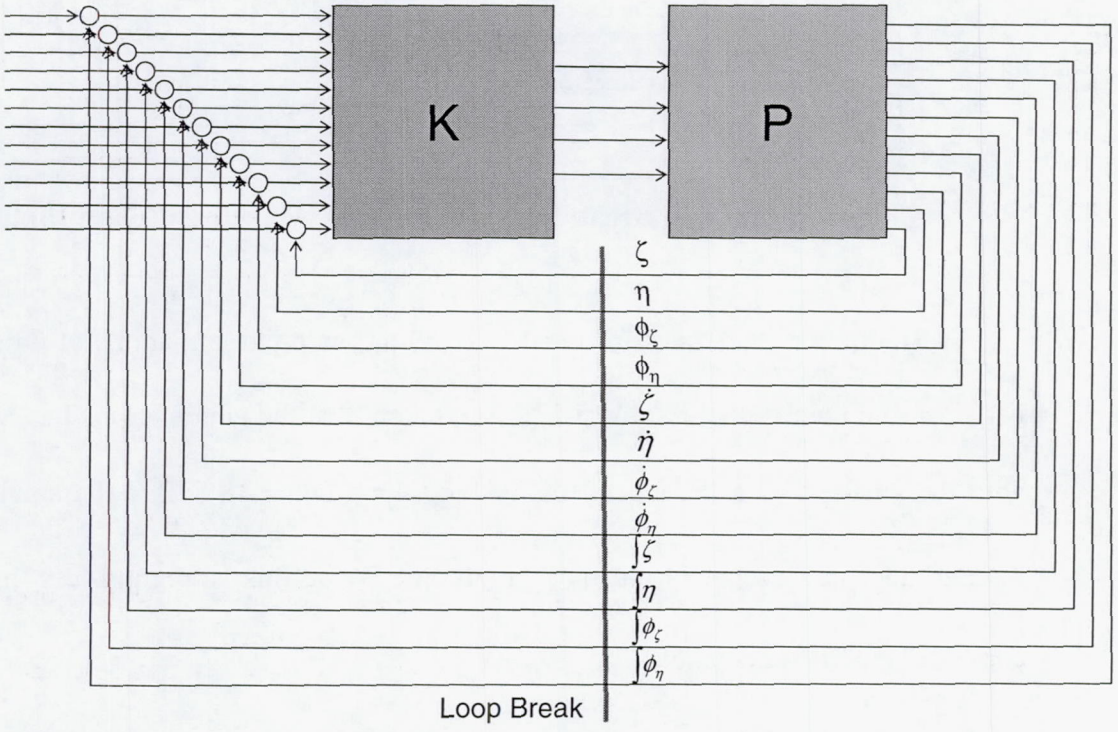

Figure 5-2. Loop Break for SISO Stability Margins at Plant Output

The results in Table 5-2 indicate that the gain margins at the output of the plant far exceed the traditional guideline of at least 6dB. Similar to the phase margin in the $\eta_{b2} \rightarrow \eta_{b2}$ loop at the input of the plant, the $\eta\_int \rightarrow \eta\_int$ loop at the output of the plant has a phase margin of approximately 28 deg. Again, while this is slightly less than 30 deg phase margin, it is acceptable. The notations _dot and _int denote the derivative and integral of the associated variable.

	Gain Margin(dB)	**Phase Margin(deg)**
$\zeta \rightarrow \zeta$	55.2	Inf
$\eta \rightarrow \eta$	44.9	Inf
$\phi_\zeta \rightarrow \phi_\zeta$	30.5	Inf
$\phi_\eta \rightarrow \phi_\eta$	45.3	Inf
$\zeta\_dot \rightarrow \zeta\_dot$	43.4	Inf
$\eta\_dot \rightarrow \eta\_dot$	37.9	Inf
$\phi_\zeta\_dot \rightarrow \phi_\zeta\_dot$	Inf	Inf
$\phi_\eta\_dot \rightarrow \phi_\eta\_dot$	21.1	Inf
$\zeta\_int \rightarrow \zeta\_int$	36.0	37.5
$\eta\_int \rightarrow \eta\_int$	35.3	27.9
$\phi_\zeta\_int \rightarrow \phi_\zeta\_int$	37.2	83.1
$\phi_\eta\_int \rightarrow \phi_\eta\_int$	43.6	100.2

Table 5-2. SISO Stability Margins at Plant Output for Nominal Spin Rate

Although gain/phase margins were not constrained during the design process, the resulting system has good gain/phase margins. This is primarily a result of two constraints that were in the design process. First, the design process required that the system be robustly stable to large parametric uncertainty in the rotor mass and the rotor

inertia. Since changing these parameters changes the gain of the plant, the controller had to be robust to gain uncertainty, yielding acceptable gain margin. Second, the constraints on the speed of the balancer masses necessitated that the controller gains stayed relatively small. The gains in the controller gain matrix could not be large values since such values would cause the controller to command the masses to move at a speed greater that the saturation speed. Having a low-gain controller corresponds to good stability margins much like a system with a zero gain controller (no control) would have infinite stability margins. However, not having a controller is not a reasonable solution since the controller is needed to meet time domain performance requirements (see Figure 5-4).

5.2 Time Domain Nonlinear Simulation

Time domain performance is analyzed using a simulation as shown in Figure 5-3. The simulation includes nonlinearities in the coordinate transformation, actuator constraints (mass rate saturation), and time delays. Also, the plant dynamic equations of motion are in the fixed (x,y) frame and the sensor measurements are rotated into the rotating frame via the coordinate transformation following the plant model.

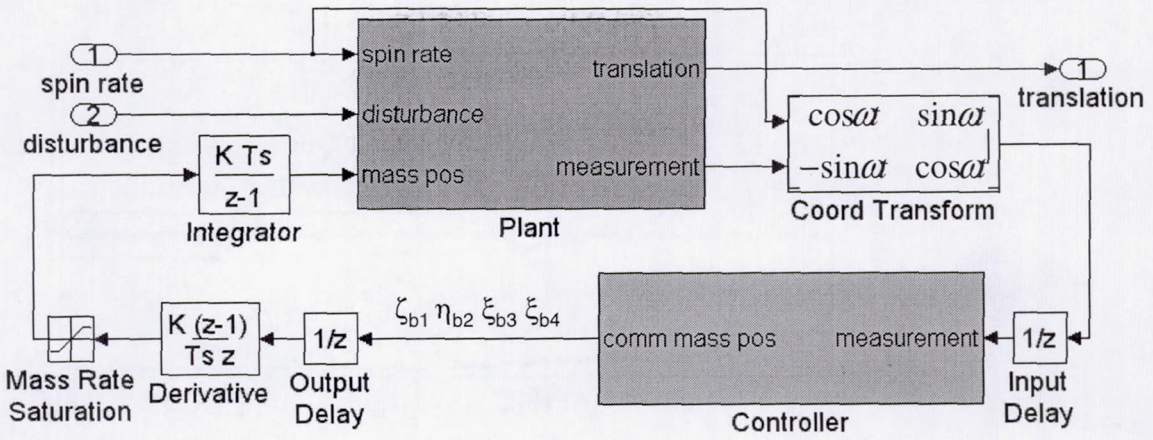

Figure 5-3. Time Domain Simulation

The scenario simulated in this section includes a spin-up of the rotor from a spin rate of 0 to the maximum spin rate. The maximum spin rate is reached in 1800 seconds and the rotor continues to spin at this rate until the simulation ends at 2500 seconds. The disturbance acting on the plant is the disturbance resulting from the rodents being stationary in positions causing the largest imbalance in the rotor as described in Section 2.1.

First, the performance of the ABC is analyzed by comparing the rotor translation for the case with no controller and the case where the controller designed in Chapter 4 is implemented. The results of these simulations are shown in Figure 5-4.

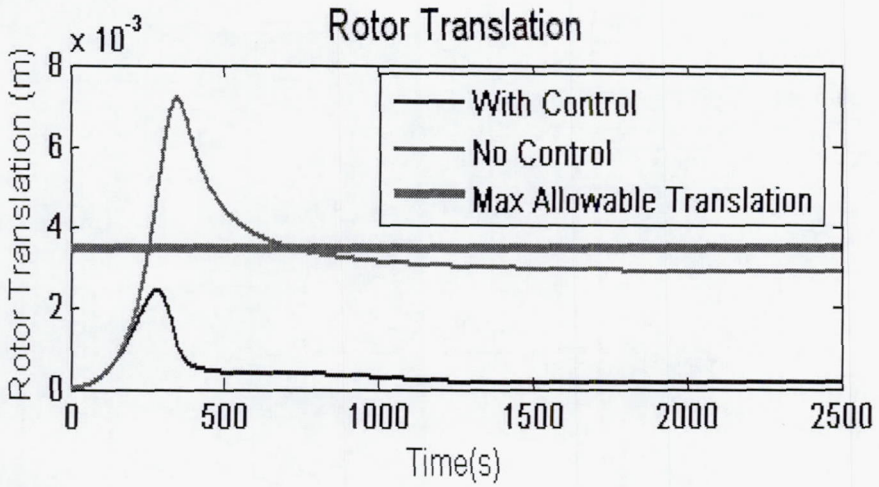

Figure 5-4. Time Domain Comparison to No Control

It is clear that control is needed to satisfy the requirement of limiting peak rotor translation to be less than 3.5mm. In fact, with the ABC the peak rotor translation is reduced from approximately 7.0mm to approximately 2.5mm.

Further, the effect of the specified variations in the rotor mass and inertia was analyzed through time domain simulation. The scenario simulated was the same as that described above that was used to compare the rotor translation with the ABC to a case with no control. In order to analyze the effect of parametric variation on the performance of the system, the corner cases of the allowed parametric variations were tested. For instance, the mass of the rotor was set at the nominal value, the nominal value + 60%, and the nominal value - 60%. Similarly, the inertias of the rotor (I_d,I_z) are allowed to vary independently between the nominal value, the nominal value + 45%, and the nominal value - 45%. Using these corner cases, 27 different parameter combinations were tested in simulation. The combinations are listed in Table 5-3. Figure 5-5 shows the response of all 27 cases tested. The peak rotor translation of the 27 cases varied

between 2.07mm and 2.87mm, all below the 3.5mm requirement. Also, the translation of the rotor at steady-state varied between 0.06mm and 0.10mm. This meets the requirement for steady-state error of 0.10mm or less.

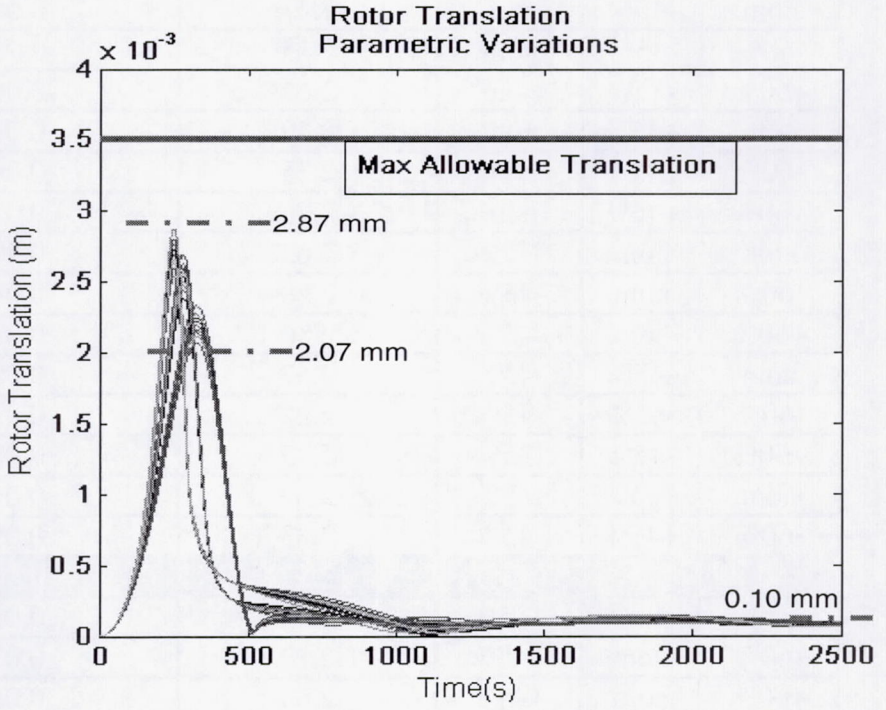

Figure 5-5. Rotor Translation with Parametric Variations

From Table 5-3 it is seen that the combination of parameter values corresponding the largest peak rotor translation and the largest steady-state error are when the mass of the rotor is +60% from nominal, the transverse moment of inertia of the rotor is +45% from nominal, and the polar moment of inertia of the rotor is -45% from nominal. This case is highlighted in Table 5-3.

M (kg)	Id (kg-m^2)	Iz (kg-m^2)	Peak Translation (mm)	Steady-State Translation (mm)
nom	nom	nom	2.53	0.093
-60%	nom	nom	2.20	0.093
+60%	nom	nom	2.70	0.076
nom	-45%	nom	2.47	0.081
-60%	-45%	nom	2.15	0.087
+60%	-45%	nom	2.64	0.062
nom	+45%	nom	2.59	0.098
-60%	+45%	nom	2.25	0.098
+60%	+45%	nom	2.76	0.084
nom	nom	-45%	2.63	0.098
-60%	nom	-45%	2.28	0.098
+60%	nom	-45%	2.80	0.087
nom	-45%	-45%	2.57	0.098
-60%	-45%	-45%	2.22	0.096
+60%	-45%	-45%	2.73	0.081
nom	+45%	-45%	2.69	0.099
-60%	+45%	-45%	2.33	0.099
+60%	+45%	-45%	2.87	0.100
nom	nom	+45%	2.44	0.081
-60%	nom	+45%	2.12	0.084
+60%	nom	+45%	2.65	0.060
nom	-45%	+45%	2.39	0.090
-60%	-45%	+45%	2.07	0.086
+60%	-45%	+45%	2.54	0.085
nom	+45%	+45%	2.50	0.087
-60%	+45%	+45%	2.17	0.091
+60%	+45%	+45%	2.66	0.066

Table 5-3. Results of Parametric Variations

The preceding time domain analysis verifies two things. First, it is apparent that without control the system will not meet the performance requirements of limiting rotor translation to a peak of less than 3.5mm or a steady-state value of 0.10mm. This verifies the need for an ABC to improve performance. Second, parametric variations in time

domain simulation verify that the performance of the system is acceptable subject to the allowable parametric uncertainty. The system performance is robust to uncertainty in the plant. The robustness is further verified through Monte Carlo Simulation.

5.3 Monte Carlo Simulation

The performance of the ABC system is further analyzed through Monte Carlo simulation. The Monte Carlo method, a numerical method of solving problems through the simulation of random variables and processes [42],[43], has been used to gain insight into many complex problems in engineering and other fields. The method allows for the repeated simulation of a given system with an unknown or uncertain input variable. Repeated random selection of this unknown variable allows one to study how a particular system's outputs are distributed given a random input.

Five separate Monte Carlo studies were performed to analyze the performance and robustness of the ABC system subject to uncertainty in the following variables: rodent motion within the habitats, mass and inertia of the rotor, actuator uncertainty, and sensor uncertainty.

The Monte Carlo studies were performed under the conditions shown in Table 5-4. 0.1 m/s is assumed to be the maximum velocity of a single rodent.

Test Case	Random Input Variables	Distribution	Disturbance	Output Variable
Test Case 1	Rodent velocity	Normal, mean = 0 m/s, 3σ = 0.1 m/s	Random variable due to rodent motion	Peak rotor translation
	Rodent direction	Uniform, random unit vector		
Test Case 2	Rotor mass	Normal, mean = nominal, 3σ = 60% variation	Rodents in fixed positions for max imbalance	Peak rotor translation
	Rotor inertia	Normal, mean = nominal, 3σ = 45% variation		
Test Case 3	Actuator gain	Normal, mean = 1, 3σ = 75% error	Rodents in fixed positions for max imbalance	Peak rotor translation
Test Case 4	Sensor gain	Normal, mean = 1, 3σ = 75% error	Rodents in fixed positions for max imbalance	Peak rotor translation
Test Case 5	Rodent velocity	Normal, mean = 0 m/s, 3σ = 0.1 m/s	Random variable due to rodent motion	Peak rotor translation
	Rodent direction	Uniform, random unit vector		
	Rotor mass	Normal, mean = nominal, 3σ = 60% variation		
	Rotor inertia	Normal, mean = nominal, 3σ = 45% variation		
	Actuator gain	Normal, mean = 1, 3σ = 75% error		
	Sensor gain	Normal, mean = 1, 3σ = 75% error		

Table 5-4. Monte Carlo Test Cases

The results of the Monte Carlo study are shown in Figure 5-6 - Figure 5-10.

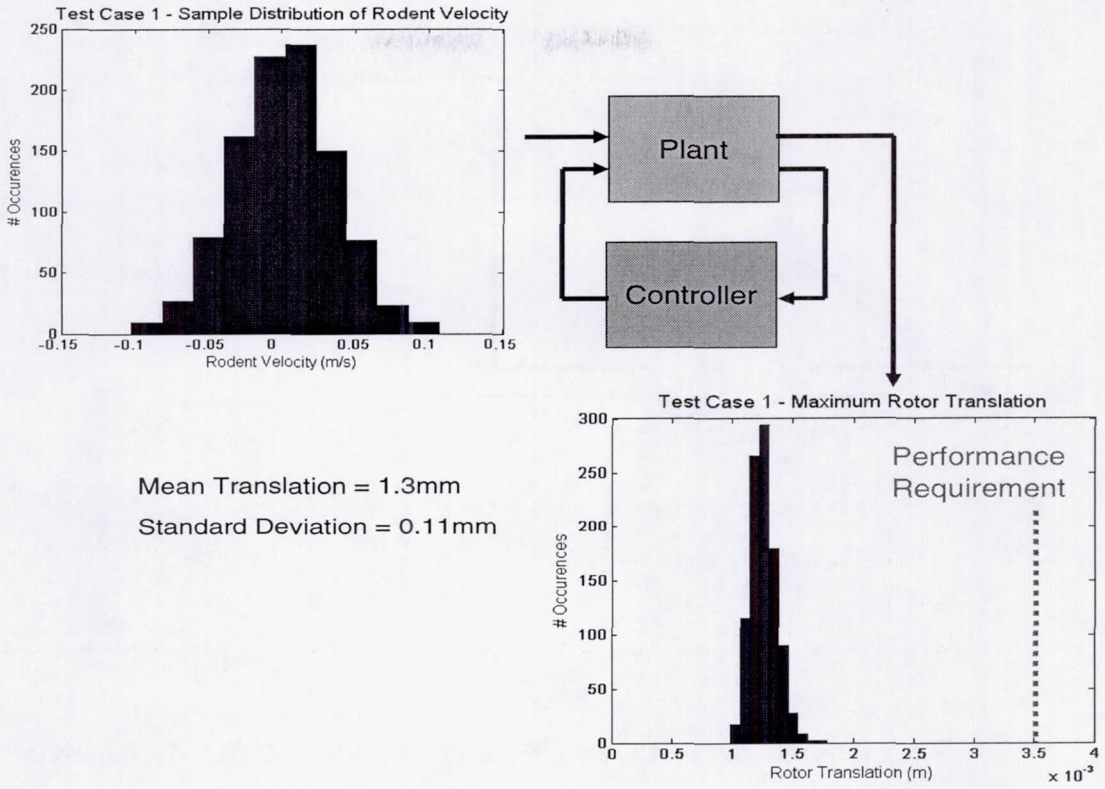

Figure 5-6. Test Case 1 Results – Random Rodent Motion

It is seen in test case 1, that the system meets the performance requirement for all 1000 runs. This result indicates that the ABC is effectively canceling the imbalance introduced by rodent motion.

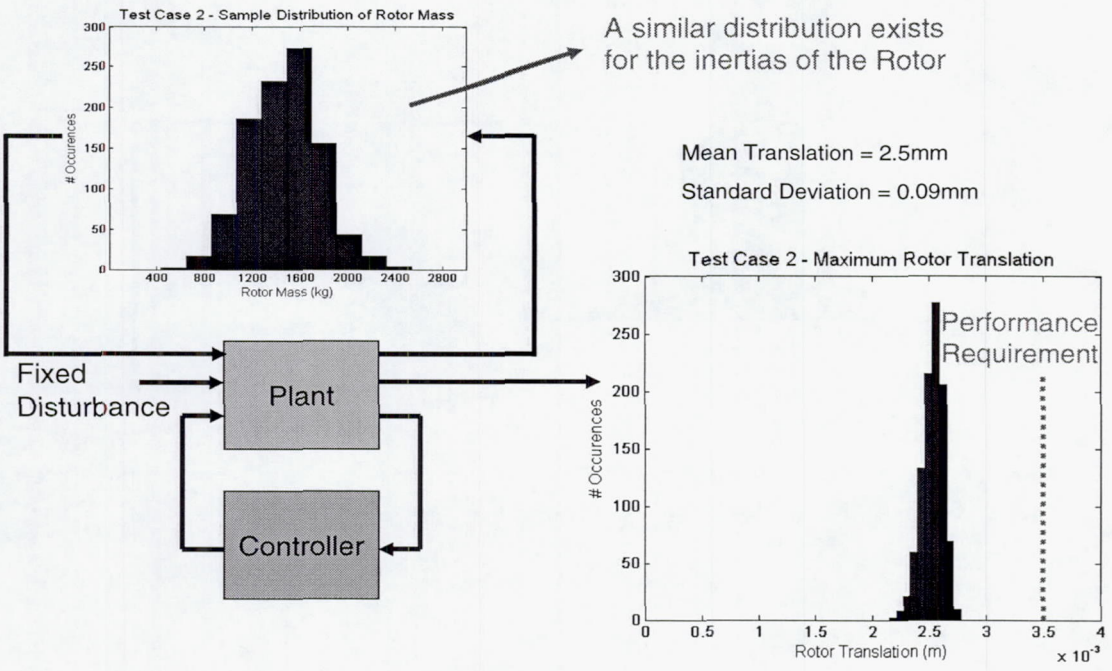

Figure 5-7. Test Case 2 Results – Random Rotor Mass/Inertia

Similarly, in test case 2, the system meets the performance requirement for all 1000 runs. This result indicates that the system with the ABC controller is robust to variations in the mass and inertia of the rotor.

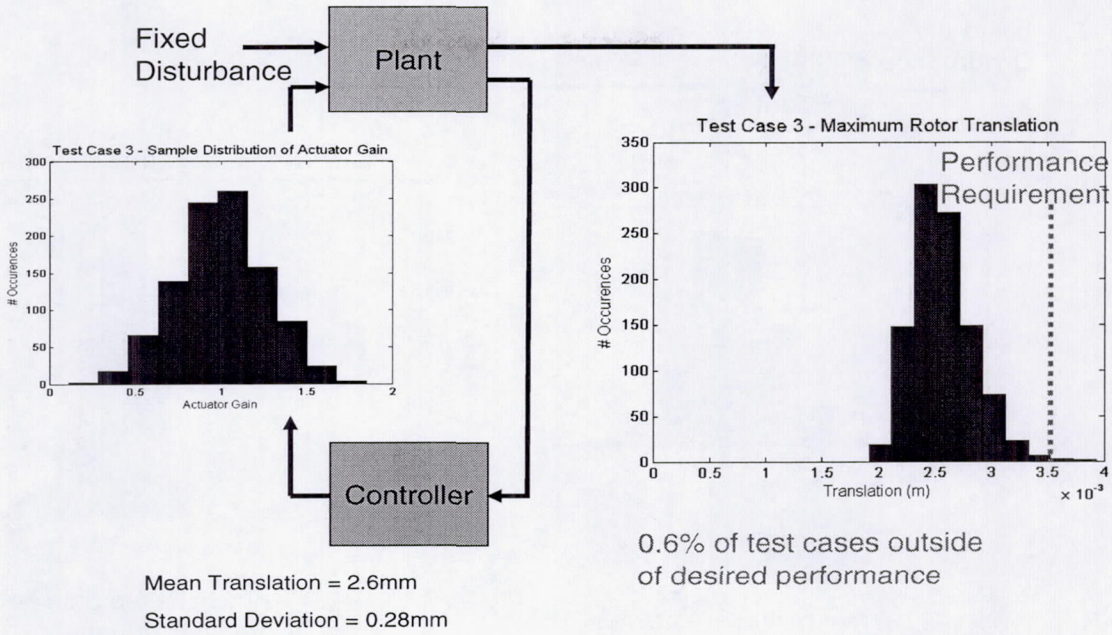

Figure 5-8. Test Case 3 Results – Random Actuator Gain

In test case 3, it is seen that the system meets the performance requirement for 99.4% of the simulations. It is not surprising that it does not meet the performance requirement in every case since a 75% uncertainty in the actuator gain is quite large. This allows the balancer mass to be up to 75% away from the position commanded by the ABC. A success rate of 99.4% is considered acceptable.

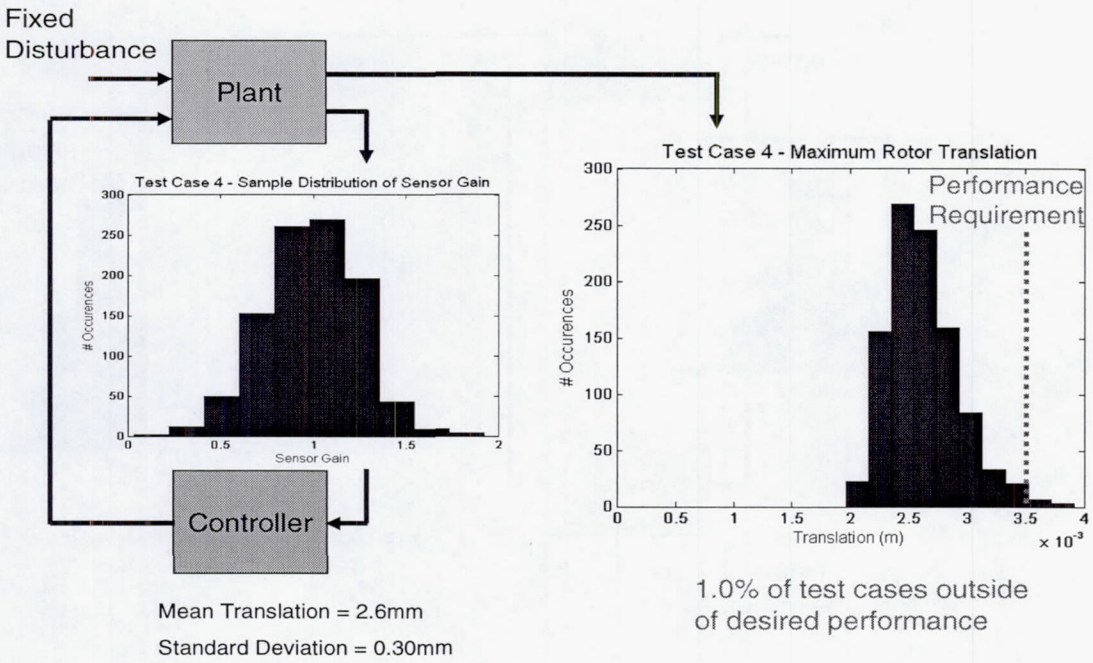

Figure 5-9. Test Case 4 Results – Random Sensor Gain

In test case 4 it is seen that the system meets the performance requirement for 99.0% of the simulations. Similar to test case 3, it is not surprising that it does not meet the performance requirement in every case since a 75% uncertainty in the sensor gain is quite large. This allows the sensor to read a displacement with up to 75% error from the actual displacement. A success rate of 99.0% is considered acceptable.

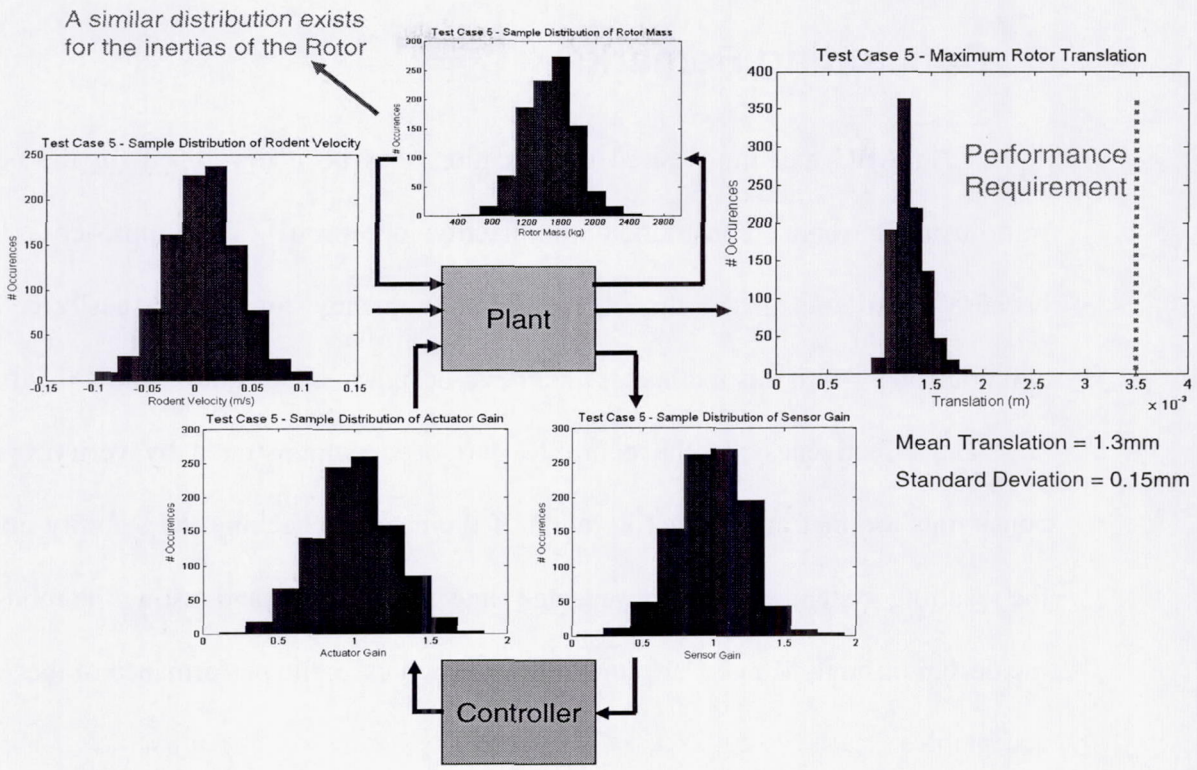

Figure 5-10. Test Case 5 Results – All Random Distributions

It is seen in test case 5 that the system meets the performance requirement for all 1000 runs. This result indicates that the ABC is effectively canceling the imbalance introduced by rodent motion and is robust to simultaneous perturbations in parameter values, actuator gains, and sensor gains. It is not surprising that the mean translation in test case 5 is significantly less than that in test cases 2-4. This is due to the fact that the disturbance in test cases 2-4 was a fixed disturbance where the rodents are stationary in the worst-case positions. The disturbance in test case 5 is a random disturbance generated from the random direction and velocity of the rodents. In general, this random disturbance will be less severe than the fixed disturbance with maximum imbalance.

6 Concluding Remarks

An ABC meeting desired specifications has been developed for the centrifuge rotor using a robust constrained optimization approach. This approach is selected because constraints in the time domain and frequency domain can easily be handled simultaneously with this method. Other ABC design methods do not allow this freedom.

The effectiveness of the controller has been demonstrated by verifying that the constraints are met at the final iteration of the design, checking the stability margins of the resulting system, performing selected time domain tests, and testing the robustness of the design through Monte Carlo methods. In each case, the performance of the ABC was acceptable.

In Chapter 2 the problem background was introduced. A description of the centrifuge rotor system and the ABC system was presented. The equations of motion for the centrifuge rotor were derived in both the fixed frame coordinate system and the rotating frame coordinate system. The system block diagram and controller structure for the ABC were presented.

In Chapter 3 the technical background for the solution of the problem is discussed. The basics of MIMO control and uncertain systems were presented. These concepts were used together to analyze system robustness with the structured singular value. Steady-state error in control systems was also discussed. Finally the robust constrained optimization approach to control design is presented.

Chapter 4 presented the method used to solve the control problem. This chapter described the implementation of the robust constrained optimization approach to control design and how it was applied to design an ABC system. The method was applied in a

three stage design procedure in order to convert the relatively large optimization problem into three smaller sub-problems. The results of the controller design are presented at the end of each individual stage and also at the end of the final design. The application of the solution method produced a controller meeting the constraints of the problem while minimizing the translation of the rotor.

Chapter 5 presented further analysis of the control design. The system was analyzed in both the time domain and frequency domain. Stability margins were analyzed in the frequency domain and performance was analyzed in the time domain. Frequency domain analysis verified that the stability margins of the system were satisfactory. The time domain simulations verified that the controller performance was robust to parametric uncertainty. The results provided further indication that the control design was acceptable. Also, the results of the Monte Carlo simulations were presented. The Monte Carlo results also verified that the control design provided satisfactory performance.

Future work in the design of an ABC for the centrifuge rotor system could include the minimization of a different performance measure, such as robust performance or robust stability. Such a controller would be able to tolerate more uncertainty, but the performance at the nominal point would suffer as a result. Also, a method could be used to treat robust performance in the time domain. This would make it possible to consider transient effects in the robust performance analysis.

7 References

[1] Space OnLine. Website. http://www.spaceonline.tv/iss_fltuf7.htm. 2004.

[2] Meirovitch, L., (1990). *Dynamics and Control of Structures*, John Wiley & Sons, New York.

[3] Knopse, C. R., Hope, R. W., Fedigan, S., and Williams, R., 1995, "Experiments in the Control of Unbalance Response Using Magnetic Bearings," *Mechanics*, Vol. 5, 385-400.

[4] Knopse, C. R., Hope, R. W., Fedigan, S., and Tamer, S. M., 1996, "Robustness of Adaptive Unbalance Control of Rotors with Magnetic Bearings," *Journal of Vibration and Control*, Vol. 2, 33-52.

[5] Knopse, C. R., Fedigan, S., and Tamer, S. M., 1997, "Robustness of Adaptive Rotor Vibration Control to Structured Uncertainty," *ASME Transactions, Journal of Dynamic Systems, Measurement, and Control*, Vol. 119, 243-250.

[6] Knopse, C. R., Tamer, S.M., Fittro, R., 1997, "Rotor Synchronous Response Control: Approaches for Addressing Speed Dependence," *Journal of Vibration and Control*, Vol. 3, 435-458.

[7] Herzog, R., Buhler, P., Gahler, C., and Larsonneur, R., 1996, "Unbalance Compensation Using Generalized Notch Filters in the Multivariable Feedback of Magnetic Bearings," *IEEE Transactions on Control Systems Technology*, Vol. 4, 580-586.

[8] Fan, Y. H., Chen, S. T., and Lee, A., 1992, "Active Control of an Asymmetrical Rigid Rotor Supported by Magnetic Bearings," *Journal of the Franklin Institute*, Vol. 329, 1153-1178.

[9] Van De Vegte, J., 1964, "Continuous Automatic Balancing of Rotating System," *Journal of Mechanical Engineering Science*, Vol. 6, 264-269.

[10] Gosiewski, Z., 1985, "Automatic Balancing of Flexible Rotors, Part 1: Theoretical Background," *Journal of Sound and Vibration*, Vol. 100, 551-567.

[11] Gosiewski, Z., 1987, "Automatic Balancing of Flexible Rotors, Part 2: Synthesis of Systems," *Journal of Sound and Vibration*, Vol. 114, 103-109.

[12] Dyer, S.W., and Ni, J., 1999, "Adaptive Influence-Coefficient Control of Single-Plane Active Balancing Systems," *Proceedings of the ASME International Mechanical Engineering Conference and Exposition, Symposium on Sensors and Controls*, MED-Vol. 10, Nashville, TN, 747-755.

[13] Zhou, S., and Shi, J., 2000, "Supervisory Adaptive Balancing of Rigid Rotors during Acceleration," *Transactions of NAMRI/SME*, Vol. 27, 425-430.

[14] Zhou, S., and Shi, J., 2001, "Optimal One-Plane Active Balancing of Rigid Rotor during Accelerations," *Journal of Sound and Vibration.*

[15] Zhou, S., and Shi, J., 2001, "Unbalance Estimation for Speed-Varying Rigid Rotors Using Time-Varying Observer," *ASME Transactions, Journal of Dynamic Systems Measurement, and Control.*

[16] Zhou, S., and Shi, J., 2001, "Active Balancing and Vibration Control of Rotating Machinery: A Survey," *The Shock and Vibration Digest*, Vol. 33, No. 4, 361-371.

[17] Sullivan, M., *State Estimation of International Space Station Centrifuge Rotor with Incomplete Knowledge of Disturbance Inputs*, Master of Thesis, Rice University, 2005.

[18] Meirovitch, L., (1985). *Introduction to Dynamics and Control*, John Wiley & Sons, New York.

[19] Yamamoto, T., and Ishida, Y., (2001). *Linear and Nonlinear Rotordynamics,* John Wiley & Sons, New York.

[20] Kailath, T., (1980). *Linear Systems*, Prentice-Hall, Inc., Englewood Cliffs, N.J.

[21] *Using Simulink*, (2002), Mathworks, Natick, Mass.

[22] Kuo, B.C, (1995). *Automatic Control Systems*, Prentice Hall, Inc., New Jersey.

[23] Strang, G., (1998). *Introduction to Linear Algebra*, Wellesley-Cambridge Press, Wellesley, MA.

[24] Skogestad, S., and Postlethwaite, I. (1996). *Multivariable Feedback Control*, John Wiley & Sons, New York.

[25] Grigoriadis, K., *Advanced Linear Controls*, Class Notes, University of Houston, 2004.

[26] Doyle, J.C., 1982, "Analysis of Feedback Systems with Structured Uncertainties," IEE Proceedings, Part D, Vol. 129, 242-250.

[27] Doyle, J.C., Wall, J.E., and Stein, G., 1982, "Performance and Robustness Analysis for Structured Uncertainty," *Proceedings of the 21st Conference on Decision and Control*, 629-636.

[28] Balas, G.J., Doyle, J.C., Glover, K., Packard, A. and Smith, R. (1993). *μ-analysis and Synthesis Toolbox User's Guide*, Mathworks, Natick, Mass.

[29] Zhou, K., Doyle, J.C., and Glover, K. (1996). *Robust and Optimal Control*, Prentice-Hall, Upper Saddle River.

[30] Barmish, B., Khargonekar, P., Shi, Z., and Tempo, R., 1989, "Robustness Margin Need not be a Continuous Function of the Problem Data," *Systems and Controls Letters*, Vol. 15, 91-98.

[31] Packard, A., Pandey, P., 1993, "Continuity Properties of the Real/Complex Structured Singular Value," *IEEE Transactions on Automatic Control*, Vol. 38, 415-428.

[32] Vidyasagar, M., (1978). *Nonlinear Systems Analysis*. Prentice-Hall, Inc., Englewood Cliffs, New Jersey.

[33] Balakrishnan, V., and Tits, A., 1996, "Numerical Optimization-Based Design," *The Control Handbook*, Ed. Levine, W., Chapter 47, 749-758.

[34] Ghaoui, L., and Balakrishnan, V., 1994, "Synthesis of Fixed-Structure Controllers via Numerical Optimization," *Proc IEEE Conference on Decision and Control*, 2678-2683.

[35] Jang, J.-W., 1995, "Design of Game Theoretic Controllers for Multiobjective Linear Regulator Problems," Ph.D. Thesis, University of Florida.

[36] Jang, J.-W., Bedrossian, N., Lee, A., and Spanos, P, 2002, "A Constrained Optimization Approach for CMG Robust Flex Filter Design," AIAA-2002-4577, AIAA Guidance, Navigation, and Control Conference, Monterey CA, 2002.

[37] Jang, J.-W., Bedrossian, N., Lee, A., and Spanos, P, 2003, "Design of Robust Nash Game Theoretic Controllers with Time Domain Constraints," AIAA-2002-4577, AIAA Guidance, Navigation, and Control Conference, Monterey CA, 2002.

[38] Branch, M.A., and Grace, A., (1996). *Optimization Toolbox User's Guide*, Mathworks, Natick, Mass.

[39] Fletcher, R., (1980). *Practical Methods of Optimization, Vol. 2, Constrained Optimization*, John Wiley & Sons.

[40] Luenberger, D.G., (1969). *Optimization by Vector Space Methods*, John Wiley & Sons, New York.

[41] Zhang, Honghai, *Improving Constrained Nonlinear Search Algorithms Through Constraint Relaxation*, Master of Science Thesis, University of Illinois at Urbana-Champaign, 2001.

[42] Sobol', I.M. (1994). *A Primer for the Monte Carlo Method*, CRC Press, Boca Raton.

[43] Spanos, P.D., and Roberts, J.B., (2004). *Random Vibration and Statistical Linearization*, Dover Publications, Inc., Mineola, N.Y.